USACERL Technical Manuscript E-89/11
July 1989

US Army Corps
of Engineers
Construction Engineering
Research Laboratory

AD-A210 826

Three-Dimensional Modelling of Heat Transfer From Slab Floors

by
William P. Bahnfleth

Earth-coupled heat transfer processes have been recognized in recent years as a potential source of significant energy savings in both conventional and earth-sheltered designs. Because of the complexity of the building/soil/atmosphere interaction, however, important aspects of earth-coupled heat transfer are not well understood. There is a particular lack of three-dimensional foundation heat loss data. In this study, a detailed three-dimensional finite difference model of a slab floor was used to generate 93 annual simulations in parametric groups focusing on effects of size and shape, soil properties, boundary conditions, climate, insulation, and building shadow. these results indicate that soil thermal conductivity, ground surface conditions, foundation design, and floor shape/size are essential elements of a general change in heat transfer rate. Effects of thermal diffusivity, and lower boundary condition variation were small (on the order of 10%) for the range of conditions considered. The building shadow produced an effect that was generally small, but much more significant in a warm sunny climate than in a cool, cloudy one. Diurnal variation in total floor heat loss also was small, indicating that a daily time step is sufficient for energy analysis purposes. Design heat loss methods based on perimeter loss coefficients were shown to be unreliable because of significant total area effect. Heat loss per unit area was found proportional to $(A/P)^d$ where A, P, and d are floor area, perimeter length, and an empirically determined exponent. A model employing this scaling and separating heat loss into mean and periodic parts may be useful as a design equation.

DTIC
ELECTE
AUG 0 2 1989
S D
B

Approved for public release; distribution is unlimited.

89 8 01 118

The contents of this report are not to be used for advertising, publication, or promotional purposes. Citation of trade names does not constitute an official indorsement or approval of the use of such commercial products. The findings of this report are not to be construed as an official Department of the Army position, unless so designated by other authorized documents.

DESTROY THIS REPORT WHEN IT IS NO LONGER NEEDED
DO NOT RETURN IT TO THE ORIGINATOR

REPORT DOCUMENTATION PAGE

Form Approved
OMB No 0704 0188
Exp Date Jun 30 1986

1a REPORT SECURITY CLASSIFICATION UNCLASSIFIED	1b RESTRICTIVE MARKINGS
2a SECURITY CLASSIFICATION AUTHORITY	3 DISTRIBUTION/AVAILABILITY OF REPORT Approved for public release; distribution is unlimited.
2b DECLASSIFICATION/DOWNGRADING SCHEDULE	
4 PERFORMING ORGANIZATION REPORT NUMBER(S) USACERL TM E-89/11	5 MONITORING ORGANIZATION REPORT NUMBER(S)
6a NAME OF PERFORMING ORGANIZATION U.S. Army Construction Engr Research Laboratory 6b OFFICE SYMBOL (If applicable)	7a NAME OF MONITORING ORGANIZATION
6c ADDRESS (City, State, and ZIP Code) PO Box 4005 Champaign, IL 61824-4005	7b ADDRESS (City, State, and ZIP Code)
8a NAME OF FUNDING/SPONSORING ORGANIZATION HQUSACE 8b OFFICE SYMBOL (If applicable)	9 PROCUREMENT INSTRUMENT IDENTIFICATION NUMBER
8c ADDRESS (City, State, and ZIP Code) 20 Massachusetts Ave, NW WASH DC 20314-1000	10 SOURCE OF FUNDING NUMBERS PROGRAM ELEMENT NO: 4A161102 | PROJECT NO: AT23 | TASK NO: EB | WORK UNIT ACCESSION NO: ER9
11 TITLE (Include Security Classification) Three-Dimensional Modelling of Heat Transfer From Slab Floors	
12 PERSONAL AUTHOR(S) William P. Bahnfleth	
13a TYPE OF REPORT Final 13b TIME COVERED FROM ____ TO ____	14 DATE OF REPORT (Year, Month, Day) 1989, July 15 PAGE COUNT 214
16 SUPPLEMENTARY NOTATION Copies are available from the National Technical Information Service, 5285 Port Royal Road, Springfield, VA 22161	

17 COSATI CODES		
FIELD	GROUP	SUB-GROUP
13	13	

18 SUBJECT TERMS (Continue on reverse if necessary and identify by block number)
heat transfer, energy consumption, foundation (structures), models

19 ABSTRACT (Continue on reverse if necessary and identify by block number)

Earth-coupled heat transfer processes have been recognized in recent years as a potential source of significant energy savings in both conventional and earth-sheltered designs. Because of the complexity of the building/soil/atmosphere interaction, however, important aspects of earth-coupled heat transfer are not well understood. There is a particular lack of three-dimensional foundation heat loss data. In this study, a detailed three-dimensional finite difference model of a slab floor was used to generate 93 annual simulations in parametric groups focusing on effects of size and shape, soil properties, boundary conditions, climate, insulation, and building shadow. these results indicate that soil thermal conductivity, ground surface conditions, foundation design, and floor shape/size are essential elements of a general change in heat transfer rate. Effects of thermal diffusivity, and lower boundary condition (Cont'd)

20 DISTRIBUTION/AVAILABILITY OF ABSTRACT ☐ UNCLASSIFIED/UNLIMITED ☒ SAME AS RPT ☐ DTIC USERS	21 ABSTRACT SECURITY CLASSIFICATION UNCLASSIFIED
22a NAME OF RESPONSIBLE INDIVIDUAL D. P. MANN	22b TELEPHONE (Include Area Code) (217) 373-7223 22c OFFICE SYMBOL CECER-IM

DD FORM 1473, 84 MAR 83 APR edition may be used until exhausted
All other editions are obsolete

SECURITY CLASSIFICATION OF THIS PAGE
UNCLASSIFIED

BLOCK 19 (Cont'd)

variation were small (on the order of 10%) for the range of conditions considered. The building shadow produced an effect that was generally small, but much more significant in a warm sunny climate than in a cool, cloudy one. Diurnal variation in total floor heat loss also was small, indicating that a daily time step is sufficient for energy analysis purposes. Design heat loss methods based on perimeter loss coefficients were shown to be unreliable because of significant total area effect. Heat loss per unit area was found proportional to $(A/P)^d$ where A, P, and d are floor area, perimeter length, and an empirically determined exponent. A model employing this scaling and separating heat loss into mean and periodic parts may be useful as a design equation.

FOREWORD

This work was conducted under Project 4A161102AT23, "Basic Research in Military Construction"; work unit EB-ER9, "Underground heat Transfer Algorithms."

This manuscript was submitted in partial fulfillment of the requirements for the degree of Doctor of Philosophy in Mechanical Engineering in the Graduate College of the University of Illinois at Urbana-Champaign. The advisor for this thesis was Professor Curtis Pedersen. Members of the examining committee: Professors J. C. Chato, T. A. Newell, L. L. Christianson, and A R. Mech. Mr Dale Herron, Team Leader in the Energy Systems Division of the U.S. Army Construction Engineering Research Laboratory (USACERL) was instrumental in obtaining funding for this research. Ms. Linda Lawrie, Team Leader, USACERL Energy Systems Division, was an understanding and supportive supervisor and helped with the production of weather data files. Finally, thanks are extended to Ms. Kimberly Ware of the University of Illinois BLAST Support Office and Ms. Athena Newcomb of the USACERL Energy Systems Division, who assisted in the production of the manuscript.

Technical guidance and support were provided by the Energy Design and Management Team of the Energy Systems Division (ES), U.S. Army Construction Engineering Research Laboratory (USACERL). Dr. G. R. Williamson is Chief of USACERL-ES.

COL Carl O. Magnell is Commander and Director of USACERL, and Dr. L. R. Shaffer is Technical Director.

Accession For
NTIS GRA&I ☑
DTIC TAB ☐
Unannounced ☐
Justification
By
Distribution/
Availability Codes
Dist | Avail and/or Special
A-1

TABLE OF CONTENTS

TABLES

FIGURES

NOMENCLATURE

Symbol	Definition and SI Units*
A	area [m^2]
D_h, D_m, D_w	turbulent transport coefficient [m/s]
E	"equation of time" [min]
G	conduction heat flux into the ground [W/m^2]
H	height [m]
K	conductance in floor heat flux model [W/m^2-K]
L	a length or length scale [m]
Long	longitude [deg]
P	perimeter [m]
Q	heat transfer rate [W]
R	a radiative flux [W/m^2]
Ri	Richardson number, dimensionless
T	temperature [C or K]
T_{db}	dry bulb temperature
T_g	ground surface temperature
T_{rcom}	room air temperature
T_{wb}	wet bulb temperature
U	wind speed [m/s]
c	Ch. II: specific heat of a solid [J/kg-K]
	Ch. III: constants in heat flux model
c_p	constant pressure specific heat [J/kg-K]
d	exponents in heat flux model (Ch. III)

* Other units, when used, are indicated in the text.

e	vapor pressure of ambient air [mbar]
g	acceleration due to gravity [m/s^2]
h	surface conductance [W/m^2-K]
k	thermal conductivity [W/m-K]
k_e	effective thermal conductivity [W/m-K]
q	unit heat flux [W/m^2]
q_{et}	evapotranspiration flux
q_{cl}	latent convective flux
q_{cs}	sensible convective flux
q_{mean}	mean component of floor heat flux
$q_{periodic}$	fluctuating component of floor heat flux
q_{total}	total time-dependent floor heat flux
r_{ins}	thermal resistance of insulation [m^2-K/W]
t	time [s]
u_{2m}	wind speed at a two meter observation height [m/s]
x	north-south coordinate [m]
y	east-west coordinate [m]
z	vertical coordinate [m]
z_0	surface roughness height [cm]
z_w	wind speed observation height [m]
$\Delta/(\Delta+\gamma)$	parameter used in potential evapotranspiration calculations
$\Delta x, \Delta y, \Delta z$	finite difference cell dimensions [m]
Θ_z	zenith angle [Deg]
α	thermal diffusivity [m^2/s]
α_{sol}	solar albedo of the ground surface, dimensionless
β	volumetric thermal expansion coefficient [C^{-1}]

γ_s	solar azimuth angle [Deg]
δ	solar declination [rad]
δx, δy, δz	distances between finite difference temperature nodes [m]
ε	emissivity, dimensionless
ϕ	latitude [deg]
ρ	density [kg/m^3]
σ	Stefan-Boltzmann radiation constant, 5.670×10^{-8} [$W/m^2\text{-}K^4$]
τ	time constant or period of a process [s]
ω	hour angle [rad]
ζ	phase shift of ground temperature [days]

I. BACKGROUND

I.A. INTRODUCTION

The impact of earth-coupled heat transfer processes on the energy consumption and thermal comfort of buildings has been a topic of concern to building scientists for more than forty years [1]*. At the time of these early studies, the basement of a typical American home might have accounted for as little as ten percent of its total energy consumption. Because leaky, lightly insulated above-grade construction was the rule, foundation heat losses could be ignored or roughly estimated with little penalty. The energy crisis brought about during the 1970s by dwindling domestic fossil fuel supplies and price increases engineered by foreign cartels led to changes in construction standards that have considerably improved the performance of typical new buildings. The same foundation that contributed only ten percent of the heating load on a 1950 building might be responsible for half the load on a comparable contemporary structure [2]. Another consequence of recent energy shortages is the growth of interest in unconventional building designs, including earth-sheltered structures [3]. Bermed walls and earth-covered roofs may be used both as moderators of the outside climate and as thermal storage media. Successful implementation of such strategies depends heavily upon a clear, quantitative understanding of the performance of the earth-sheltered envelope

* Numbers in brackets refer to entries in REFERENCES.

components. Consequently, the need for accurate modelling of earth-coupled building heat transfer is greater today than ever before.

A truly satisfactory modelling capability for design purposes is not yet a reality, however. The theoretical background needed to support such models is incomplete. Experimental studies, being limited in number and narrow in scope, provide only clues to the general heat transfer behavior of foundations. Analytical methods (those which are distinguishable from numerical methods) deal with simple geometries and boundary conditions. Detailed simulation of foundations still requires computer resources and expertise in numerical methods that are not commonly available to the building designer. Indeed, most research via numerical modelling has been restricted to two-dimensional analysis because of computer hardware limitations. Thus, understanding of three-dimensional effects is incomplete. Nor have other aspects of modelling, such as the effect of ground surface boundary conditions, soil properties, and deep ground conditions received sufficient scrutiny. The predictions of design models based on this incomplete science vary considerably. MacDonald, Claridge, and Oatman, for example, reported disagreements as large as 1000% between the basement heat loss predictions of seven simplified methods [4]. This unsatisfactory state of affairs is likely to persist until new models are developed that account for more of the parameters that influence earth-coupled heat loss.

The present study was undertaken in the belief that highly detailed models, while not yet suited to design applications, can be

valuable aids to the development of simplified models. This is particularly true when it is impractical to conduct sufficiently detailed or numerous experimental studies. The three broad objectives of this work were:

i) Construct a detailed three-dimensional numerical model of earth-coupled heat transfer that could be used to evaluate basic assumptions employed in simplified analytical and numerical models.

ii) Reexamine the slab-on-grade problem, focusing on the significance of three-dimensional geometric effects.

iii) Investigate the influence of environmental and building parameters on model predictions in order to identify potential modelling simplifications that do not seriously degrade accuracy.

While the scope of this study was limited to slab-on-grade floors, many of its observations and conclusions apply to the general case of earth-coupled heat transfer.

The sections which follow give a brief review of the literature to place the present inquiry in historical perspective, describe in detail the development of the numerical model and test plan, and present an analysis of results from seven parametric studies comprising more than ninety simulations.

I.B. HISTORICAL REVIEW*

Prior to the 1970s, essentially all knowledge about the heat loss characteristics of building foundations had been obtained from field studies. The 1948 study by Bareither, *et al.*, [1] gave a description of slab-on-grade heat loss which, while incomplete, remains essentially valid and widely referenced today. Measurements were taken of floor heat loss, floor surface temperature, soil temperature beneath the floor, and moisture transport through the floor. Three months of heating season measurements provided validation data for two simple models of unheated slab floor heat loss:

$$Q = F_1 \cdot P \cdot (T_{inside} - T_{outside}) + 2 \cdot A_{inside} \qquad (I\text{-}1a)$$

and

$$Q = F_2 \cdot P \cdot (T_{inside} - T_{outside}) \qquad (I\text{-}1b\dagger)$$

where Q is the total rate of floor heat loss in BTU/hr. Equation I-1a, which they found to be more accurate, distinguishes between heat lost at the slab perimeter and heat lost to the ground through the "inner area" of the floor (total floor area less the area of a two foot strip around the perimeter). The former component is a function of floor perimeter length [ft], indoor-outdoor air temperature difference [F], and a construction-dependent perimeter heat loss

---

* This review of previous work makes no pretense to being exhaustive. It is an overview intended only to provide a context for the present study.

† Dill, *et al.* [5] had proposed this form several years earlier.

factor "F_1" [BTU/hr/ft]. The latter component was found to be approximately 2 BTU/hr/ft^2 of inner floor area. Eqn. I-1b predicts whole-floor loss on the basis of perimeter length only, using a different set of factors, "F_2". Bareither believed this model to be sufficiently accurate for load calculations for area to perimeter ratios of 12 ft or less. For larger values of A/P, the neglected loss from the inner area caused large errors.

Two features of this analysis deserve special attention. First, recognition of the need to account for heat transfer from the "core" or "inner" floor area of medium-to-large buildings is an important observation that is generally forgotten by designers today. The current ASHRAE Handbook of Fundamentals [6] contains up-to-date perimeter loss factors based on detailed two-dimensional finite element analysis [7], but recommends the "F_2" method (Eqn. I-1b) as a design procedure without any caveats concerning the limits of its applicability. Secondly, the scaling of slab floors through the use of the length scale A/P is a useful approach which has seen little, if any, subsequent use. Regrettably, the use of scaling and dimensional analysis in the study of foundation heat loss has been very limited. (The basement heat loss method developed by Yard, *et al.* [8] is a recent example of the use of similitude in earth-coupled heat loss studies.)

Estimates of heat loss based solely on the indoor-outdoor air temperature difference, such as Equations I-1a and I-1b, do not work well outside of the heating season. An annual model must take the yearly cycle of ground temperature into consideration. Kusuda and his colleagues at the National Bureau of Standards [9] helped to

clarify the nature of seasonal variation in floor heat loss through the interpretation of Green's function [10, 11] and Fourier transform [12] solutions. These analytical solutions revealed that the temperature distribution in the soil under a slab floor changes markedly from season to season. In the winter, isotherms are closely bunched near the edge of the floor and heat flux lines approximate circular arcs from the bottom of the floor to the ground surface. Consequently, most winter heat loss occurs at the perimeter. As the ground warms during the spring and summer, however, isotherms spread out and more closely approximate horizontal surfaces. During these warmer seasons, heat loss is much more uniform over the entire floor. Clearly, this seasonal difference in soil thermal regime is responsible for the limited applicability of Equations 1.1.

The rigorous analytical approach to the study of foundations promoted by Kusuda and others spawned a generation of improved, albeit more complicated, models of floor heat loss [e.g., 13-16]. These models are themselves derived from analytical and numerical solutions of the conduction equation, and so, are generally referred to as "simplified" methods.

The Kusuda method [13] employs a "monthly average subfloor temperature" derived from Lachenbruch's Green's function solution [10]. Kusuda provides empirical expressions which allow the user to approximate the analytical solution as a function of soil thermal diffusivity, mean ground temperature, floor dimensions, and other important parameters.

Shen and Ramsey [14] constructed a numerical two-dimensional Fourier series solution suitable for micro-computer application. Its primary advantage over more detailed numerical methods is its reduced storage requirement--an important consideration in 1983, but much less of a concern today.

The interzonal temperature profile estimation (ITPE) method of Krarti, *et al.* [15], is an approximate analytical technique based on certain arbitrary (but physically motivated) assumptions about the nature of the solution. The two-dimensional domain is divided into three zones, one directly beneath the floor, and two beyond the edge of the floor. Solutions in the three regions are matched to an assumed temperature profile specified on the interzonal boundary (from whence the name of the method derives). The selection of an exponential function as the interzonal temperature profile was motivated by the form of Kelvin's well-known analytical solution for ground temperature [17].

The three previous approaches are somewhat limited in application because of their origin in classical analysis. Modelling of details such as partial insulation and variable thermal properties is not possible with these methods. Mitalas [16] avoided this shortcoming by using a rather detailed finite element simulation to generate the "data" for his method. He compiled tables of monthly heat loss factors for two values of soil thermal conductivity and a variety of foundation types and insulation treatments. An estimate of heat loss is obtained by decomposing the foundation into zones as directed by Mitalas and summing the losses of the parts using the appropriate tabulated factors. Although it can be performed

manually, this procedure is better suited for computer implementation [18, 19].

The use of computer-based analysis for design heat loss calculations is limited but growing. Detailed numerical modelling has been a major mode of basic earth coupled heat transfer research for over a decade, however. Most numerical models have employed either finite difference (FDM) or finite element (FEM) methods. FDM models are more numerous than FEM models, probably because the finite difference method is both older and more straightforward to program. The advantage of finite element analysis is its capability to model complex geometry more easily. Although the selection of numerical methods used has been small, the assumptions concerning, boundary conditions, soil properties, and time step have varied greatly from model to model. Since the effect of such assumptions is a major concern of the present study, it is appropriate to consider in some detail several representative examples of research-oriented numerical models.

Wang [7] used a two-dimensional, transient FEM model to investigate basement and slab-on-grade heat loss. The model was very detailed with respect to the description of the foundation and the model of soil heat transfer (although only one soil type was considered). Phase change of moisture in the soil was simulated, but snow cover and moisture movement were not. The wall section connected to the edge of the foundation was included in the model because of possibly significant fin effects*. An adjustment to the

* Indeed, they were found to be quite important. Wang's demonstration of the magnitude of this effect is one of the more significant findings of his study.

thermal conductivity of hollow block foundation walls served to approximate the effect of internal convection. In contrast, several potentially significant features of the model were treated in a rather unsophisticated manner. The ground surface, for instance, was considered a simple convective boundary even though the program allowed specification of radiative boundaries. Air temperature was approximated by a sinusoidal function that was varied to simulate three different "climates" as measured by heating degree days. The dimensions of the modelled buildings are not mentioned in the cited reference, perhaps indicating that core effects were considered negligible. In any case, it would appear that floor width was not varied to determine the effect of core area on heat loss. Two annual cycles of air temperature with a one week time step were found sufficient to obtain a steady solution. As noted above, Wang's slab simulations are the basis for the current "F_2" coefficients of the ASHRAE recommended design procedure.

The two-dimensional transient FDM created by Shipp [20] and used in numerous investigations by a host of others connected with the Underground Space Center at the University of Minnesota has been one of the most influential earth-coupled heat transfer models. The program employs the discretization method and implicit iterative solution technique of Patankar and Spalding [21]. Because it was developed in conjunction with an extensive experimental study of a large earth-sheltered building on the University of Minnesota campus, Shipp's model has been validated quite thoroughly. The model permits variable soil properties and has a ground surface boundary condition which includes both convection

and radiation based on actual meteorological data. Shipp used the model for parametric studies of the effects of berming, wall insulation, soil properties, and surface cover on heat loss from the monitored building. Differences in ground cover were simulated by adjustments to the solar absorptivity of the ground. Absorptivity values of 0.33, 0.15, and 0.0 were used to represent concrete, short grass, and long grass, respectively. Values for vegetative cover were based on interpretation of Kusuda's experimental data [22]. The extensive use of this model for a variety of other purposes, for example, the study of regional variation in earth-shelter performance [23] and optimization of foundation insulation [24] has demonstrated the capability of numerical models quite forcefully.

Szydlowski and Kuehn [25] developed a transient two-dimensional FDM model of an underground building. The model was validated against basement heat loss measurements made by McBride, *et al.* [26]. In many respects, Szydlowski and Kuehn's approach resembles that of Shipp. Like Wang, however, they specified constant coefficient convection at earth-air interfaces and neglected evaporative and radiative effects. Time steps of 24 and 48 hours were used for the calculations, the choice depending upon whether daily weather data or approximate forcing functions were being used as input. A steady state overrelaxation solution provided the initial condition for the transient model. Additional transient calculations of 1.33 years were needed to achieve a converged periodic solution. Szydlowski and Kuehn found their model to agree well (considering the simplifying assumptions it contained) with validation data. They concluded that accurate

predictions of earth-sheltered building heat loss can be obtained from models employing simple approximations to climate variables and time steps of several days.

Speltz [27] adopted a highly detailed approach in constructing an hourly simulation of an earth-sheltered house. The performance of a 1500 ft^2 earth-sheltered building was compared to that of a slab-on-grade building of the same area in seven different geographic locations. This eclectic model combined one-dimensional transfer function analysis of building walls with a two-dimensional finite difference model of the soil surrounding the structure. Speltz' soil heat transfer model is particularly notable for its detailed treatment of the ground surface boundary condition. The energy balance at the ground surface included not only convection and solar radiation, but also, infrared radiation and evaporation. Evaporation was modeled as a constant rate of loss based on average annual precipitation*. The two-dimensional soil heat transfer results were corrected to give approximate three-dimensional values through the use of factors derived from a limited number of 3-D simulations. Because Speltz "simplified" the solution of the soil heat transfer problem by separating it into steady and time-varying components, independent correction factors were computed for each part. The transient three-dimensional model predicted heat losses that were 28% and 38% greater than the transient two-dimensional model for the two sets of soil properties considered in

* In a subsequent investigation of earth covered roof performance with Meixel [28], Speltz replaced this crude approximation of latent loss with a potential evapotranspiration model. This model is discussed at length in the following chapter.

the study. The greater difference was obtained with the lower value of soil conductivity, k. For the steady component, the differences were 18% and 21%, however, the larger difference corresponded to the *larger* value of k in this case.

While a number of other detailed numerical models should be mentioned in a more complete review, the four described above display a representative variety of approaches to the major choices that must be made in the construction of an earth-coupled heat transfer model: two- or three-dimensional analysis, level of building description detail, soil property model, ground surface boundary condition, weather representation, and time step. As these examples demonstrate, developers of numerical models generally treat some of these areas in much greater detail than others. Very few have investigated three-dimensional effects at all, and there are practically no such studies that would qualify as "large scale". The need for additional research into three-dimensional effects is underscored by the recent work of Walton [29], which shows that discrepancies between two- and three-dimensional predictions may be even larger than those observed by Speltz*. The importance of this issue will persist as long as full three-dimensional modelling is beyond the practical capacity of the computers found in the architectural/engineering workplace.

Regardless of future growth in computer hardware and software capabilities, a premium always will be placed on

* Labs [2] claims that Walton's 3-D and 2-D results, which differed by as much as 50%, can be reconciled to within 9% by an area weighting correction. Such procedures are clearly empirical and of uncertain validity in the general case, however.

efficiency in modelling. In this regard, three "simplified" numerical methods deserve mention. Walton, in the paper cited above, proposes a pseudo-three-dimensional numerical method in which a three-dimensional basement or slab-on-grade is decomposed into a combination of axisymmetric and Cartesian two-dimensional parts. The sizes of these elements are chosen to preserve both the area and perimeter of the original foundation. He found this approach to agree with his 3-D model to within two percent. Another promising avenue is that of multi-dimensional response factor methods [30]. One of the most attractive features of such methods is their conceptual compatibility with existing detailed hourly energy analysis programs. Finally, The non-dimensional superposition technique of Shen, *et al.* [31], has brought two-dimensional finite difference analysis a step closer to practical applicability. This model has been coupled to the DOE-2.1C energy analysis program [32] to generate data for the extensive tables of foundation design data contained in a recently published U. S. Department of Energy handbook [2].

As this brief review indicates, the use of numerical methods in the study of earth-coupled heat transfer has become widespread. In many respects, however, the background research needed to generate confidence in numerical models remains incomplete. Most prior models have been two-dimensional, leaving open questions concerning the nature and magnitude of three-dimensional effects. Ground-surface boundary conditions frequently have been modelled in a simplified manner. Evaporative and radiative effects generally are neglected, and smoothed approximations to weather variables

usually substitute for actual data. Additionally, the relatively long time steps used in most transient simulations do not resolve diurnal effects which may be important influences on thermal loads and comfort. Consequently, a need exists to evaluate the implications of model assumptions and simplifications both through validation in the field and through parametric studies with detailed models. The hourly, three-dimensional model described in the following chapter was designed to address the latter need.

II. METHOD AND TEST PLAN

II.A. MATHEMATICAL MODEL

II.A.1. HEAT TRANSFER IN SOIL

In its natural state, soil is an inhomogeneous porous medium through which energy may be transported by a variety of mechanisms, including conduction, advection by ground water, and convection of water vapor through voids in the soil matrix. Laboratory studies have shown that soil moisture content exerts far more influence on heat transfer than does the composition of the solid matrix, even at very low moisture content [33]. Over the range from zero to twelve percent moisture content, the conductivity of a given soil may increase by a factor of seven. In comparison, a 30 C change in temperature for the same soil at fixed moisture content might cause conductivity to change by only twenty percent [34]. Similarly, variation in the thermal conductivity of dry soils is much smaller than the variation with moisture of the conductivity of a particular soil.

In the low moisture regime, the large void fraction of the matrix allows easy passage to water vapor. Thermally induced motion of vapor not only enhances heat transfer, but also, causes drying of the soil near sources of heat [35]. Because of this effect, thermal conductivity values obtained from steady-state measurements are of questionable accuracy. Interstitial vapor movement is most significant in the vicinity of ten percent volume

fraction of liquid water and at elevated temperatures [34]. As moisture content increases, liquid water displaces the lower conductivity gases in the void space of the soil matrix and conductivity increases markedly.

The influence of moisture on soil heat transfer is further manifested in the form of phase change effects. These are of two types. First, because the conductivity of ice is over four times that of liquid water, the conductivity of frozen soil may be substantially larger than the conductivity of unfrozen soil [36]. Secondly, the "heat valve" phenomenon* investigated by Gilpin and Wong [37] tends to elevate soil temperature by limiting heat loss in the phase change region. These effects may be significant influences on the heat loss from buildings located in cold climates.

Borrowing from electromagnetic theory, Philip and deVries [38] developed a model of soil conductivity which accounts for vapor convection with some success, but is quite complicated and impractical for most engineering applications. As Eckert and Pfender [34] note, however, the conditions which prevail in the soil near a typical building foundation are such that coupled heat and mass transfer can be neglected. Therefore, in the absence of the boundary data needed to define a moisture distribution, it is not harmful to assume that there is no mass transfer in the soil. Under these assumptions, only the heat conduction equation with appropriately specified boundary conditions and thermal property values needs to be considered for the purpose of earth-coupled

* Freezing and thawing of the ground in phase with seasonal changes in ground surface properties can cause rates of winter soil heat loss to decrease.

building heat transfer analysis. This simplification makes modelling considerably easier, but the specification of soil properties for a given site remains problematic. In practice, the knowledge of soil composition and moisture distribution needed to establish properties and boundary conditions accurately is seldom available.

A constant thermal property model of the soil was employed in the present study. The research summarized above suggests that it is not necessarily worthwhile to consider a more detailed treatment of soil properties unless comparisons are to be made with situations in which large seasonal or spatial variations are known to exist. Since direct comparison of this model with experimental data was not planned, there was no compelling motivation to adopt a variable property model. Likewise, phase change was omitted on the grounds that, in most inhabited climates, freezing of the soil is essentially a boundary effect. The presence or absence of phase change does not alter the character of the heat transfer process in most of the soil surrounding a building, and comparisons between simulations should not be invalidated by its neglect except in *bona fide* cold region applications. Given these assumptions, the basis for the present model becomes the three-dimensional, transient heat conduction equation without heat generation, i. e.,

$$\rho c \frac{\partial T}{\partial t} = \nabla \cdot (k \cdot \nabla T) \qquad (II\text{-}1)$$

Effects of moisture and phase change may enter this model only through thermal properties and boundary conditions. The variable property form of Eqn. II-1 is necessitated by thermal property changes across interfaces between the soil and building materials.

II.A.2. BOUNDARY CONDITIONS

The four boundary types most commonly encountered in the analysis of earth-coupled buildings are:

- Earth-coupled building surfaces
- Far-field boundaries
- The deep ground
- The ground surface

The following discussion describes the heat transfer processes at these boundaries and the mathematical models of these processes used as boundary conditions on Eqn. II-1 in this study.

Interior Building Surface Conditions

The primary purpose of a building's heating, ventilating, and air-conditioning system is to maintain conditions inside the conditioned space consistent with occupant comfort and well-being. Although more sophisticated indices are available, the most common measure of comfort is the dry-bulb temperature of the air. HVAC systems generally attempt to maintain this parameter within fairly narrow limits (which may vary seasonally, for reasons of energy

conservation). A constant indoor air temperature of 22 C (71.6 F) was assumed to exist year-round above the slab floors simulated by the present model. In order to simplify interpretation of results, seasonally varying set points were not used. Heat transfer to interior building envelope surfaces occurs through combined convection and radiation. This flux can be approximated by expressions of the form:

$$Q = h_i \cdot A \cdot (T_{room} - T_{floor}) \qquad (II\text{-}2)$$

where T_{room} and T_{floor} are, respectively, room air and floor surface temperatures and h_i is a combined convective-radiative surface conductance [W/m^2-C]. The ASHRAE Handbook of Fundamentals [6] gives tables of h_i for a variety of surface orientations and emittances. Values appropriate for non-reflective horizontal surfaces in still air (6.13 and 9.26 W/m^2-C for upward and downward heat flow, respectively) were used throughout this study.

Far-Field Soil Conditions

Conditions in the ground several building widths removed from the edge of an isolated structure approach those of the undisturbed ground, in which the temperature distribution is a function of depth and time only. It is common to state this condition as one of zero lateral flux. When applied at a finite distance from the building (as in numerical models), this condition implies the existence of a mirror image building reflected about the zero flux boundary. When

neighboring structures of different shape are too near to be ignored, they must be modeled explicitly. Shipp [20] encountered this situation in modelling Williamson Hall on the University of Minnesota campus. In the present study, the case of an isolated building was assumed and a numerical boundary condition approximating zero lateral flux at infinity was applied. This choice removed the influence of side boundaries on the soil temperature field near the building.

Deep Ground Conditions

In the deep ground, either zero flux or specified temperature conditions may be applied, depending on circumstances, i. e.,

$$\frac{\partial T}{\partial z} = 0 \quad \text{for} \quad z \to \infty \tag{II-3a}$$

or

$$T = \text{constant} \quad \text{at some} \quad z > 0 \tag{II-3b}$$

where z is the vertical coordinate, assumed positive into the ground. A specified temperature condition is particularly appropriate when conditions exist (such as a high water table) that tend to maintain a fixed temperature at a finite depth. Data summarized by Kusuda and Achenbach [39] show that annual average earth temperature is well approximated by either average air temperature or well-water temperature, irrespective of depth. Consequently, many prior models have assumed a fixed temperature equal to the average dry

bulb at some large depth. The data of Kusuda and Achenbach also imply that surface conditions are the driving force behind the temperature distribution in the upper few meters of the soil. On this basis, an asymptotic zero flux boundary condition is justified in some cases. This choice would be most appropriate in the absence of ground temperature data and when the local water table is not likely to be very near the surface. The base case boundary condition in the present study was fixed temperature equal to the average air temperature at a depth of 15 m.

Heat Transfer at the Earth's Surface

Heat transfer occurs at the surface of the earth through coupled processes of conduction from the ground, convection, evaporation, and radiant exchange in both long (sky and ground infrared) and short (solar) wavelength bands. The balance between these modes depends upon a great many parameters, including soil properties, soil moisture content, ground cover, and weather variables. A number of prior investigations have considered the effects of surface conditions on the soil thermal regime [22, 37, 39-41]. Since the level of temperature in the soil has a great impact on the heat transfer from earth-coupled building surfaces, it is appropriate to consider the findings of this research in some detail.

Gilpin and Wong [37, 40] also considered the effect of ground cover in their previously cited study. A sinusoidally varying surface conductance approximated seasonal changes in ground cover. Their one-dimensional model predicted a range in average ground

temperature of as much as 7 C due to ground cover variation. Annual average ground surface temperature typically exceeded average air temperature by about 4 C. Evaporation, which would have tended to lower ground temperature was not included in this model, so a hypothesis that average ground temperature always exceeds air temperature is not proved by these results. The important point demonstrated theoretically by this study is that ground temperature *may differ substantially from* air temperature.

Gold [41] conducted an experimental study in which temperatures were measured at various depths beneath the surface of a grassy plot and two parking lots. One parking lot was 38 x 46 m and the other was 24 x 46 m. He observed that the monthly-averaged surface temperature of the parking lots exceeded the average air temperature by as much as 15 C during the summer, while the grass covered plot remained within 1.7 C of air temperature. Gold hypothesized that the lower temperatures observed in the grass covered plot resulted from evaporative losses that were suppressed by the asphalt ground cover of the parking lots.

In the winter, one of the lots was cleared of snow and the other was not. The insulating effect of snow on the uncleared parking lot and grassy plot kept their surface temperatures up to 10 C above air temperature. During the same period, the temperature of the cleared lot fell below that of the air because of its lower surface resistance.

Differences in temperature observed beneath the test plots diminished with depth and were negligible at 6 m, regardless of the season. It might be expected, however, that the effect of a change in

the surface conditions over a larger area would cause a more far-reaching modification of mean soil temperature.

Kusuda [22] conducted a similar study in which data were taken from five 50 x 50 ft plots with different surface conditions (plain asphalt, asphalt painted white, bare earth, short grass, and uncut grass). Data from the plain asphalt plot are in good agreement with Gold's measurements with respect to the elevation of surface temperature above ambient air temperature. The monthly averaged surface temperatures of the grass covered plots fell somewhat below averaged air temperature, with the greatest difference occurring in the unmowed plot during the summer. Kusuda also observed that differences between plots diminished rapidly with depth.

Despite the extensive evidence that surface conditions can and do have a major effect on the level of temperature in the ground (and therefore, on heat transfer through earth-coupled building components) models of the ground surface in building simulation studies are frequently of improbable simplicity. More complete models, (e. g., Shipp [20]) include solar gain in the surface boundary condition and account for evaporative effects in an *ad hoc* manner. Only the model of Speltz and Meixel [27, 28], however, attempts to deal directly with all of the identified influences on the surface energy balance. It is interesting (and perplexing) to note that all of the cited numerical models gave reasonable results when compared with field data. It seems unlikely that the variety of boundary conditions used in these studies are really equivalent. Rather, model

tuning or experimental uncertainty probably underlie the perceived success of all of these approaches.

The choice of weather data representation used in modelling is closely linked to the model of surface heat transfer employed. Simple models, such as one limited to constant film coefficient convection, require only the dry-bulb temperature. When long time steps are employed, air temperature is often approximated by a sinusoidal function. A detailed model, on the other hand, requires frequent input of many weather variables, including dry- and wet-bulb temperatures, barometric pressure, solar radiation, and wind speed. Previous studies (e. g., [31]) indicate that the use of smoothed approximations to outdoor dry-bulb temperature does not cause significant loss of accuracy relative to actual data used in the same model. This is because the thermal mass of the soil damps short-term variations quite effectively even at shallow depths. The equally important issue of whether a particular climate variable ought to be included or omitted from a model has not been investigated in much detail, however. In part because detailed representations of the surface boundary have not received extensive use, a boundary condition model similar to that of Speltz was employed in this study. Actual hourly weather data from "typical meteorological year" (TMY) tapes were used in order to permit the study of diurnal effects.

The ground surface boundary condition may be stated mathematically as a specified flux condition on Eqn. II-1:

$$-k\left.\frac{\partial T}{\partial z}\right|_{z=0} = G(t) \qquad (II\text{-}4)$$

where the flux G(t) is determined by an energy balance at the ground surface. The surface energy balance, as described in [42] and [43], has the general form

$$G = R_t - q_{cs} - q_{et} \qquad (II\text{-}5)$$

Eqn. II-5 states that the rate of conduction of heat into the ground (G) is equal to the net radiation absorbed at the ground surface (R_t) less sensible convection (q_{cs}) and evapotranspiration* (q_{et}). Fig. II-1 shows these fluxes in relation to a control volume at the surface of the earth. Fluxes are positive in the direction of their respective arrows. Procedures for estimating the components of Eqn. II-5 were drawn from a number of reliable sources and incorporated into the present model.

R_t is equal to the sum of absorbed solar radiation (R_{sol}) and incoming infrared sky radiation (R_{sky}) less the infrared radiation emitted by the ground surface (R_g), i. e.,

$$R_t = R_{sol} + R_{sky} - R_g \qquad (II\text{-}6)$$

* Evapotranspiration is an umbrella term denoting all forms of latent heat transport from the ground surface. This includes both evaporation of moisture directly from the soil and transpiration by vegetative ground cover. It also is referred to as consumptive loss in some parts of the agricultural literature.

R_{sol} depends on the absorptivity of the ground surface and on incident short wave radiation, both of which may vary seasonally. The albedo of the ground, α_{sol} is more commonly recorded than its absorptivity, so R_{sol} is determined by application of Eqn. II-7:

$$R_{sol} = (1 - \alpha_{sol}) \cdot R_{sol,i} \qquad (II\text{-}7)$$

where $R_{sol,i}$ denotes total incident solar radiation on a horizontal surface, a readily available item of weather data. According to measurements summarized by Sellers [42], values of α_{sol} may vary from as low as 0.05 for blacktop to as high as 0.95 for fresh snow. Representative average values for North America are 0.16 in the summer and 0.40 in winter.

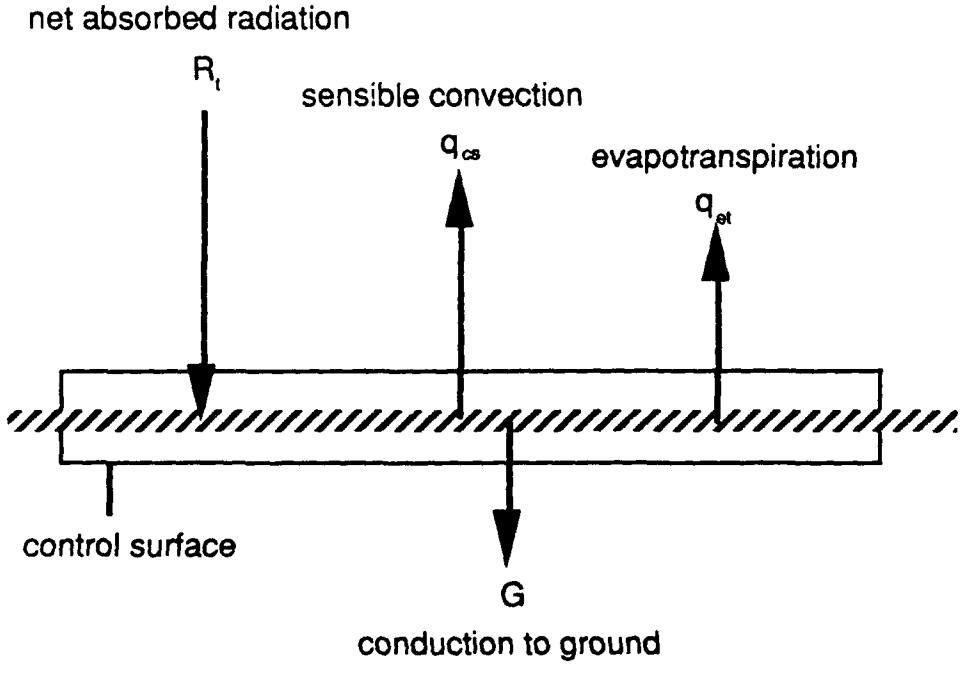

Figure II-1. Ground surface energy balance components.

Infrared radiation makes a much smaller contribution to the ground energy balance during daylight hours than does solar radiation. At night, however, it increases in significance and plays a role in such phenomena as the formation of frost while air temperature remains above freezing. Sky radiation data are not so generally available as solar radiation data. Consequently, R_{sky} is computed by means of Ångstrom's empirical correlation [44]:

$$R_{sky} = \varepsilon_{sky} \sigma T_{db}^4 [a - b \cdot \exp(-2.3\, c \cdot e)] \qquad (II\text{-}8)$$

The term in square brackets functions as a multiplier on the gray emissive power of the sky evaluated at the ambient dry bulb temperature (T_{db}). This correction factor depends on the moisture content of the air, indicated by the ambient vapor pressure, e [millibars]. Note that sky radiation increases with air moisture content. The infrared emissivity of the sky may be assumed to be unity without serious error. Following the recommendation of Geiger [44], values adopted for the empirical coefficients a, b, and c are, respectively, 0.820, 0.250, and 0.094. The radiative flux predicted by Eqn. II-8 is a clear sky value and should, in principle, be corrected for cloud cover. Cloud cover values were not recorded in the weather files used in this study, however, so clear sky values were used without correction. Ground surface infrared radiation is given by the Stefan-Boltzmann equation:

$$R_g = \varepsilon_g \sigma T_g^4 \qquad (II\text{-}9)$$

where T_g is the ground surface temperature. The infrared emissivity, ε_g, is on the order of 0.9 or greater for most natural surfaces.

Convective transfer processes at the earth's surface are inherently turbulent, and are influenced by the nature of the ground cover as well as by deviations from conditions of neutral stability in the atmosphere. The fundamental parameter of turbulent atmospheric convection is the Richardson number (Ri), which indicates the importance of buoyancy effects by its magnitude and stability or instability by its sign. The Richardson number appears in several guises in the literature. A typical form is

$$Ri = \frac{g\beta(\Delta T)L}{U^2} \qquad (II\text{-}10)$$

in which ΔT is the surface-ambient temperature difference, L is a characteristic length (e.g., the boundary layer thickness), and U is a characteristic velocity. If ΔT is positive (ground warmer than the air), buoyancy forces promote convection and an unstable condition exists. In the opposite case, body forces tend to suppress turbulence.

At present, the gap between a general theory of turbulence and practical methods for engineering analysis has not been completely bridged. The conceptual superiority of models based on the theory of stochastic processes over earlier methods derived by analogy to molecular transport is universally acknowledged. Nevertheless, engineering models of turbulent processes based on dated theories,

but supported by experimental measurements, remain in widespread use. Although such models are restricted in application to special cases and narrow ranges of conditions, they can be quite useful within their limits.

An eddy diffusivity model of atmospheric boundary layer convection, with empirical coefficients derived from the measurements of Sellers and Dryden [43, 45], is used to simulate convection of both heat and moisture in the present model. The sensible and potential (i.e., maximum possible) latent convective fluxes are denoted by, respectively, q_{cs} and q_{cl}. Sellers and Dryden approximate these fluxes by expressions of the form:

$$q_{cs} = \rho_{air} c_{p,air} D_h (T_g - T_{db}) \qquad \text{(II-11a)}$$

and

$$q_{cl} = \rho_{air} c_{p,air} D_w (T_{db} - T_{wb}) \qquad \text{(II-11b)}$$

where D_h and D_w are turbulent transport coefficients for heat and water vapor [m/s], and T_{wb} is the ambient wet-bulb temperature. Potential, rather than actual, latent convection is employed in this model for reasons explained below.

Sellers and Dryden derived D_h and D_w by analogy to D_m, the neutral stability momentum transfer coefficient:

$$D_m = 0.164\, u_{2m} \left(\ln \frac{z_w}{z_0} \right)^{-2} \qquad \text{(II-12)}$$

To extend the analogy to non-neutral conditions, they modify the neutral stability expressions with corrections that depend on the atmospheric temperature gradient at the ground. The corrected expressions are:

$$D_h = \begin{cases} D_m \left[1 + 14 \left(\dfrac{T_g - T_{db}}{u_{2m}^2} \right) \right]^{\frac{1}{3}} & \text{if } T_g \geq T_{db} \\ D_m \left[1 - 14 \left(\dfrac{T_g - T_{db}}{u_{2m}^2} \right) \right]^{-\frac{1}{3}} & \text{if } T_g < T_{db} \end{cases} \qquad \text{(II-13)}$$

and

$$D_w = \begin{cases} D_m \left[1 + 10.5 \left(\dfrac{T_g - T_{db}}{u_{2m}^2} \right) \right]^{\frac{1}{3}} & \text{if } T_g \geq T_{db} \\ D_m \left[1 - 10.5 \left(\dfrac{T_g - T_{db}}{u_{2m}^2} \right) \right]^{-\frac{1}{3}} & \text{if } T_g < T_{db} \end{cases} \qquad \text{(II-14)}$$

In Eqn. II-12, u_{2m} is the wind speed measured at a height of two meters, z_w is the wind speed observation height (i.e., two meters), and z_0 is the "roughness height" of the ground cover. Roughness height may be as small as a millimeter for a very smooth surface or larger than two meters for a forested surface [42]. While z_0 frequently is close to the actual height of ground cover, the relationship is not as direct as the name "roughness height" implies. Because z_0 is defined merely to be the z-intercept of the velocity

profile (i. e., the theoretical height at which an experimentally measured velocity profile goes to zero), it is quite possible to obtain negative values of roughness height from data sets that do not fit the logarithmic boundary layer model very well.

Although this model is open to certain scientific objections, it is a valid representation of the atmospheric boundary layer from an engineering standpoint*. It is well suited to implementation in a computer model and is capable of simulating the effects of hourly fluctuations of weather conditions--unlike other models that employ transfer coefficients averaged over long time periods.

The evapotranspiration term in Eqn. II-5, q_{et}, comprises all processes at the the surface of the ground which involve exchanges of latent heat. These include the convection of latent heat (Eqn. II-11b), evaporative conversion of sensible heat to latent heat, and transpiration of latent heat by vegetation. Limits on evapotranspiration are imposed by the saturation conditions of the ambient air, by the mixing efficiency of the boundary layer, and by the supply of moisture available to the surface. For analytical purposes, it is useful to distinguish between evapotranspiration that is limited by the supply of moisture and that which is not. The latter regime is referred to as potential evapotranspiration. It is the maximum rate for a surface and is limited solely by meteorological conditions. An actual evapotranspiration model requires knowledge of the degree of saturation at the ground surface

* Note, for instance, that the bracketed correction factors in Eqns. II-13 and II-14 have the same functional dependence on wind velocity and temperature difference as does the Richardson number.

and could not be used in this study because the soil moisture distribution was not modelled.

Although it is a limiting case, potential evapotranspiration is approximated in a number of naturally occurring situations, most often through the action of vegetation. Grasses and other similar ground cover, when well watered, transpire moisture into the atmosphere at near the potential rate even when the ground surface is relatively dry. The potential evapotranspiration model is, thus, of wider applicability than its definition suggests. Also, the zero and potential evapotranspiration cases bracket the range of boundary evaporation effects. Because it is frequently a good model of actual conditions, does not require specification of moisture conditions at the surface, and is a useful asymptotic case, potential evapotranspiration was assumed in the present model.

Expressions for potential evapotranspiration are derived in [42] and [46]. The working equation given by Sellers [42], and used by Speltz and Meixel in their earth-covered roof model [28], is:

$$q_{et} = \left[\frac{\Delta}{\Delta + \gamma}\right](R_t - G) + \rho_{air} c_{p,air} D_w (T_{db} - T_{wb}) \qquad \text{(II-15)}$$

The first term on the right-hand side of Eqn. II-15 represents sensible heat transferred to the surface by radiation or conduction that is converted to latent heat. The dimensionless group $[\Delta/(\Delta+\gamma)]$ is a physical property of the air that is tabulated in [46]. It represents the fraction of a unit of sensible heat transferred to a saturated surface that is converted into latent heat. Parameter Δ is

the change in saturation vapor pressure with temperature and γ is the "psychrometer constant" (the change in vapor pressure per unit temperature difference during an adiabatic saturation process). The second term represents convection of latent heat.

The final form of the surface boundary condition is obtained by substituting from Eqns. II-7, 8, 9, 11a, and 15 into Eqn. II-4:

$$G = -k\frac{\partial T}{\partial z} = (1-\alpha_{sol})R_{sol,i} + \varepsilon_{sky}\sigma T_{db}^4[a - b\cdot\exp(-2.3\,c\cdot e)] - \varepsilon_g\sigma T_g^4 - \rho_{air}c_{p,air}D_h(T_g - T_{db}) - \left[\frac{\Delta}{\Delta+\gamma}\right](R_t - G) - \rho_{air}c_{p,air}D_w(T_{db} - T_{wb})$$

$$\text{at } z = 0 \qquad \text{(II-16)}$$

II.B. NUMERICAL SOLUTION FOR SLAB-ON-GRADE FLOORS

The boundary value problem developed in the preceding section was solved by means of standard numerical techniques. The following sections describe both the numerical method and its implementation in a computer program.

II.B.1. DEFINITIONS AND CONVENTIONS

The numerical model employed in this study simulates a slab floor and the soil on which it rests. Neither the above grade portion of the building nor the mechanical system are modelled. Instead, a

constant room air temperature is maintained above the floor. Floor plans may be either rectangular or L-shaped. These shapes are most easily described in a Cartesian coordinate system, for which the appropriate form of Eqn. II-1 is:

$$\rho c \frac{\partial T}{\partial t} = \frac{\partial}{\partial x}\left(k \frac{\partial T}{\partial x}\right) + \frac{\partial}{\partial y}\left(k \frac{\partial T}{\partial y}\right) + \frac{\partial}{\partial z}\left(k \frac{\partial T}{\partial z}\right) \qquad \text{(II-17)}$$

Building axes are aligned with a right-handed system in which x is positive south, y is positive west, and z is positive into the ground. These coordinate conventions are shown in Fig. II-2. For rectangular floors, the coordinate origin is at the top-center of the slab. In L-shaped cases, the origin is at the interior bend of the "L".

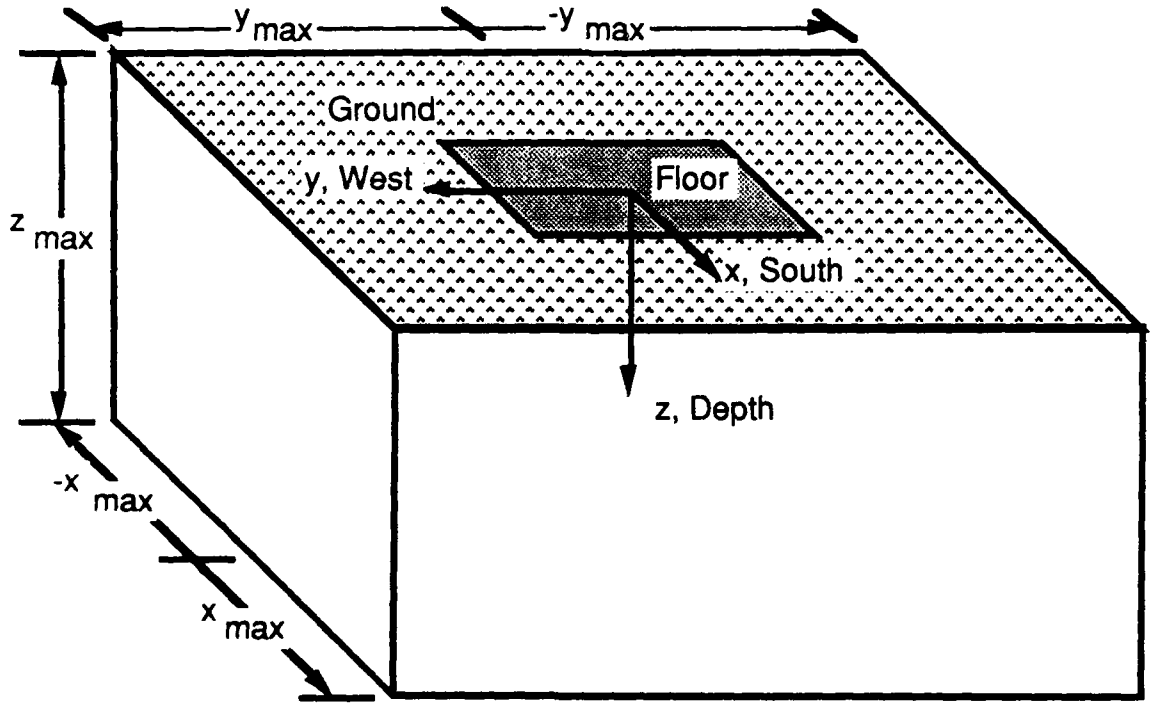

Figure II-2. Domain coordinate definitions.

Conditions on Eqn. II-17 are applied at the boundaries of the domain in a manner consistent with the discussion of the preceding section. In the plane z = 0, Eqns. II-2 and II-16 apply at the floor and ground surfaces, respectively. The four vertical boundary planes at $x = \pm x_{max}$ and $y = \pm y_{max}$ are "far-field" boundaries on which the undisturbed soil temperature distribution is imposed. The lower boundary, $z = z_{max}$, may be either a specified flux or specified temperature surface.

The numerical solution employed the Patankar-Spalding finite difference procedure [21]. The conceptual basis of this method is the representation of the continuum physical domain by a computational domain comprising a finite number of lumped parameter cells. These cells must be sufficiently small that 1) their properties may be assumed uniform and 2) temperature variations between adjacent cells are approximately linear. These assumptions permit the integration of Eqn. II-17 over each cell to produce a more easily solved simultaneous linear system approximating the original problem.

In the present case, the domain is divided into rectangular solid cells of varying dimensions by plane surfaces aligned with the coordinate directions. Definitions for the computational domain are indicated in Figure II-3, which shows the surface (x-y) plane. The cell face indices i, j, and k are associated with the x, y, and z directions, respectively. The modelled floor lies within a one cell thick box centered on the origin and defined by the cell faces ±IBOX in the x direction and ±JBOX in the y direction. If the floor is rectangular, it fills this area completely. An L-shaped floor fills

three of the four quadrants of the box. The outer limits of the domain are defined by the cell faces ±NX in the x direction, ±NY in the y direction, and in the z direction, by zero and NZ.

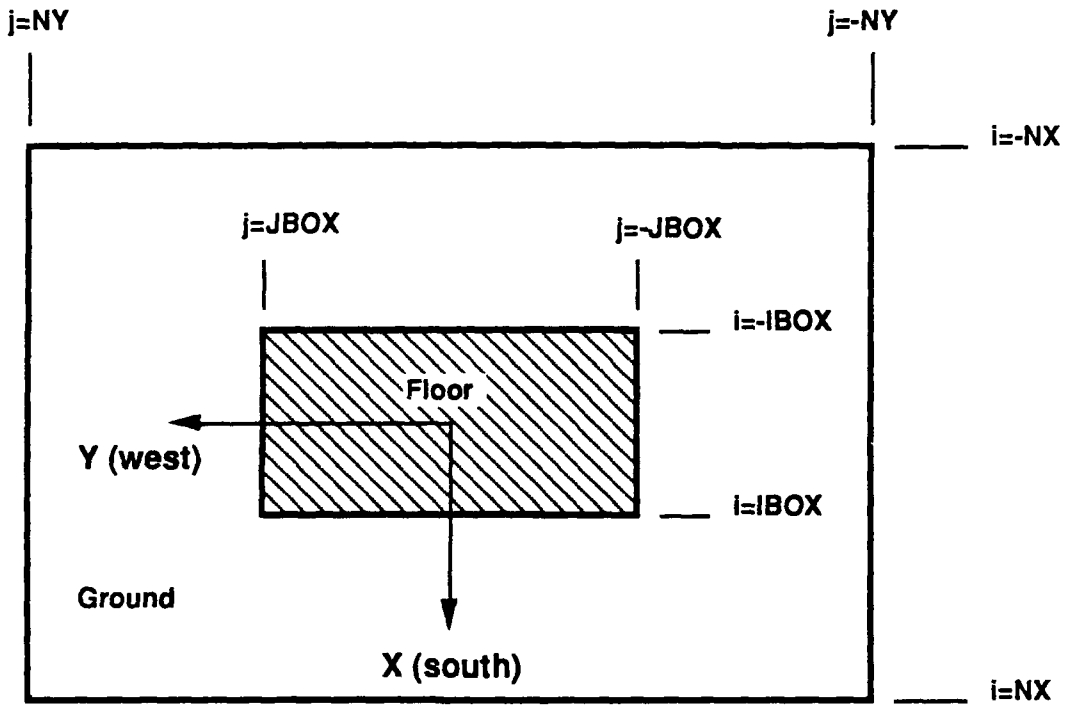

Figure II-3. Finite difference domain definitions.

II.B.2. DISCRETIZATION EQUATIONS

Interior Cells

A typical interior cell (i. e., one having neighbor cells on all sides) will be used to illustrate the Patankar-Spalding approach to discretization. A vertical (x-z) cross-section of such an interior cell and its neighbors is shown in Figure II-4.

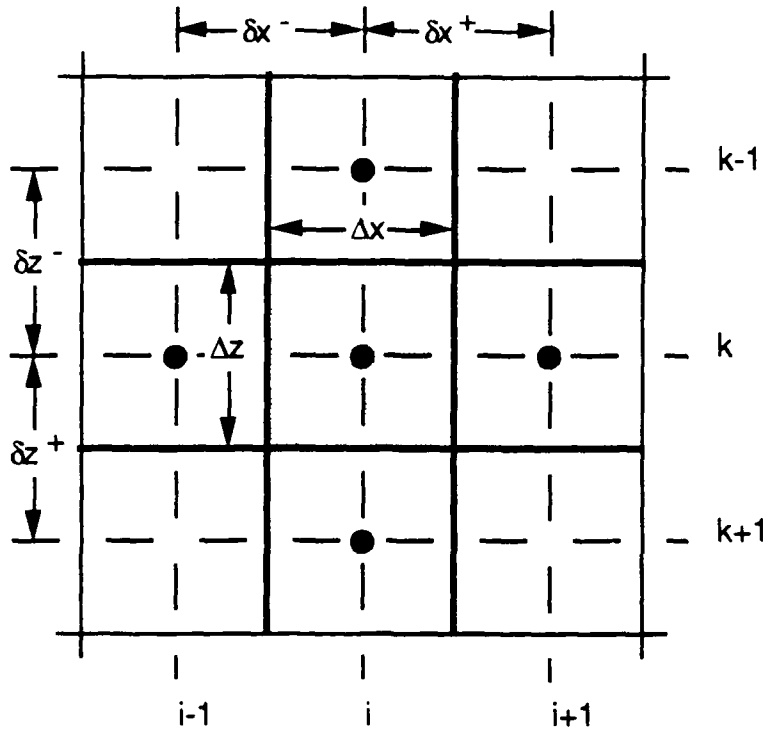

Figure II-4. Interior finite difference cell definitions.

Cell boundaries are shown as solid lines and the grid of cell centerlines is shown dashed. Temperature nodes are centered in their respective cells. Since a variable grid is permitted, cell faces do not necessarily lie midway between temperature nodes. The dimensions of the cell of interest (i. e., the distances between faces of the center cell) are Δx, Δy, and Δz, along the x, y, and z axes, respectively. The distances between the temperature node of this cell and the temperature nodes of its neighbor cells are indicated by, for example, δx^+ and δx^- for neighbor cells in the positive and negative x direction. A similar notational scheme is used to identify cell faces. For instance, the cell faces in the positive and negative

directions from the center of the cell are indicated by x^+ and x^-, respectively.

The first step in the derivation of the discretization equation is to integrate Eqn. II-17 once over a control volume identical with this cell, assuming constant thermal properties within its boundaries:

$$\rho c \frac{\partial T}{\partial t} \cdot \Delta x \cdot \Delta y \cdot \Delta z = \left[\left(k \frac{\partial T}{\partial x}\right)_{x^+} - \left(k \frac{\partial T}{\partial x}\right)_{x^-}\right] \cdot \Delta y \cdot \Delta z + \left[\left(k \frac{\partial T}{\partial y}\right)_{y^+} - \left(k \frac{\partial T}{\partial y}\right)_{y^-}\right] \cdot \Delta x \cdot \Delta z + \left[\left(k \frac{\partial T}{\partial z}\right)_{z^+} - \left(k \frac{\partial T}{\partial z}\right)_{z^-}\right] \cdot \Delta x \cdot \Delta y \qquad \text{(II-18)}$$

As indicated by the notation, flux terms on the right-hand side are evaluated at the surfaces of the cell.

The derivation is completed by replacing the remaining first derivative terms in Eqn. II-18 with first-order linear difference approximations (consistent with the second basic assumption of the method) and clearing the cell volume from both sides:

$$\rho c \frac{T^{t+\Delta t}_{i,j,k} - T^{t}_{i,j,k}}{\Delta t} = \frac{1}{\Delta x}\left(k_{x^+} \frac{T^{t}_{i+1,j,k} - T^{t}_{i,j,k}}{\delta x^+} - k_{x^-} \frac{T^{t}_{i,j,k} - T^{t}_{i-1,j,k}}{\delta x^-}\right) + \frac{1}{\Delta y}\left(k_{y^+} \frac{T^{t}_{i,j+1,k} - T^{t}_{i,j,k}}{\delta y^+} - k_{y^-} \frac{T^{t}_{i,j,k} - T^{t}_{i,j-1,k}}{\delta y^-}\right) + \frac{1}{\Delta z}\left(k_{z^+} \frac{T^{t}_{i,j,k+1} - T^{t}_{i,j,k}}{\delta z^+} - k_{z^-} \frac{T^{t}_{i,j,k} - T^{t}_{i,j,k-1}}{\delta z^-}\right) \qquad \text{(II-19)}$$

Temperature subscripts in Eqn. II-19 denote the indices of the node at which T is evaluated. Superscripts on T indicate time level. Note that all but one temperature is evaluated at the current time level, "t", making this an explicit formulation (i. e., one which may be solved directly for the cell temperature at the new time level "t + Δt"). The Patankar-Spalding method is not bound to a particular method for solving the discretized problem, so implicit differencing might have been employed instead. In the three-dimensional Cartesian case, stability exists as long as the inequality of Eqn. II-20 is satisfied for every cell:

$$\alpha \cdot \Delta t \cdot \left[\frac{1}{\Delta x^2} + \frac{1}{\Delta y^2} + \frac{1}{\Delta z^2} \right] \leq \frac{1}{2} \qquad \text{(II-20)}$$

(where α is thermal diffusivity). If this criterion is met for a given combination of thermal diffusivity, grid size, and time step, then it is more advantageous to use the explicit formulation since it requires fewer operations per nodal temperature update [47]. For the time step (one hour), minimum cell dimensions (20 x 20 x 10 cm), and diffusivity values (on the order of 10^{-7} m^2/s) encountered in this study, the stability criterion was satisfied. Therefore, the explicit method of solution was employed.

Effective Thermal Conductivity

Interface subscripts on thermal conductivity values in Eqn. II-19 ("x+", "y-", etc.) indicate that these are "effective" conductivities

pertaining to the flux across a particular interface. The need for effective conductivity arises from the possibility of heat flow across an interface between cells of different conductivity. If no allowance was made for variable properties and the conductivity of the center cell was used in all of the right-hand side flux terms of Eqn. II-29, then the same temperature difference between two cells of different conductivity would simultaneously cause two different fluxes across a single interface. The interface flux implied by the discretization equation of one cell would differ from that implied by the equation of its neighbor by an amount proportional to the difference in their conductivities. This erroneous production or destruction of energy could lead to serious error. Accordingly, a single representative value of conductivity must be chosen to guarantee conservation across such cell boundaries.

The effective conductivity may be derived by analogy to the procedure for calculating the steady-state thermal resistance of a composite material. The resistance per unit cross-sectional area of a planar layer of a homogeneous material is equal to its thickness divided by its conductivity. The total resistance of a composite material equals the sum of the resistances of its parts. By analogy to the homogeneous case, there is an effective conductivity which, divided into the total path length, gives the same value of thermal resistance as the sum of the component resistances. This is precisely the condition that must be met in the finite difference formulation in order to conserve energy.

By way of example, if two plane layers with conductivities k_1 and k_2 [W/m-K] have thicknesses L_1 and L_2 [m], then their component resistances are L_1/k_1 and L_2/k_2 [m^2-K/W], respectively. The effective conductivity, k_e, is the value which satisfies the equation:

$$\frac{L_1+L_2}{k_e}=\frac{L_1}{k_1}+\frac{L_2}{k_2} \qquad \text{(II-21)}$$

i. e.,

$$k_e=\frac{L_1+L_2}{L_1/k_1+L_2/k_2} \qquad \text{(II-22)}$$

In the discretized Cartesian problem, each flux between neighbor cells may be viewed as a locally one-dimensional quasi-steady process. Referring to Fig. II-4, it is clear that L_1 and L_2 correspond to the half-widths of adjacent cells (e.g., $\Delta x/2$), and that the total path length ($L_1 + L_2$) is analogous to the distance between the nodes separated by a given interface (e.g., δx^+).

In addition to maintaining conservation of energy in the model, this treatment of variable conductivity provides an easy way to incorporate the effect of insulation without redefining the grid. If it is assumed that a layer of insulation is thin and of negligible thermal mass, then the insulation may be modelled as a pure thermal resistance added to the total path resistance on the right-hand side of Eqn. II-21. The resulting expression for effective

conductivity, analogous to Eqn. II-22, becomes:

$$k_e = \frac{L_1 + L_2}{L_1 / k_1 + L_2 / k_2 + r_{ins}} \qquad \text{(II-23)}$$

where r_{ins} [m^2-K/W] is the unit thermal resistance of the insulation.

Boundary Cells

Equations for boundary cells may be derived from the interior cell result by making appropriate substitutions in Eqns. II-18 and II-19. Cells at the ground or slab surface require special treatment on their upper surfaces. In both cases, the surface boundary condition has the form

$$-k\left(\frac{\partial T}{\partial z}\right)_{z=0} = q_0 \qquad \text{(II-24)}$$

where q_0 is a flux which depends on the surface temperature. For exterior surface cells,

$$q_0 = G(t) \qquad \text{(II-25)}$$

where G(t) is determined by the surface energy balance. At interior slab surfaces, q_0 is derived from Eqn. II-2:

$$q_0 = h_i \cdot \left(T^t_{room} - T^t_{i,j,0}\right) \qquad \text{(II-26)}$$

Because the conditions II-25 and 26 depend on surface temperature, it is important to evaluate surface temperature as accurately as possible. Soil temperature near the ground surface may vary substantially over a distance of a few centimeters. To avoid the error associated with use of the temperature at a below surface node to represent the boundary temperature, the temperature nodes of surface cells are defined to be the centered in their upper faces, as depicted in Figure II-5.

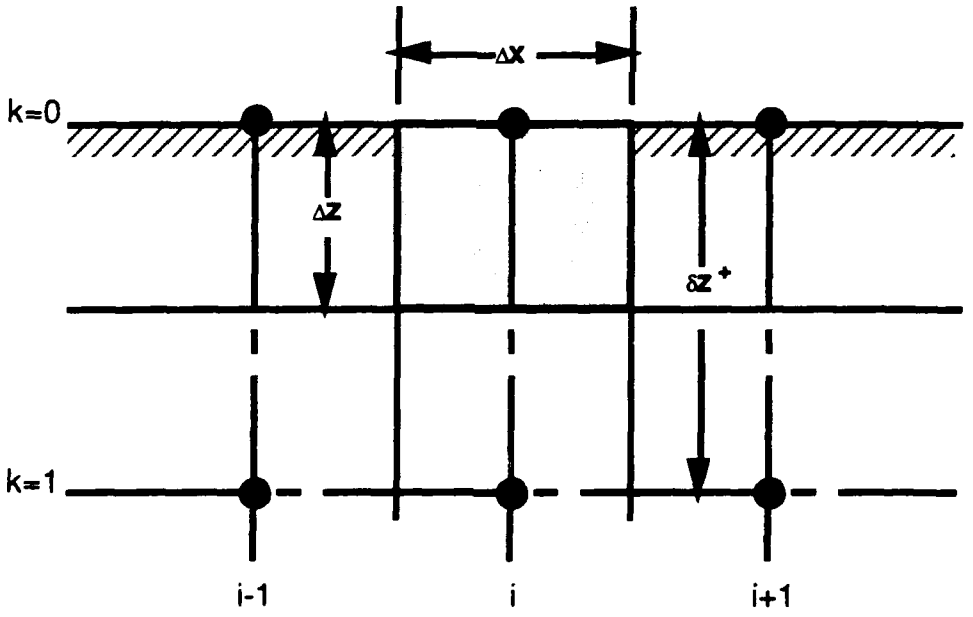

Figure II-5. Surface cell definitions.

Substitution from Eqns. II-24, 25, and 26 into Eqn. II-18 yields the desired boundary forms, i.e:

$$\rho c \frac{T^{t+\Delta t}_{i,j,k} - T^{t}_{i,j,k}}{\Delta t} =$$
$$\frac{k_{x^+}}{\Delta x \cdot \delta x^+} T^{t}_{i+1,j,k} - \left(\frac{k_{x^+}}{\Delta x \cdot \delta x^+} + \frac{k_{x^-}}{\Delta x \cdot \delta x^-} \right) T^{t}_{i,j,k} + \frac{k_{x^-}}{\Delta x \cdot \delta x^-} T^{t}_{i-1,j,k}$$
$$\frac{k_{y^+}}{\Delta y \cdot \delta y^+} T^{t}_{i,j+1,k} - \left(\frac{k_{y^+}}{\Delta y \cdot \delta y^+} + \frac{k_{y^-}}{\Delta y \cdot \delta y^-} \right) T^{t}_{i,j,k} + \frac{k_{y^-}}{\Delta y \cdot \delta y^-} T^{t}_{i,j-1,k} +$$
$$\frac{k_{z^+}}{\Delta z \cdot \delta z^+} \left(T^{t}_{i,j,k+1} - T^{t}_{i,j,k} \right) + \frac{1}{\Delta z} \cdot G(t)$$

(II-27)

for the ground, and

$$\rho c \frac{T^{t+\Delta t}_{i,j,k} - T^{t}_{i,j,k}}{\Delta t} =$$
$$\frac{k_{x^+}}{\Delta x \cdot \delta x^+} T^{t}_{i+1,j,k} - \left(\frac{k_{x^+}}{\Delta x \cdot \delta x^+} + \frac{k_{x^-}}{\Delta x \cdot \delta x^-} \right) T^{t}_{i,j,k} + \frac{k_{x^-}}{\Delta x \cdot \delta x^-} T^{t}_{i-1,j,k}$$
$$\frac{k_{y^+}}{\Delta y \cdot \delta y^+} T^{t}_{i,j+1,k} - \left(\frac{k_{y^+}}{\Delta y \cdot \delta y^+} + \frac{k_{y^-}}{\Delta y \cdot \delta y^-} \right) T^{t}_{i,j,k} + \frac{k_{y^-}}{\Delta y \cdot \delta y^-} T^{t}_{i,j-1,k} +$$
$$\frac{k_{z^+}}{\Delta z \cdot \delta z^+} \left(T^{t}_{i,j,k+1} - T^{t}_{i,j,k} \right) + \frac{h_i}{\Delta z} \left(T^{t}_{room} - T^{t}_{i,j,k} \right)$$

(II-28)

for the fioor.

The remaining boundaries, those in the far field and deep ground, were converted to specified temperature boundaries on which the undisturbed soil temperature distribution was imposed. This was accomplished by pre-calculating and saving the one-dimensional ground temperature solution prior to execution of the three-dimensional simulation. The calculation was performed in

this manner because test runs converged more rapidly when specified temperature conditions were used and because it reduced the number of calculated nodes in the model. Preliminary tests were conducted to obtain an estimate of how far from the perimeter of the building the specified temperature side boundaries should be located in order to approximate zero-flux boundaries. On the basis of these results, far field boundaries were placed a minimum of 12 m beyond the slab edge.

The formulation of the one-dimensional boundary temperature routine was analogous to that of the three-dimensional program in all respects with the exception that implicit differencing was employed. The unconditionally-stable implicit formulation was required because the minimum cell z dimension violated the one dimensional stability criterion for a one hour time step.

II.B.3. SIMULATION OF GROUND SHADING

A possible influence on foundation heat loss which does not seem to have been studied before is the shadowing of the ground by the building itself. By reducing the beam radiation incident on the ground surface at and near the edge of the floor, a regularly occurring pattern of shade could alter the local average ground temperature sufficiently to cause noticeable changes in heat loss patterns. In order to assess the magnitude of ground shading, a simulation of the building shadow cast on the ground was included in this model. The building was assigned an exterior wall height and assumed to be flat-roofed for this purpose.

The method used to create a discretized approximation of the shadow is quite simple in concept, although rather laborious in practice. A cell on the ground surface was considered to be entirely in the shade during a given hour if the view of the sun from its center was obstructed at the beginning of the hour. For each potentially shaded surface cell, a simple coordinate geometry computation was made to determine whether the line defined by the hourly beam direction and the cell center intersected any above grade surface of the building. If a cell was determined to be unshaded, it was assigned a beam radiation multiplier of 1. If it was determined to be in the shade, this multiplier was set to zero. This radiation multiplier was then applied to the incident beam portion of solar radiation (from the weather file) in the calculation of G(t). An entire year of shading factors was generated and saved prior to execution of the heat transfer simulation of the building. During the simulation proper, these hourly shade switch values were read in from the file.

The geometric description of a horizontal shadow is shown in Figure II-6. For a given obstruction height "H", the length and direction of its shadow are determined by two solar angles: the zenith angle (Θ_Z), and the solar azimuth angle (γ_S) [48]. The former is the angle between beam radiation and vertical, and the latter is the angle between the horizontal projection of beam radiation and south. The length of the shadow, L, is given by:

$$L = H \cdot \tan(\Theta_z) \qquad \text{(II-29)}$$

and its components in a horizontal plane are, respectively:

$$L_x = H \cdot \tan(\Theta_z) \cdot \cos(\gamma_s) \qquad \text{(II-30a)}$$

and

$$L_y = H \cdot \tan(\Theta_z) \cdot \sin(\gamma_s) \qquad \text{(II-30b)}$$

The procedure used to compute the zenith and solar azimuth angles is described in Appendix A.

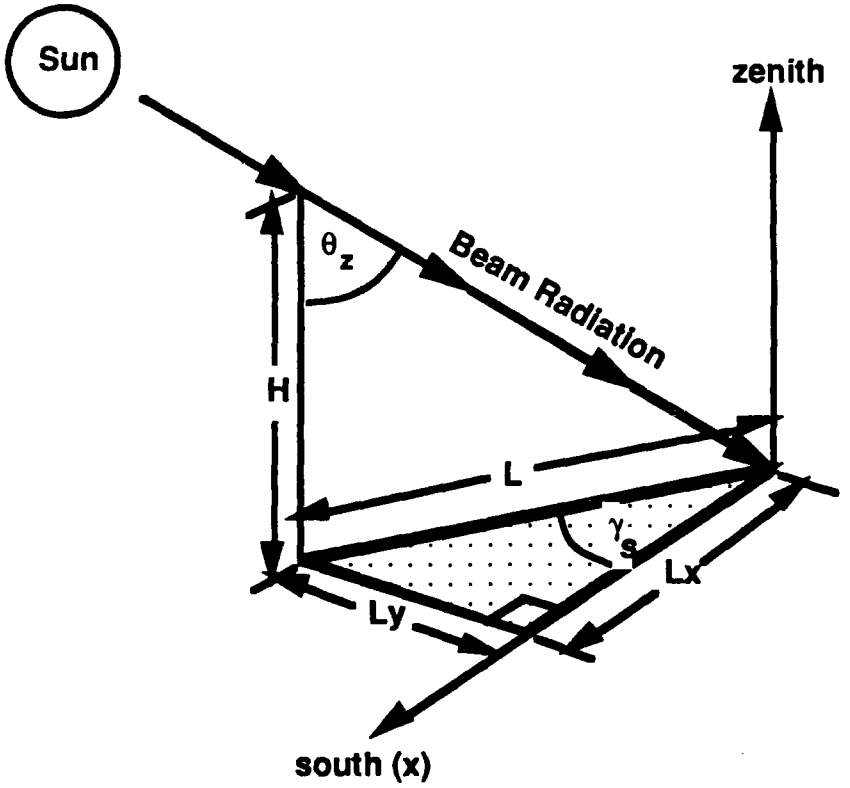

Figure II-6. Solar geometry definitions.

When H is taken to be the building height, the lengths L_x and L_y may be used in conjunction with the solar azimuth angle to limit the

area which must be searched for shaded cells. If, as in Figure II-7, beam radiation strikes a rectangular solid building from the south and west (as indicated by the azimuth), a shadow is cast only on the north and east sides within an L-shaped patch defined by L_x and L_y. This *a priori* limitation of the search area reduced the number of evaluations required by more than 75%.

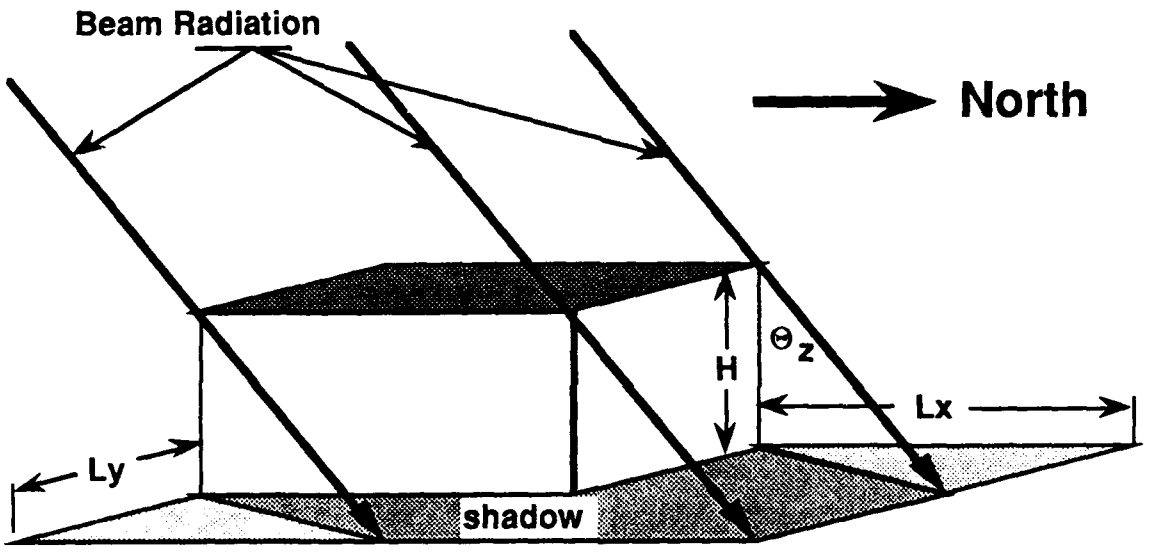

Figure II-7. Search area for shadowed surface cells.

II.B.4. COMPUTER PROGRAM DESCRIPTION

The numerical solution described above was implemented in Fortran 77 on a VAX 11-785 minicomputer. This section gives an overview of the program. Commented source listings of the main program and its six subroutines contained in Appendix B may be consulted if more detailed information is desired.

The main program SLAB3D controls the simulation as directed by data read from a short input file, performs the actual solution of the difference equations, and prepares output reports. The contents of the input file include:

- the geographic location to be simulated (which identifies the appropriate TMY weather file)
- thermal properties of the soil and floor materials
- ground surface properties for snow-covered and no-snow conditions
- the indoor dry bulb temperature and convection coefficients
- coordinates of cell faces (temperature node coordinates and cell dimensions are computed by the main program from the cell face coordinates)
- the size and shape of the floor to be modelled
- insulation thermal resistance and width*
- the building height to be used in shadowing calculations
- an initial ground temperature distribution based on the analytical semi-infinite medium solution (if a new ground temperature file must be calculated)
- logical switches indicating whether existing shade and ground temperature files are to be used, what type of deep ground boundary condition is to be applied, and whether shadowing and/or evapotranspiration are to be included in the ground surface boundary condition

* The only configuration modelled is vertical insulation on the slab edge and exterior horizontal insulation extending a specified distance in from the edge beneath the slab.

A sample input worksheet used in the preparation of this file is attached as Appendix C. Data items requested by the worksheet are supplied to the program in the order shown via an unformatted ASCII file.

Several steps occur between the reading of the input file and the beginning of the three-dimensional simulation:

- If an existing soil temperature file is not available for the current run, SLAB3D calls the subroutine TEARTH, which computes the steady-periodic ground temperature solution for the given data and writes a new file. Hourly sky infrared radiation, convective heat and mass transfer coefficient, and $\Delta/(\Delta+\gamma)$ values are also saved in this file.
- If a shadowing calculation is desired and no shadow file exists, the subroutine SHADE is called to create one.
- Coefficients used in three-dimensional difference equations which do not vary during a constant property simulation are calculated by the subroutine COEFFS and stored in arrays that are passed back to the main program.
- An input summary report is written.

Once these steps are accomplished, the remainder of program execution occurs in the main program.

At the beginning of the annual simulation loop, the entire domain is initialized to the undisturbed ground temperature. At the end of the second year of simulated time, and every year thereafter, a convergence test is performed. If every nodal temperature is

within an arbitrary, small tolerance of the previous year's values, convergence is assumed. One additional year of calculations is performed during which the following output reports are written:

- Hourly surface temperatures on January 21.
- Daily averaged surface temperatures and heat fluxes on the 21st of each month.
- Daily averaged temperatures in a vertical plane along the x axis on the 21st of each month.
- Daily high, low, and average values of outdoor dry bulb temperature, surface temperature and heat flux.

Execution times for the program ranged from slightly less than four hours to as long as fifty-two hours (on a dedicated machine). Excluding runs which considered shadowing and runs with L-shaped floor plans, the upper limit was closer to twelve hours. The execution time for rectangular floors without shadowing was greatly reduced through the use of the two planes of symmetry available in such cases. The 75% reduction in domain size achieved through the use of symmetry conditions resulted in a commensurate reduction of run time. The decision to take advantage of symmetry conditions was made internally by SLAB3D on the basis of the input file contents and required no user intervention. Typically, five to seven years of simulated time were required to achieve a converged periodic temperature distribution throughout the domain. Longer runs occurred for deeper domains and for zero flux lower boundary conditions.

II.C. TEST PLAN

II.C.1. PARAMETER RANGES

Climate

Four TMY weather locations were selected to represent the range of climates found in the continental United States. Geographic and climatic data for these sites are given in Table II-1. Minneapolis and Phoenix are typical of the cold and hot extremes of U. S. weather. Philadelphia and Medford are situated in moderate climate zones having similar mean temperatures, but different degree days. Oregon's coastal climate is responsible for the less severe conditions observed in Medford. Three of these sites, Medford, Minneapolis, and Phoenix, are located in regions identified by Labs [49] as being well-suited for earth-sheltered construction.

	Medford, OR	Minneapolis, MN	Philadelphia, PA	Phoenix, AZ
Latitude [Deg]	42° 2'	44° 5'	39° 5'	33° 3'
Longitude [Deg]	122° 5'	93° 1'	75° 2'	112° 0'
Elevation [m]	396	251	2	340
T_{mean} [C]	11.7	7.0	12.2	21.8
HDD [C]	2735	4636	2855	773
CDD [C]	315	506	614	2023

Table II-1. Test site geographic and climate data.

Soil Properties

Soil properties were chosen to represent the range of naturally occurring conditions. Data gathered by Kersten [33], as presented graphically by Andersland and Anderson [50], were the primary source of guidance for property selection. A mid-range set of properties simulating a moist soil was used as the base case in most of the simulations. Four other sets representative of both drier (lower conductivity) and wetter (higher conductivity) extremes were used in a parametric study of property effects. These five sets of properties are shown in Table II-2. Properties were varied from one set to another in such a way that it was possible to compare thermal conductivity and thermal diffusivity effects independently. (For example, in set A, α remains constant while k doubles with respect to the base case. Diffusivity is halved with respect to the base case while conductivity remains constant in set B.) Density and specific heat always appear as a product in this analysis, so they were assigned equal values purely for convenience. No such constraint exists in reality.

	Base Case	A	B	C	D
k [W/m-K]	1.0	2.0	1.0	0.5	2.0
ρ [kg/m^3]	1200	1700	1700	1200	1500
c [J/Kg-K]	1200	1700	1700	1200	1500
α [m^2/s]	6.9×10^{-7}	6.9×10^{-7}	3.5×10^{-7}	3.5×10^{-7}	8.9×10^{-7}

Table II-2. Soil property sets.

Ground Surface Properties

Ground surface properties were drawn from a number of sources summarized by Sellers [43]. A surface ordinarily covered by short grass was assumed. Average solar albedo values were taken from the extensive measurements of Kung, Bryson, and Lenschow [51], who compiled tables of continental averages as a function of latitude and snow cover on the basis of optical measurements taken from an airplane. Values used in this study were:

- 30-35° North Latitude (Phoenix)--Snow: 0.191, No Snow: 0.172
- 35-40° North Latitude (Philadelphia)--0.285/0.165
- 40-45° North Latitude (Medford, Minneapolis)--0.379/0.158

Data reported by Geiger [44] and others indicate that infrared emissivity is 0.90 or higher for most natural surfaces, including snow and grass. Accordingly, a value of 0.90 was used in all runs. Surface roughness height values of 0.75 cm for short, bare grass and 0.03 cm for snow were used in the convection model.

Building Parameters

A number of floor parameters were held constant throughout this study so attention could be focused on the central questions of size and shape. Consequently, issues such as details of floor construction, material property differences, and floor coverings were not considered. All floors were 10 cm thick concrete slabs. Thermal properties of concrete were those given in the ASHRAE Handbook of Fundamentals [45], 0.93 W/m-K, 2300 kg/m^3, and 653 J/kg-K for, respectively, conductivity, density, and specific heat.

Insulation, when specified, was polystyrene board with a thermal conductivity of 0.029 W/m-K (i. e., a thermal resistance of 34.5 m-K/W). As noted previously, floor surface conductances of 9.26 W/m^2 and 6.13 W/m^2 were used for heat transfer to and from the room, respectively.

Rectangular and L-shaped floors covering a large range of size and aspect ratio were considered. Values of area varied from a minimum of 144 m^2 to a maximum of 3600 m^2. For most runs, either a "residential" size of 144 m^2 or a "commercial" size of 2025 m^2 was used. Aspect ratio varied from unity (for a square floor) to nine (180 m x 20 m rectangle). Area to perimeter ratios ran from 2.4 m to 15 m. Four cases of insulation were considered: one inch on the slab edge and under the first meter of the floor, one inch of insulation covering the entire outer surface of the slab, and two inches of insulation in both of the preceding configurations.

II.C.2. PARAMETRIC GROUPS

The ninety-three simulations which form the basis of this study are catalogued in Appendix D. They are grouped into seven series which isolate various effects of interest:

- Series G: Floor shape and size/domain depth
- Series W: Climate
- Series E: No evapotranspiration
- Series S: Shadowing of the ground by the building
- Series K: Soil thermal property effects
- Series Z: Zero-flux deep ground boundary condition
- Series I: Insulation

The ground surface boundary condition included potential evapotranspiration except in series "E" and as otherwise noted in Appendix D. All floors other than those in series "I" were uninsulated. The deep ground boundary condition in all series except "Z" was a specified temperature condition equal to the annual average air temperature at a depth of either 10 m or 15 m (again, as indicated in the appendix). In each series, several area and aspect ratio combinations were considered in order to show the dependence on geometric factors of the effect produced by the parameter under study.

III. RESULTS

III.A. OVERVIEW

This section describes some qualitative characteristics of the results of this study. Later sections consider results of the parametric studies in a more quantitative way.

III.A.1. THE THERMAL REGIME OF THE UNDISTURBED GROUND

Because soil is the environment with which earth-coupled building surfaces interact, earth-coupled heat transfer rates depend strongly on the soil temperature regime. The semi-infinite medium analysis of heat transfer in the earth's crust [17] reveals the following characteristics of the soil temperature distribution:

- Annual and diurnal cycles each with an associated penetration depth of order $\sqrt{\alpha\tau}$, where τ is the appropriate period.
- Exponentially increasing attenuation of the surface temperature disturbance as a function of depth.
- Phase lag that is a linearly increasing function of depth.

These features are apparent in Figures III-1 and III-2, which show profiles for Minneapolis weather in a 15 m deep domain, base case soil properties (approximating a moist soil--see Table II-2), a zero flux deep ground boundary condition, and a surface boundary

condition that includes potential evapotranspiration. (These and subsequent soil temperature plots are based on boundary condition data generated by subroutine TEARTH.)

Fig. III-1 shows full profiles at 8 am on January 21 and 10 am on July 21, the respective hours of low and high surface temperature on those days. The positions of these profiles suggest the extent of the exponential envelope of the annual cycle. Phase lag is evidenced by the fact that July temperatures below four meters are less than January values. Below ten meters, soil temperature is essentially constant at a value near 5 C. According to the semi-infinite medium

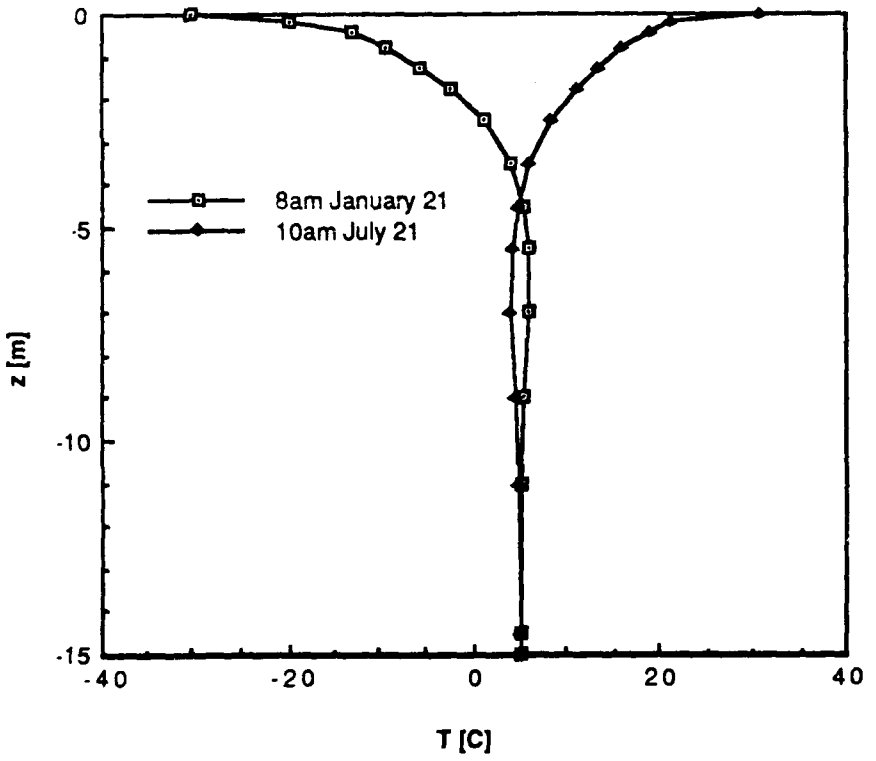

Figure III-1. Typical Minneapolis winter and summer soil temperature profiles (potential evapotranspiration, zero flux lower boundary).

analysis, this deep ground temperature is equal to the annual average ground surface temperature. The deep ground temperature (and so, the average surface temperature) is slightly lower than the annual average air temperature of 7 C due to the effect of evapotranspiration.

Fig. III-2 shows the upper half meter of the July 21 profile at the hours of minimum and maximum surface temperature. The qualitative similarity between the diurnal and annual cycles is apparent. Note that for these soil properties, daily variations are almost completely damped below 20 cm.

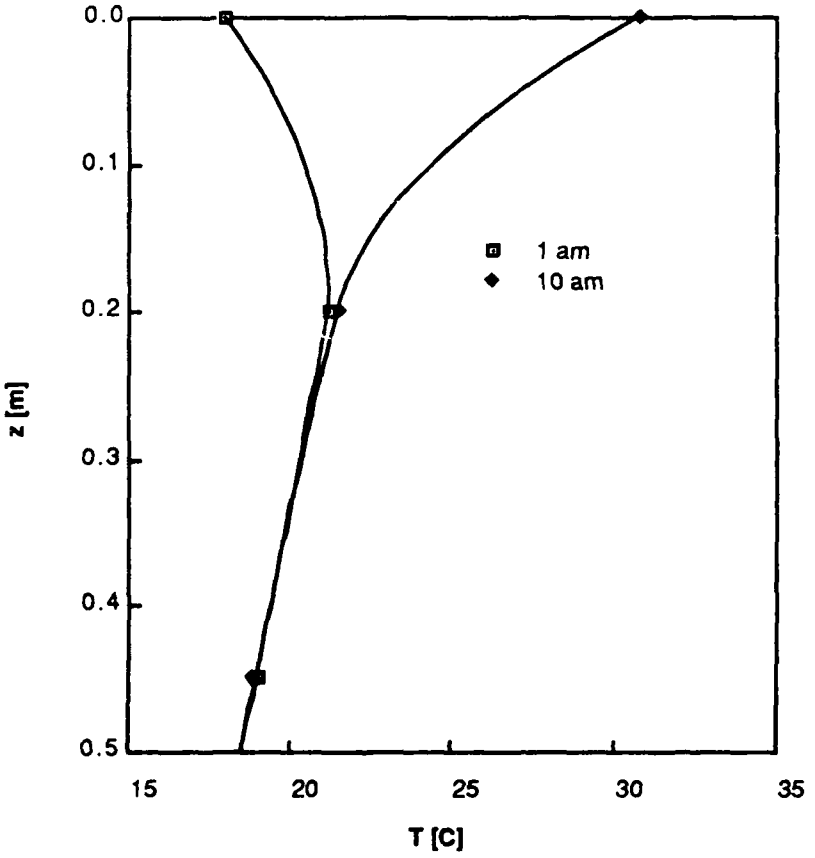

Figure III-2. Soil temperature variation near ground surface, Minneapolis, July 21.

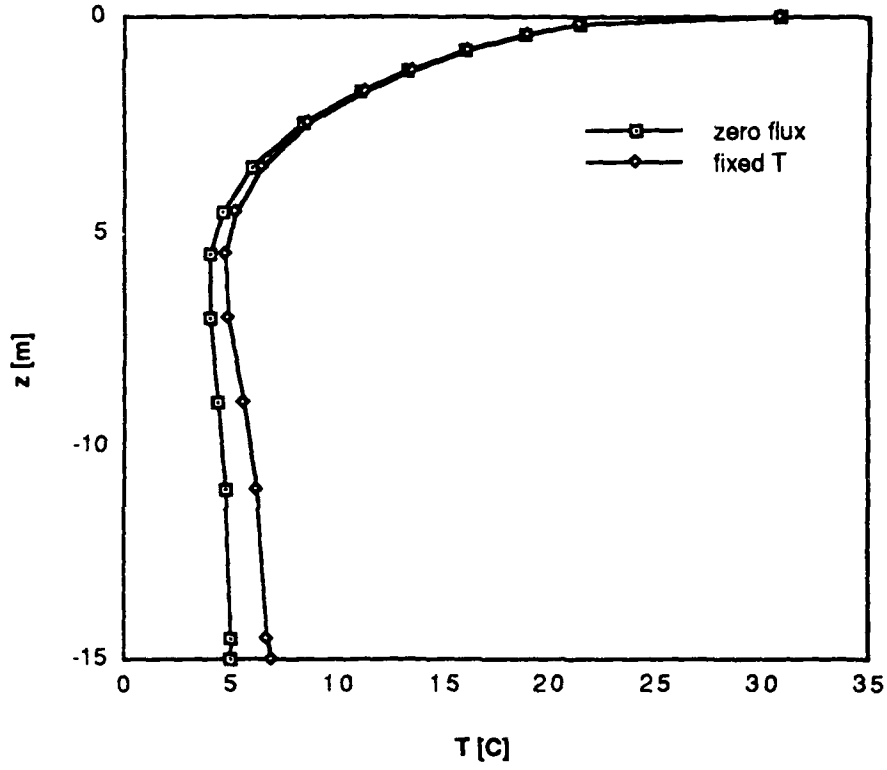

Figure III-3. Effect of zero-flux and fixed temperature lower boundaries on July 21 Minneapolis ground temperatures.

The relatively small influence of deep ground conditions on near-surface conditions is indicated by Fig. III-3, which shows the 10 am, July 21 zero flux boundary case of Fig. III-1 superimposed on the profile obtained when the lower boundary temperature is set equal to the mean annual air temperature (7 C in this case). Despite a two degree difference at the bottom of the domain, the influence of surface conditions is sufficiently strong to make the two profiles indistinguishable in the upper three meters of soil. This is not proof, however, that heat loss from slab floors is uninfluenced by changes in deep ground conditions. In fact, the temperature disturbance caused by a slab-on-grade building can extend to

considerable depths and may be sensitive to the lower boundary condition.

An example of ground temperature sensitivity to *surface* conditions is given in Figures III-4a and III-4b. These figures compare hourly ground temperatures with and without potential evapotranspiration for typical winter and summer days. On January 21 (Fig. III-4a), both boundary conditions give essentially the same result. Peak ground temperature exceeds dry bulb air temperature by approximately 10 C during the middle of the day, when solar gain is greatest. Late in the day, ground surface temperature falls several degrees below air temperature--a phenomenon made possible by night infrared loss. The close resemblance of the profiles in this case is due to the extremely small driving force for latent transfer processes existing in the low air temperature range recorded for this day. Both the wet bulb depression and $\Delta/(\Delta+\gamma)$ were essentially zero.

During the summer, potential for evaporation increases greatly. As Figure III-4b shows, the July 21 mid-day wet bulb depression for Minneapolis is in excess of 10 C. For this day, $\Delta/(\Delta+\gamma)$ averaged 0.75, indicating very efficient conversion of incoming radiation to latent heat in the potential evapotranspiration case. As a result, ground temperature with potential evapotranspiration is near or below dry bulb temperature throughout the day while, with no evaporation, the ground temperature rises above the dry bulb by an even greater amount than during the winter. The daily range of surface temperature is larger in Fig. III-4b than in III-4a because solar input is much greater in summer than during the winter.

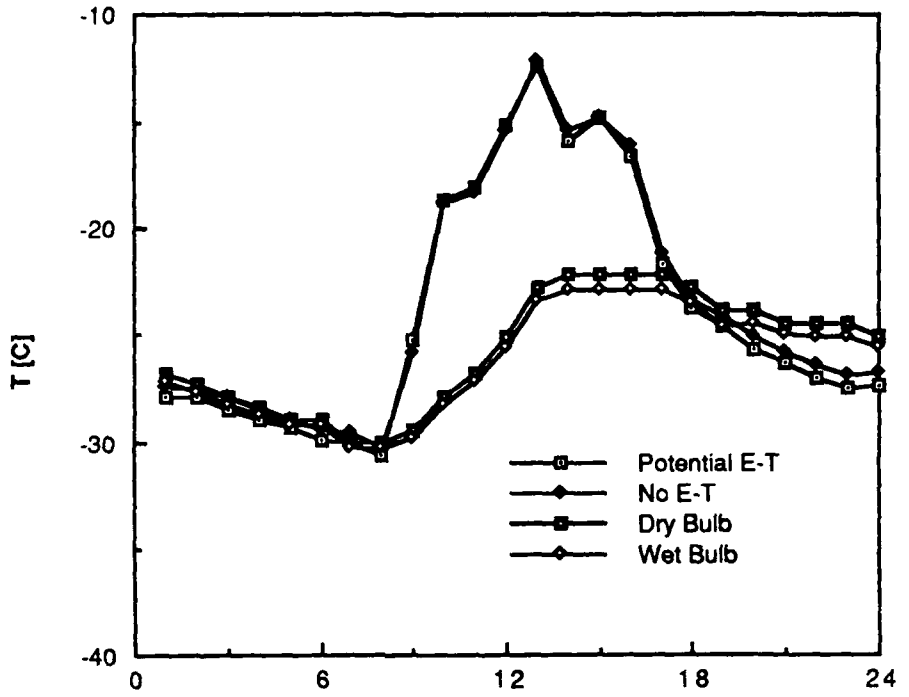

a) January 21

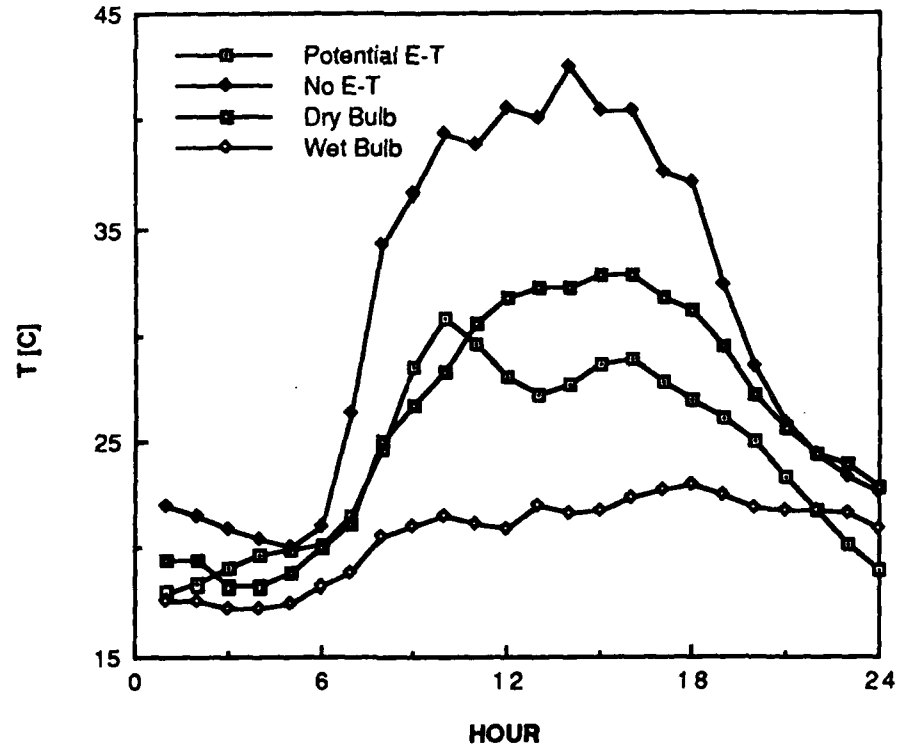

b) July 21

Figure III-4. Hourly variation of Minneapolis ground and air temperatures.

III.A.2. SOIL TEMPERATURE DISTRIBUTION NEAR A SLAB-ON-GRADE BUILDING

The undisturbed soil temperature profile fluctuates more or less symmetrically about its mean value during an annual cycle. In the vicinity of a slab-on-grade building, however, the soil thermal regime undergoes marked changes in character from season to season as a result of the time-varying difference between indoor and ground surface temperatures. In temperate or cold climates, the indoor-outdoor temperature difference is much larger during the winter than in the summer. When the temperature difference is large, as in the winter, a high flux region forms at the perimeter of a slab floor. During such periods, use of the F_2 type method for load estimation purposes has some legitimacy. In the summer, however, flux levels near the floor perimeter are not substantially different from those near the center. Consequently, the entire floor area contributes equally to heat loss and perimeter loss coefficient methods are invalid.

A typical seasonal cycle is shown in Fig. III-5, a series of daily averaged soil isotherm plots in a vertical plane running north-south through the center of a 12 x 12 m building in Minneapolis, MN. Shadowing was not included, so the isotherm patterns are symmetric about the floor center. Isotherms are labelled with temperatures in degrees centigrade. January isotherms are closely bunched and nearly vertical near the edge of the slab. The heat flow paths of largest gradient are arcs from the floor to the ground. Although the upper meter of far-field soil is below freezing, a large

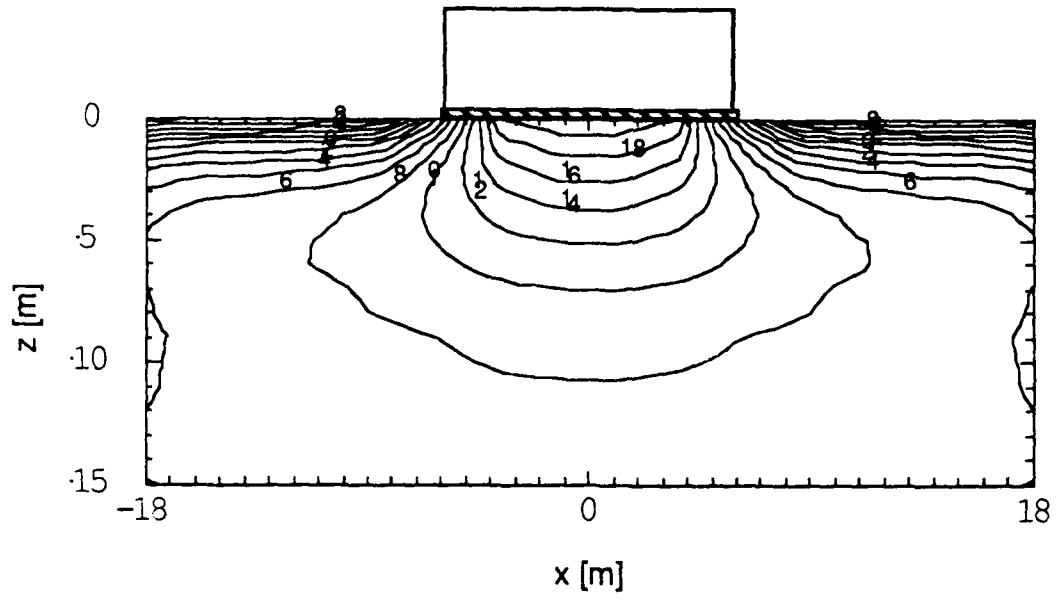

a) January 21

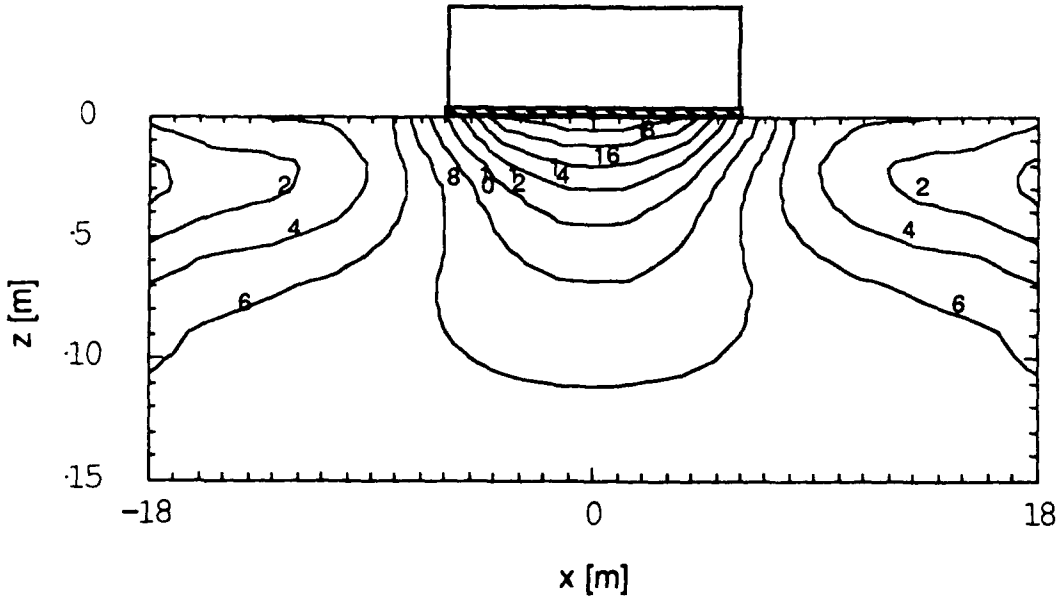

b) April 21

Figure III-5. Soil isotherms beneath an uninsulated 12 x 12 m slab in Minneapolis, MN.

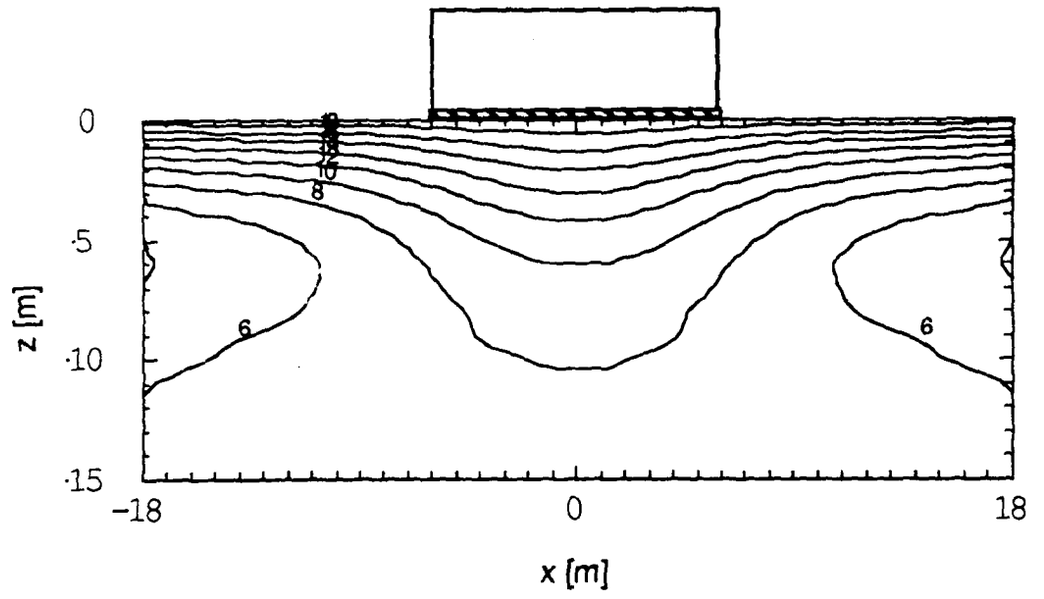

c) July 21

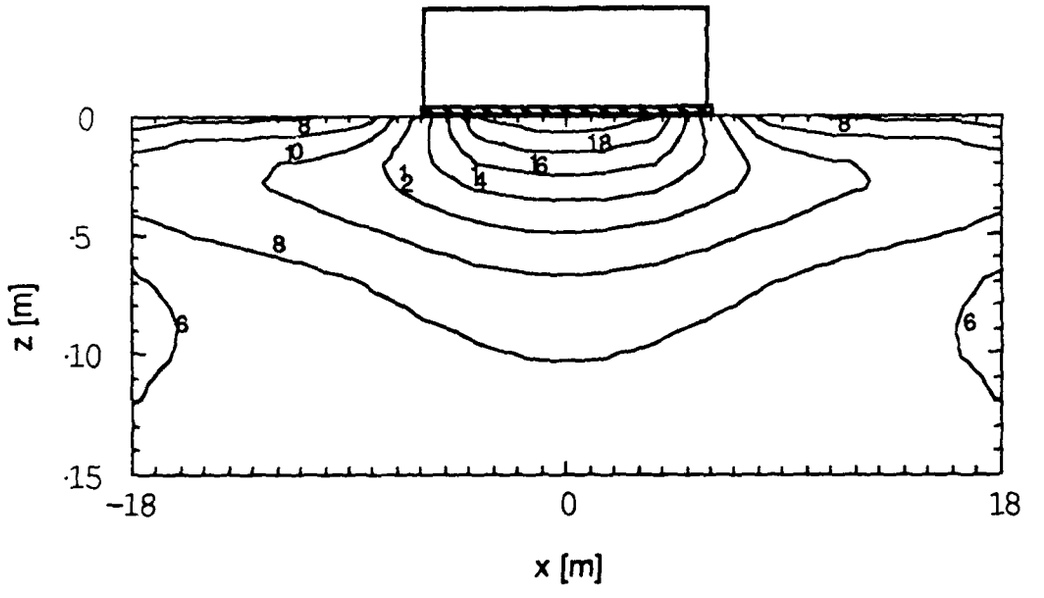

d) October 21

Figure III-5. Soil isotherms beneath an uninsulated 12 x 12 m slab in Minneapolis (continued).

subsurface region of warm soil extends into the earth beneath the slab center. Seasonal variations in the size and temperature of this region are quite small except near the floor perimeter. The association of this large soil mass with the floor is responsible for the relative stability of the core heat flux. The center of this earth-coupled zone is warmest in winter and coolest during the summer--a fortunate coincidence that tends to reduce both heating and cooling loads.

By April, as Fig. III-5b shows, the soil temperature gradient near the surface is much smaller and isotherms beneath the building are nearly horizontal. On either side of the building, a downward moving region of low temperature may be observed--the slowly dissipating, phase-lagged remnant of the cold winter weather. By July (Fig. III-5b), this region has expanded, warmed, and moved further into the earth. During the same period, isotherms beneath the floor have become horizontal surfaces and the distinction between core and edge regions has vanished. In the final plot, one may see the features of the winter distribution beginning to return as fall weather cools the ground surface.

III.A.3. SPATIAL VARIATION OF FLOOR TEMPERATURE AND HEAT LOSS

Floor temperature and heat flux distributions follow the same patterns as the soil temperature distribution. They may be divided conceptually into core and edge regions whose heat loss contributions vary in relative significance from season to season. Perimeter effects dominate during cold periods when high gradient

regions surround the slab edge. The precipitous nature of the perimeter zone temperature change during winter is indicated by Figure III-6. The upper curve in this figure shows the surface temperature distribution along a cross-section through the floor center. Adjustment from the core temperature to the adjacent soil surface temperature, a change of nearly 30 C, occurs in a zone extending approximately one meter on either side of the edge. The lower curve is a temperature profile along the outer edge of the slab. It shows that edge temperature varies in a manner similar to

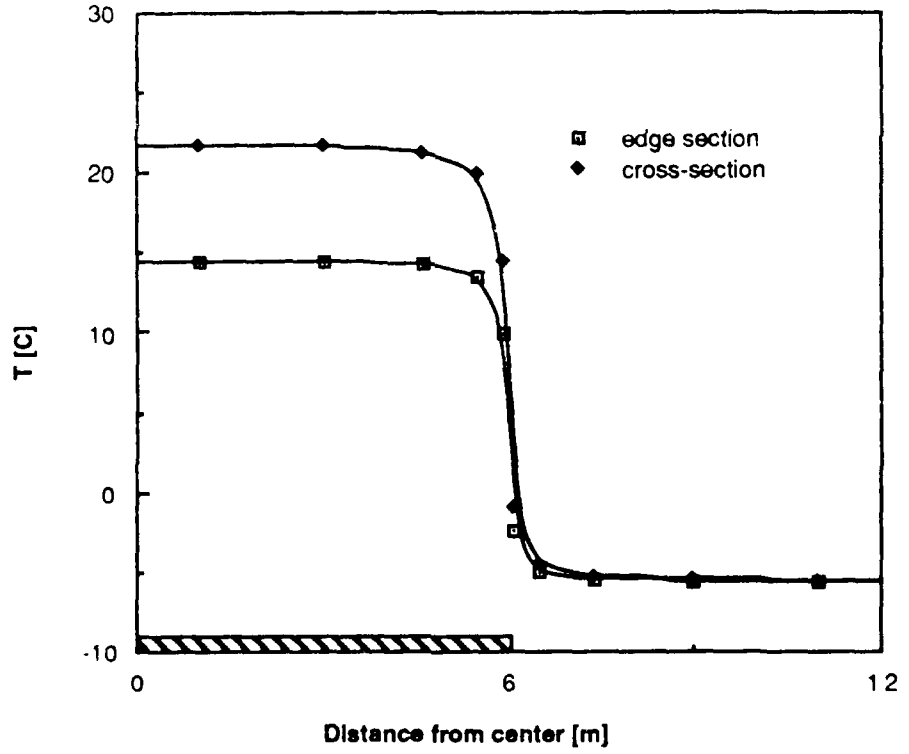

Figure III-6. Daily averaged edge and cross-sectional surface temperature distributions for a 12 x 12 m uninsulated slab-on-grade. January 21, Medford, OR.

cross-sectional temperature. The "fin" effect of the corner depresses the edge temperature approximately 5 C beneath the value at the center of the edge. Edge temperature rises to the edge center value over a distance similar to that required for the edge to core transition--about one meter.

January 21 average cross-sectional heat flux profiles for this floor and two others of different dimensions are shown in Figure III-7a. Two features of these distributions are particularly significant. First, regardless of the size and aspect ratio of the floor, the flux profile in the outer half meter is invariant. This observation supports the findings of Barəither, *et al.* [1] that the F_1 coefficients of Eqn. II-1a are independent of building size. Second, although the core heat fluxes of the three slabs are quite uniform, the precise value of this flux depends significantly upon geometric factors. This conflicts with the assumption implicit in Eqn. II-1a that the magnitude of the core flux is independent of core area. The magnified vertical scale of Figure III-7b (otherwise identical to III-7a) reveals an increase in core heat flux of almost 300% as the ratio of area to perimeter decreases from 11.25 m to 2.6.m.

The sharp perimeter zone changes that characterize the winter regime diminish substantially during the summer. Figure III-8a shows that the well-defined boundary region near the the slab edge in Fig. III-6 has become nearly isothermal by July. Note that the core temperature in July is essentially unchanged from its January value because of the thermal inertia of the soil coupled to the floor center. The magnified view in Fig. III-8b shows that the core flux rose by ten percent between January and July due to the arrival

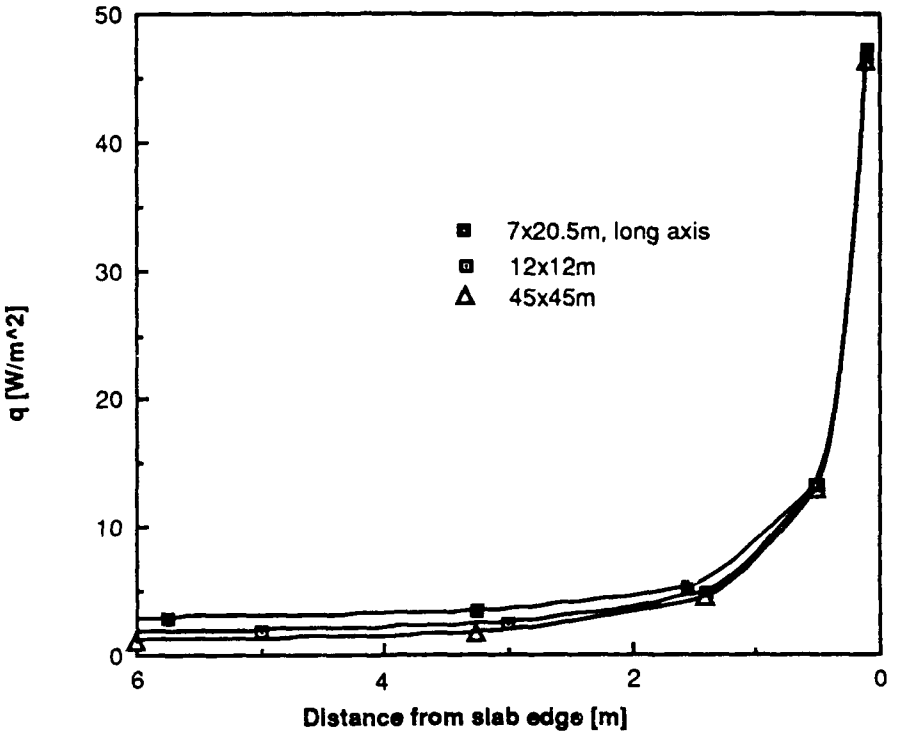

a)

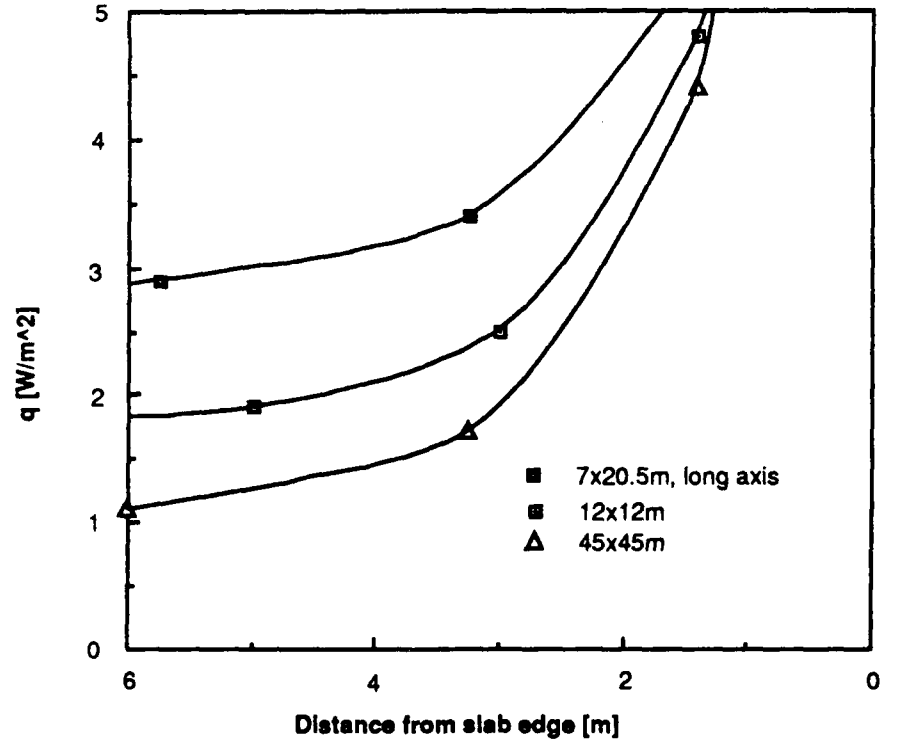

b)

Figure III-7. Daily averaged surface heat flux profiles for three slab-on-grade floors. Medford OR, January 21.

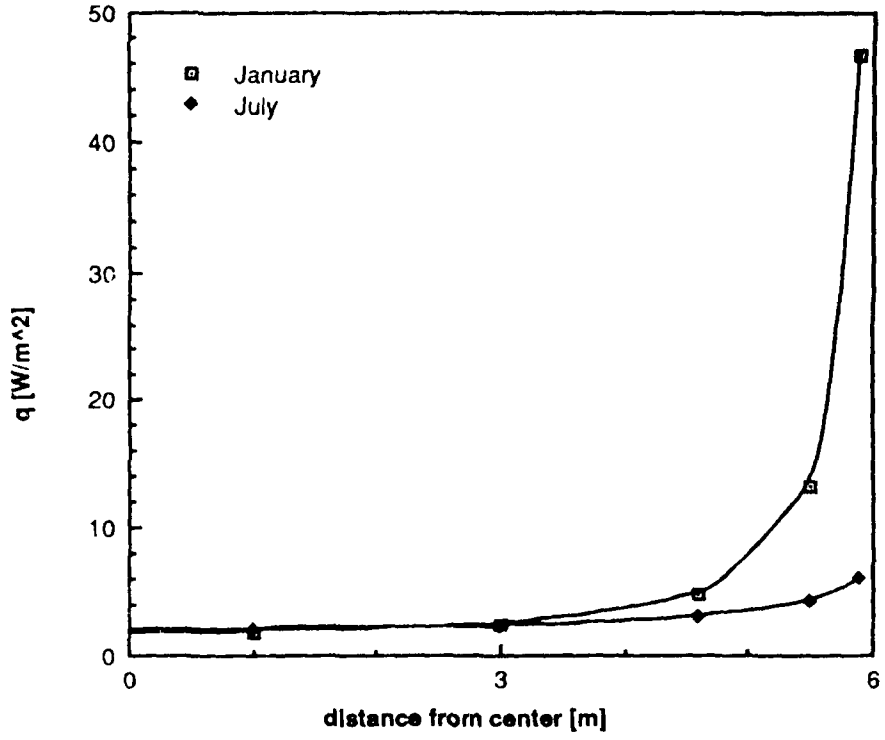

a)

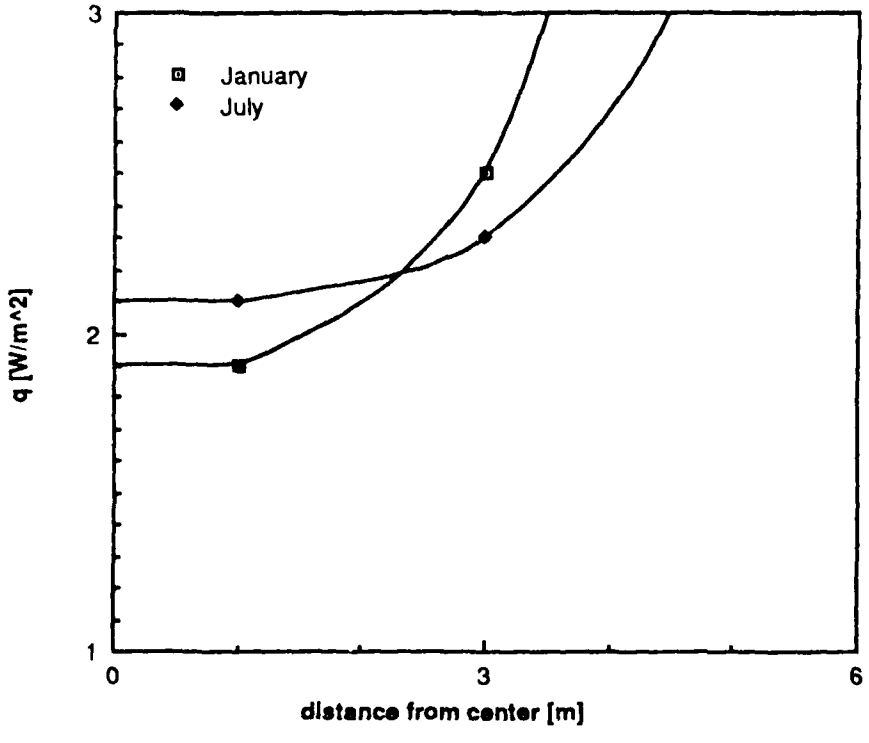

b)

Figure III-8. Winter and summer Medford, OR floor surface cross-section heat flux profiles.

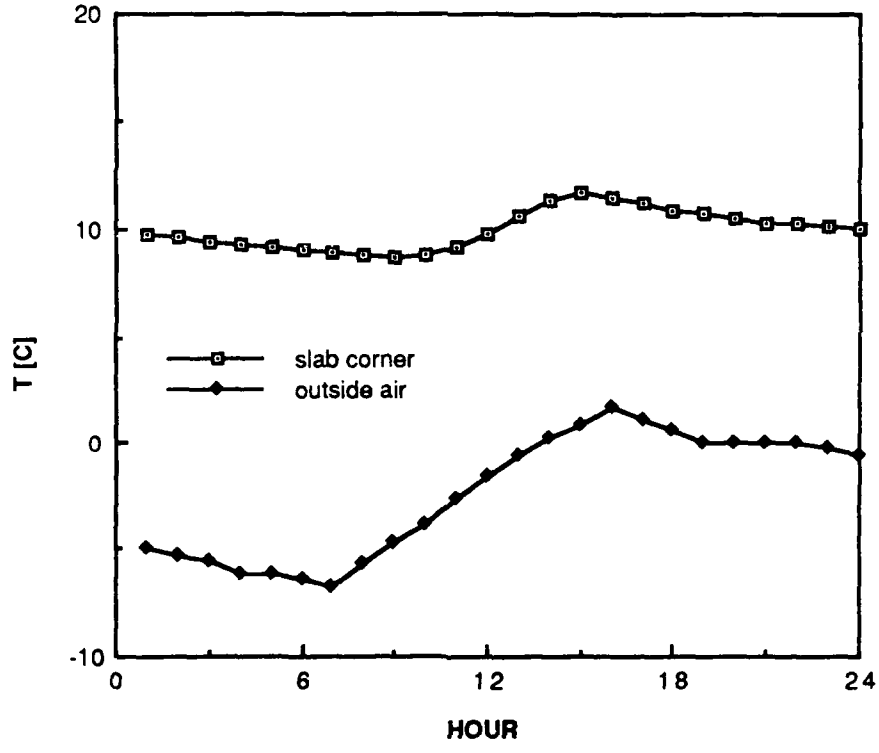

Figure III-9. Hourly variation of floor surface temperature at the corner of a 12 x 12 m uninsulated slab, Medford, OR, January 21.

under the slab of the winter cold front. During the summer, when core flux is comparable to perimeter flux, total floor area exerts relatively more influence on heat loss than in the winter. Therefore, the variation in core flux as a function of floor geometry is of great importance to the summer heat loss.

Surface temperature near the edge of a slab floor undergoes modest diurnal fluctuations. Because the penetration depth for daily disturbances is small, the effect of this variation on whole-floor heat loss is not very significant. Figure III-9 shows the January 21

temperature history of a corner floor surface node from the 12 x 12 m Medford, OR case considered previously. The daily range of 3 C at this node is considerably smaller than the outdoor air temperature range of 9 C. The results of this study indicate that hourly fluctuations in whole floor heat loss are negligible and that for energy analysis purposes, a 24 hour average is probably sufficient.

III.A.4. WHOLE-FLOOR HEAT LOSS

The primary factors determining whole-floor rates of heat loss are average conditions in the ground and weather events on a scale of several days or longer. Figure III-10 gives a comparison of heat loss per unit of perimeter for the 12 x 12 m and 45 x 45 m Medford, OR cases considered previously. Although fluctuations with a period of a week or less are evident, the predominant pattern is a single annual cycle of approximately sinusoidal shape. Note that the two curves are offset from one another by approximately 8 W/m over the entire year due to the greater core loss per unit of perimeter of the larger building. This example indicates the significant role played by core losses in larger buildings and the considerable error that can be introduced by the use of F_2 coefficients (Eqn. I-1b) based on small building data. Heat loss estimates for the 45 x 45 m floor extrapolated from the flux per unit perimeter length of the 12 x 12 m floor would be low by roughly 25% in the winter and 50% in the summer for this case. Clearly, the perimeter loss factor method is inadequate when there is real concern for accurate prediction of slab-on-grade heat loss.

Over the short term, i. e., periods of less than a week, both floors experience heat loss fluctuations of about the same magnitude per unit of perimeter. The similarity in this respect is due to the insensitivity of the edge loss to the area of the floor (as shown above in Fig. III-7). This example demonstrates that the load on a floor depends on several time scales as well as on geometry. The quantification of geometric effects is a major topic of the following sections.

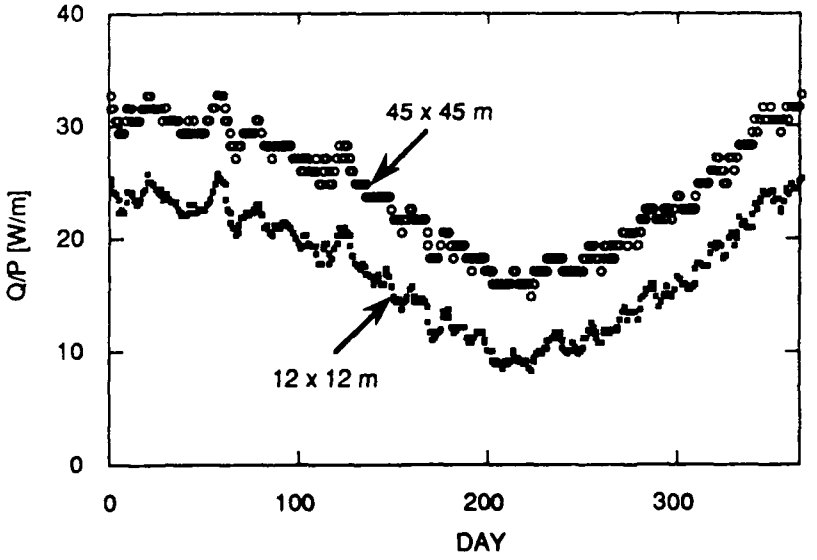

Figure III-10. Daily-averaged heat loss per unit perimeter length for large and small slabs, Medford, OR.

III.B. PARAMETRIC STUDIES

This section presents results from the parametric studies described in Ch. II.C.2.

III.B.1. EFFECTS OF SHAPE AND SIZE

The group of runs designated series "G" provided data for the investigation of geometric effects including size, shape, aspect ratio, and domain depth while other parameters were held constant. In all of these runs, Medford weather, base case soil properties, potential evapotranspiration at the surface, and a fixed temperature lower boundary equal to the annual average dry bulb were specified. Area ranged from 144 to 3600 m^2 and area/perimeter varied from 2.4 to 15 m. The plan shape in most cases was rectangular, however one L-shaped case was simulated for areas of 144, 900, and 2025 m^2. On the basis of these three runs, it was concluded that shape alone is not a strong influence on slab-on-grade heat transfer.

Figure III-11 shows annual average heat loss as a function of perimeter for twenty runs in a 15 m deep domain. In each group, the case having the smallest perimeter is a square (aspect ratio of one). Increasing perimeter for a fixed area corresponds to increasing aspect ratio. Clearly, the data do not fall on a single Q vs. P curve. For a given perimeter length, there is a significant total area effect on average loss. Heat loss increases with increasing area beyond the amount predicted by a "proportional to perimeter" model. For the limited variety of plan shapes considered, there is no significant

effect due to shape alone. L-shaped floors fall comfortably into place among rectangles of the same area in Fig. III-11. (For example, the middle point of the five 2025 m^2 cases is an L-shaped slab.) The relationship between area and perimeter, not the particular shape seems more important. (However, this might not hold for special cases such as a floor that completely encloses an area that is open to the atmosphere.)

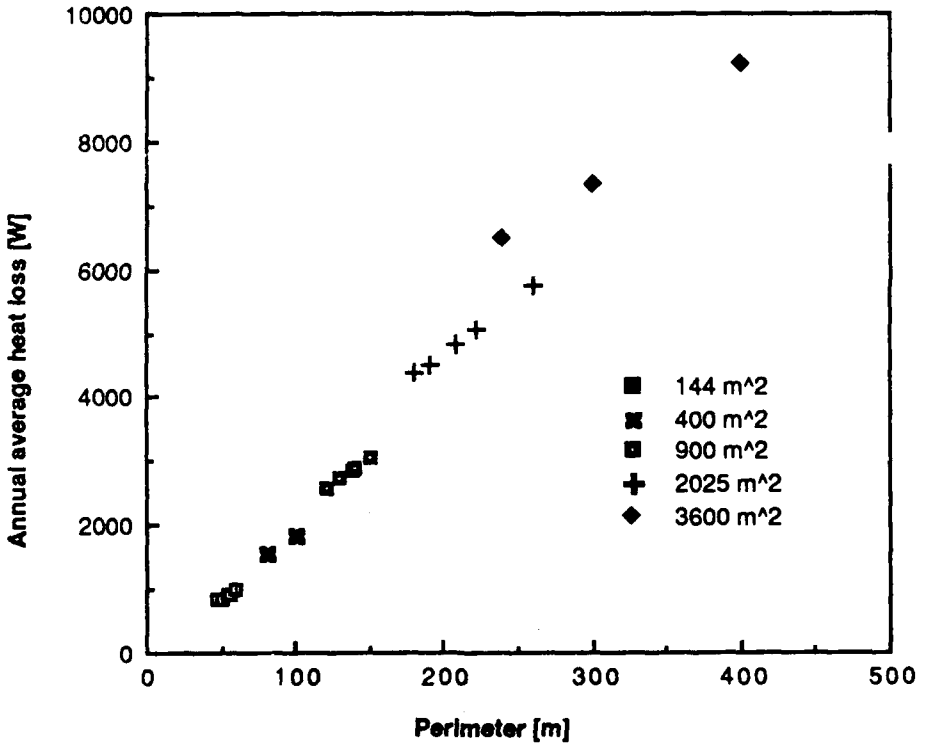

Figure III-11. Heat loss vs. perimeter length for uninsulated floors in Medford, OR. 15 m deep domain.

One method of dealing with the area dependence revealed by Fig. III-11 is to construct a family of Q vs. P curves with area as a parameter. However, this approach does not provide any insight into

the nature of the area-perimeter relationship. Another method is represented by Eqn. II-1a, namely, to divide a floor into a core zone with a constant rate of loss and a perimeter zone with a constant heat transfer coefficient. This partitioning of the floor, however, is arbitrary and the core loss is, itself, a function of area (cf. the profiles of Fig. II-7). A third method, the one adopted in this study, is to seek an area-perimeter scaling relationship that provides both a useful model and a more satisfactory explanation of the observed phenomena.

The length scale defined by the ratio of area to perimeter (A/P) is a measure of the narrowest dimension of a planar shape. For a square of side "L", A/P is equal to L/4. In the general case of a rectangle with short side "L" and aspect ratio "μ" (defined ≥ 1), A/P is equal to $L/[2(1+1/\mu)]$. An infinite strip of length "L" has an aspect ratio of infinity and an A/P of L/2. When the data of Fig. III-11 are replotted as annual-averaged heat loss per unit area vs. A/P, the result is Figure III-12. All of the data lie on a single curve approximated by the logarithmic function:

$$q = c \cdot \left(\frac{A}{P}\right)^{d} \qquad \text{(III-1)}$$

where c and d are constants. For a given rectangular area, a square has the largest value of A/P, so for each group of data plotted in Figure III-12, the square case is the rightmost point. Note that there is overlap between the A/P values of the 2025 m^2 and 3600 m^2 data, and that the heat flux values for these overlapping cases

fall into place quite well on the same curve. As the characteristic width of a slab increases, its average rate of heat loss decreases. This reflects that fact that floors with large A/P have proportionately more core area than those with small values of A/P.

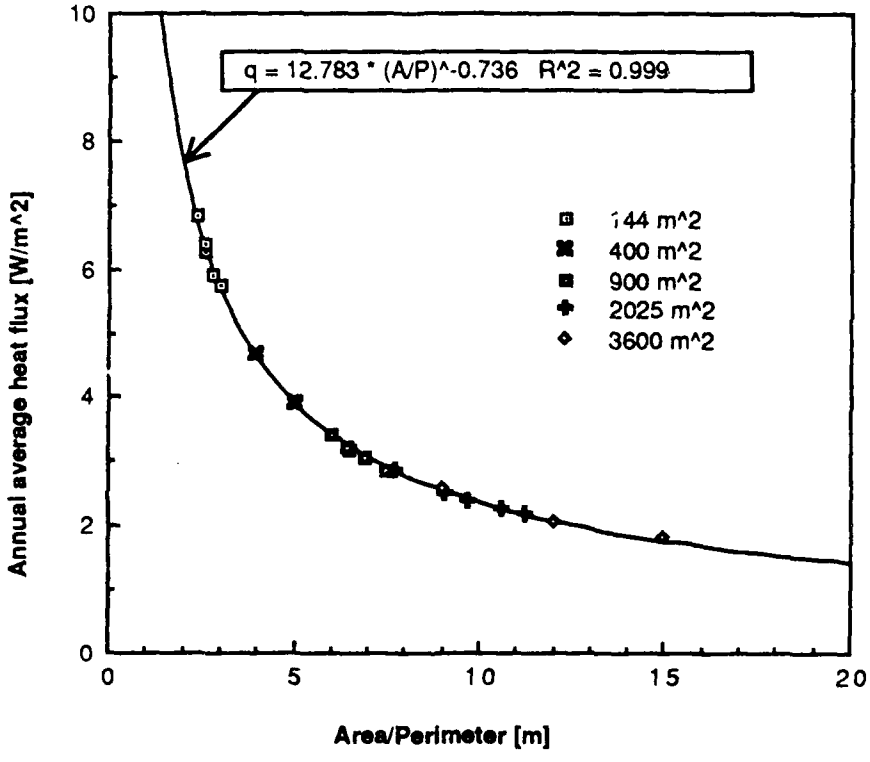

Figure III-12. Heat loss per unit area vs. A/P for uninsulated slabs, Medford OR, 15 m deep domain.

Two points should be kept in mind concerning the model of Eqn. III-1. First, the constants "c" and "d" depend on a great many parameters, including the annual average temperature difference, soil properties, domain geometry, and details of foundation design. There is no reason to suppose that the value -0.736 of exponent "d"

is universal in any sense. Secondly, the fluctuating component of heat loss may obey a different rule. The extension of Eqn. III-1 to include temperature and time-dependent effects will be considered subsequently.

It is worthwhile to consider the implications of the heat flux relation Eqn. III-1 for average whole-floor heat loss. In consequence of Eqn. III-1,

$$Q = c \cdot \left(\frac{A}{P}\right)^{d} \cdot A = c \cdot P^{-d} \cdot A^{1+d} \qquad \text{(III-2)}$$

If d has a value of -1, then Eqn. III-2 is independent of area and a linear function of perimeter. Values of d greater than -1 indicate a combined dependence on total area and perimeter. A value of 0 would indicate linear dependence on area and independence of perimeter. On physical grounds, it seems that possible values of d must lie between these limiting cases of 0 and -1. If d is greater than zero, Eqn. III-2 implies that an increase in perimeter would lead to decreased heat loss for a fixed area. A value of d less than -1 would imply that heat loss decreases as area increases. Both of these behaviors are implausible. For the Medford data presented above, Eqn. III-2 takes the particular form

$$Q = 12.783 \cdot P^{0.736} \cdot A^{0.264} \qquad \text{(III-3)}$$

The success of Eqn. III-1 as a model for the annual averaged flux provided motivation to investigate the application of this scaling

relationship to the daily averaged transient heat loss. Linear conduction theory permits the decomposition of the total floor heat flux into mean and fluctuating parts:

$$q_{total}(t) = q_{mean} + q_{periodic}(t) \qquad \text{(III-4)}$$

If it is assumed that the mean heat loss is proportional to the difference between the indoor air and outdoor ground surface temperatures and that the periodic loss is a function of the difference between the daily averaged and annual mean ground surface temperatures, then for a given floor:

$$q_{total}(t) = K_1 \cdot (T_{room} - T_{g,\,mean}) + K_2 \cdot (T_{g,\,mean} - T_{g,\,\phi}) \qquad \text{(III-5)}$$

Where K_1 and K_2 are constant mean and periodic conductances (SI units W/m^2-K) for that floor. $T_{g,\,\phi}$ is the time-dependent, phase lagged ground surface temperature. Ground surface temperature was chosen in preference to air and deep ground temperatures as an ambient reference because it more nearly represents conditions in the soil near the slab. As shown previously, air temperature may be considerably different than ground temperature (Fig. III-4) and deep ground temperature does not seem to influence the surface temperature (Fig. III-3). One must allow for the phase lag "ϕ" to account for the possibility that soil mass beneath a slab-on-grade will delay the effect of above-ground conditions on heat transfer.

The ground temperature, T_g, was approximated by a sinusoidal least squares model of data from soil temperature boundary condition files:

$$T_g = T_{g,mean} + \Delta T_g \cdot \sin\left(2\pi \frac{(Day+\zeta)}{365}\right) \qquad \text{(III-6)}$$

where ΔT_g is the amplitude of the annual ground temperature cycle, "Day" is the day of the year (1-365), and ζ is the phase shift (in days) of the ground temperature with respect to the calendar. $T_{g,\phi}$ differs from T_g only by virtue of the additional phase shift, ϕ:

$$T_{g,\phi} = T_{g,mean} + \Delta T_g \cdot \sin\left(2\pi \frac{(Day+\zeta+\phi)}{365}\right) \qquad \text{(III-7)}$$

To complete the model, the geometric scaling approach of Eqn. III-1 is used to approximate the geometric dependence of K_1 and K_2 for arbitrary floors. Each conductance is presumed to vary independently of the other, so each is equated with an expression of the same form as Eqn. III-1:

$$K_1 = c_1 \cdot \left(\frac{A}{P}\right)^{d_1} \qquad \text{(III-8a)}$$

$$K_2 = c_2 \cdot \left(\frac{A}{P}\right)^{d_2} \qquad \text{(III-8b)}$$

With substitution from Eqns. III-7 and 8, the complete daily averaged heat flux model of Eqn. III-5 becomes:

$$q_{total}(t) = c_1 \cdot \left(\frac{A}{P}\right)^{d_1} \cdot (T_{room} - T_{g,mean})$$

$$- c_2 \cdot \left(\frac{A}{P}\right)^{d_2} \cdot \Delta T_g \cdot \sin\left(2\pi \frac{(Day + \zeta + \phi)}{365}\right) \qquad \text{(III-9)}$$

Values of the constants c_1, c_2, d_1, and d_2 are determined by a two stage process. First, K_1 and K_2 values are calculated for a number of floor A/P values by least squares approximation of daily averaged heat flux results. Then, c_1, c_2, d_1, and d_2 are obtained by a second round of approximations using Eqns. III-8.

Numerical ground temperature "data" and the sinusoidal least squares ground temperature approximation "T_g" for the Medford, OR cases of Figs. III-11 and 12 are shown in Figure III-13a. Daily averaged heat flux results and the approximate model "q_{total}" for the 12 x 12 m uninsulated slab appear in Figure III-13b. Ground surface temperatures show much more scatter with respect to T_g than do heat flux results with respect to q_{total}. The relatively smoother heat flux data reflect the damping effect of soil thermal mass coupled to the floor. Another mass effect, the phase lag "ϕ", causes an offset between the day of peak heat loss and the day of minimum ground surface temperature in Fig. III-13. For this small building, ϕ is approximately eighteen days. (In fact, phase lag varied little with building size in this study. An average value of ϕ could be used with no significant error.)

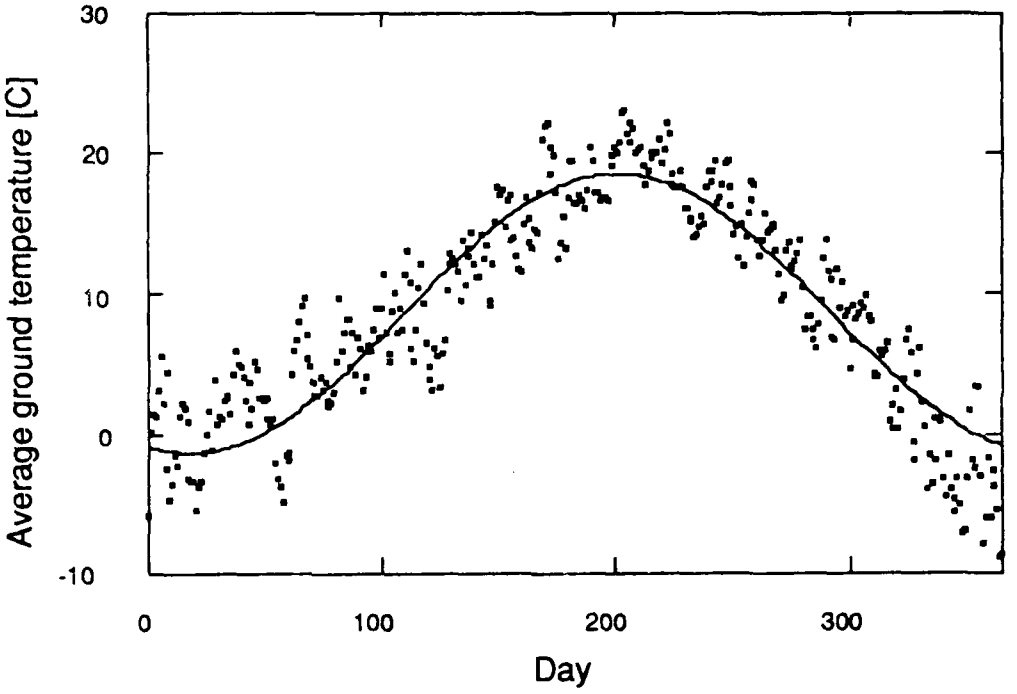

a)

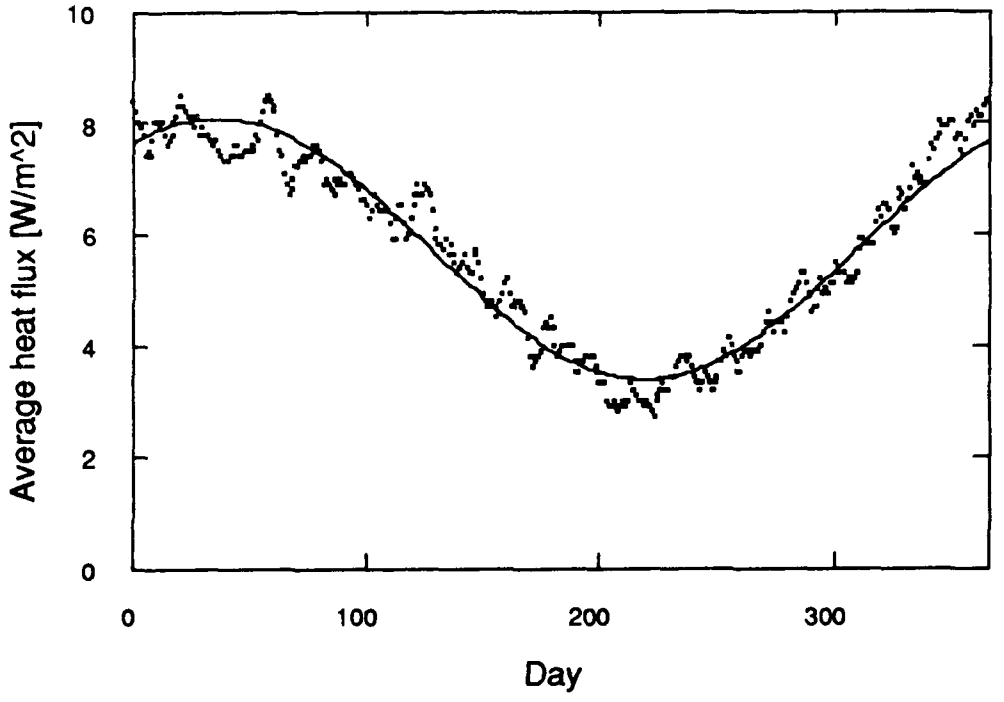

b)

Figure III-13. Daily-averaged heat loss model for a 12 x 12 m floor in Medford, OR. a) Average ground surface temperature. b) Average heat flux.

Table III-1 gives model coefficients for four representative uninsulated floors in Medford, OR. Values of K_1 and K_2 decrease with increasing A/P. Phase lag, on the other hand, increases slightly (by approximately one day) as area increases from 144 m^2 to 2025 m^2, but decreases as A/P increases for a given area. Values of c_1, c_2, d_1, and d_2 derived from these four cases are, respectively, 0.978, 0.713, -0.747, and -0.999. The values of c_1 and d_1, which pertain to the annual average component of heat loss, agree very well with the values of c and d (Eqn. III-1) computed for the entire Medford data set and shown in Fig. III-12. Exponents d_1 and d differ by only 1.5% of their mean value. The product of c_1 and the average indoor to ground surface temperature difference is similarly close to analogous constant, c (13.105 vs. 12.783). The good agreement between coefficients derived from both large and small sets of results is encouraging evidence that the scaling approach of Eqn III-1 has physical significance. Floor area seems to affect only the mean heat transfer rate. The value of d_2 differs from the area independent limit of -1 by less than 0.01%. Thus, the periodic component of heat loss is a strong function of perimeter and essentially independent of area.

Run ID	Dimensions	Area	A/P	K_1	K_2	$-\phi$
GR04	6 x 24 m	144 m^2	2.4 m	0.510 W/m^2	0.299 W/m^2	17.885 days
GR1A	12 x 12	144	3.0	0.428	0.236	17.811
GR8A	18 x 112	2016	7.75	0.212	0.093	18.812
GR5B	45 x 45	2025	11.25	0.161	0.064	18.381

Table III-1. Daily average heat loss model coefficients for Medford, OR. 15 m deep domain.

The effect of domain depth was investigated by comparing results for z_{max} = 10 m with the z_{max} = 15 m Medford results already presented. In all cases, the annual average heat loss was greater for z_{max} = 10 m, but the magnitude of the difference depended on A/P. Table III-2 compares the annual average heat loss for several floors as a function of z_{max}. For the smallest area, 144 m^2, there is no appreciable difference between the two cases. As area (and more particularly, A/P) increases, differences become

Dimensions	Area	A/P	$Q_{15\ m}$	$Q_{10\ m}$	Δ%
12 x 12 m	144 m^2	3.0 m	822.97 W	825.69 W	0.33
15 x 60	900	6.0	3062.71	3142.60	2.61
30 x 30	900	7.5	2583.86	2702.96	4.61
23 x 88	2024	9.1	5076.08	5386.06	6.11
45 x 45	2025	11.25	4367.89	4760.13	8.98
30 x 120	3600	12.0	7319.34	8001.86	9.32
60 x 60	3600	15.0	6467.18	7281.86	12.60

Table III-2. Effect of lower boundary depth on mean heat loss for uninsulated floors in Medford, OR.

larger. An explanation consistent with these results is that the strength of interaction between a floor and a lower boundary surface is related to the comparative magnitudes of A/P and the lower boundary depth. A small building with small A/P creates a temperature disturbance that does not penetrate very deeply into the ground. As size increases, the boundaries of the building-induced disturbance expand and the building's heat loss becomes sensitive to changes in conditions at greater and greater distances. In this sense, a boundary is only "deep" if it satisfies the twin criteria of

being beyond the annual penetration depth of the soil temperature distribution *and* deeper than the length scale of the building in question.

If the primary effect of the lower boundary is to influence the average loss from the entire floor area, and if proximity of the floor increases that influence, then raising the lower boundary will cause the exponent "d" in Eqn. III-1 to become smaller (since this would indicate an increased area effect). This, in fact, occurred when z_{max} was changed from 15 m to 10 m. For a set of four runs otherwise identical to those with z_{max} = 15 m, c and d values were 11.95 and -0.677, respectively. This result indicates that heat loss will grow more rapidly as A/P increases when z_{max} = 10 m than when z_{max} = 15 m. This effect could be caused by the interaction of a high water table with a slab floor.

III.B.2. EFFECTS OF CLIMATE

Assessment of climatic influences was based on simulations of four rectangular uninsulated slabs in each of four climates: Medford, OR; Minneapolis, MN; Philadelphia, PA; and Phoenix, AZ. Medford results were taken from series G. The other cases are grouped as series W in Appendix D. All had potential evapotranspiration ground surface conditions and mean outside dry bulb fixed temperature lower boundary conditions. Following the approach of the previous section, least squares models of daily averaged heat flux were computed and their coefficients were compared.

Table III-3 contains the parameters of sinusoidal least squares models (cf. Eqn. III-6) for air and ground temperature in each location. It is interesting to note the varying degrees of difference between ground surface and air temperature for the four sites. For the three temperate cases: Medford, Minneapolis, and Philadelphia, the mean ground temperature is depressed from 2.4 to 2.9 C beneath the average dry bulb and the amplitude* of the daily average ground temperature is within a degree of the air temperature amplitude. For Phoenix, however, which has a warm dry climate with year-round high evapotranspiration potential, the mean ground temperature is a full 6 C less than mean air temperature and the ground temperature model amplitude is 3.4 C smaller than the dry bulb amplitude.

	$I_{air,\ mean}$	ΔI_{air}	ζ_{air}	$I_{g,\ mean}$	ΔI_g	ζ_g
Medford, OR	11.4 C	-9.7 C	69.2 Days	8.6 C	-9.9 C	73.0 Days
Minneapolis, MN	7.2	-17.0	72.3	4.8	-16.3	72.6
Philadelphia, PA	12.4	-12.6	68.9	9.5	-12.1	68.8
Phoenix, AZ	21.9	-11.7	72.2	15.9	-8.3	68.3

Table III-3. Mean, amplitude, and phase shift for models of daily averaged air and ground surface temperatures.

According the data summarized by Kusuda and Achenbach [39], the average ground temperature depression obtained for Phoenix is larger than would occur naturally. The large amount of precipitation needed to maintain potential evapotranspiration conditions in this

* Values of amplitude in Table III-3 are negative as a result of the form of the model and the choice of representation for phase shift. Only the magnitude is of significance to this discussion.

environment simply is not available. It is not impossible, however, that such a condition could be induced locally by watering and/or shading. These results demonstrate that air temperature may not be a reliable indicator of ground temperature when accuracy is important. Because mean losses depend on relatively small temperature differences, large uncertainty is introduced by using the indoor/outdoor air temperature difference as the reference for floor heat loss. Figure III-14 compares the models for air and ground temperature in Phoenix, AZ, the case of worst agreement. The two curves are closest during the winter when evaporation potential is lowest and farthest apart during the summer when it is highest. The maximum summer difference is in excess of 10 C.

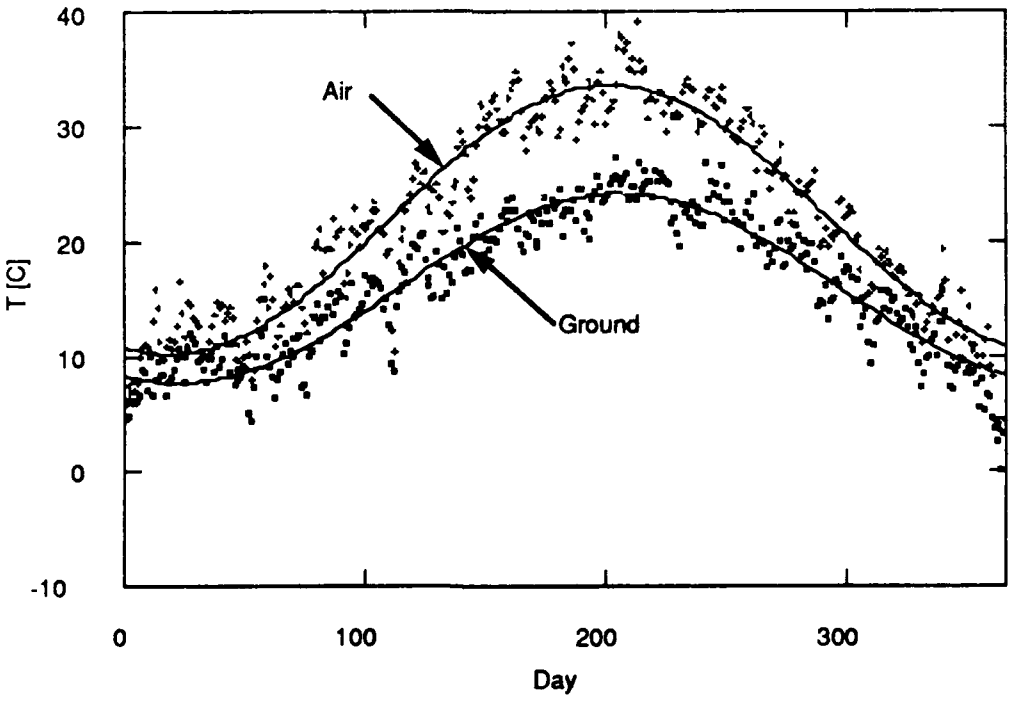

Figure III-14. Daily averaged air and ground surface temperatures for Phoenix, AZ (potential evapotranspiration).

Table III-4 gives K_1, K_2, and ϕ values for the Minneapolis, Philadelphia, and Phoenix series "W" runs. The corresponding results for Medford were tabulated previously in Table III-1. Comparing coefficients K_1 and K_2 case by case, it is evident that the models for Medford, Minneapolis, and Philadelphia are quite consistent with one another. Differences between the amplitudes of annual temperature variation in Medford and Philadelphia, which have similar mean conditions, are responsible for the somewhat higher Philadelphia K_2 values. The spread among these three sites is on the order of 10% or less of the mean. Because their model coefficients are so similar, it is reasonable to conclude that differences in climate reduce to differences in ground temperature annual mean and amplitude in these cases*. K_2 values for Phoenix are in good agreement with the other three sites, but values of K_1 are significantly lower.

This set of runs confirmed the correctness and importance of choosing soil temperature rather than air temperature as the exterior reference condition in Eqn. III-5. Values of K_1 and K_2 obtained relative to an air temperature reference showed a systematic variation with annual average temperature from one climate to another. Values obtained with a ground temperature reference were more nearly independent of climatic changes. The

* It should not be forgotten, however, that more subtle effects of climate variation are not explicitly incorporated in this model. For instance, the effect of evaporative heat transfer is greatest in warm weather and practically vanishes during cold weather. Consequently, (as will be shown in a subsequent section) evapotranspiration may be relatively uniform over the entire year in a warm climate such as Phoenix and quite seasonal in a cold climate similar to Minneapolis. In the present case, this effect is apparent only in the differing ground temperature depressions recorded in Table III-3.

a) Minneapolis, MN

Run ID	Dimensions	Area	A/P	K_1	K_2	$-\phi$
WMN3	6 x 24 m	144 m^2	2.4 m	0.527 W/m^2	0.318 W/m^2	16.503 days
WMN1	12 x 12	144	3.0	0.440	0.251	16.467
WMN4	18 x 112	2016	7.75	0.221	0.099	17.226
WMN2	45 x 45	2025	11.25	0.170	0.068	17.413

b) Philadelphia, PA

Run ID	Dimensions	Area	A/P	K_1	K_2	$-\phi$
WPH3	6 x 24 m	144 m^2	2.4 m	0.525 W/m^2	0.322 W/m^2	16.104 days
WPH1	12 x 12	144	3.0	0.437	0.254	15.854
WPH4	18 x 112	2016	7.75	0.217	0.101	16.681
WPH2	45 x 45	2025	11.25	0.165	0.069	16.822

c) Phoenix, AZ

Run ID	Dimensions	Area	A/P	K_1	K_2	$-\phi$
WPX3	6 x 24 m	144 m^2	2.4 m	0.473 W/m^2	0.323 W/m^2	15.930 days
WPX1	12 x 12	144	3.0	0.386	0.255	15.833
WPX4	18 x 112	2016	7.75	0.167	0.101	16.504
WPX2	45 x 45	2025	11.25	0.115	0.069	16.722

Table III-4. Daily heat loss model coefficients for climate variation tests. (Case by case).

cause of strong climate dependence in the former case is the increase in fractional error due to the presumed equivalence of air and ground temperatures as these values approach the reference indoor temperature. For example, if the indoor set point is 22 C, the outdoor air mean is 7.2 C, and the mean ground temperature is 4.8 C (as in Minneapolis), then the ratio of the mean indoor/outdoor air temperature difference to the mean indoor/ground surface temperature difference is (22 - 7.2)/(22 - 4.8), i. e., 0.86. The two differ by only fourteen percent. In Phoenix, however, where the mean air and ground temperatures were, respectively, 21.9 C and 15.9 C, the corresponding ratio of temperature differences was 0.016. In this case, the indoor/outdoor air temperature difference is nearly two orders of magnitude smaller than the mean difference actually imposed on the floor. When the air reference temperature differs from the "actual" temperature difference, K_1 must change by an amount proportional to the error in order to obtain the correct mean heat loss. As this example shows, that correction would be much larger for Phoenix than for Minneapolis, so K_1 and K_2 would lose their independence of climate. The obvious way to avoid this problem is to adopt a ground temperature reference as was done in this study.

Table III-5 gives coefficients of daily averaged heat flux models for arbitrary A/P derived from the data of Table III-4. These also show the strong similarity between results for Medford, Minneapolis, and Philadelphia. In all four locations the time varying component of heat loss was linearly proportional to perimeter length and independent of area ($d_2 \approx -1.0$). The primary difference

between Phoenix and the other sites is the degree of area dependence of the steady state heat transfer component (much weaker for Phoenix). It may be that d_1 was larger for Phoenix because the deep ground and indoor temperatures were nearly identical. When there is no mean temperature difference between the floor and the deep ground, any mean loss must be toward the ground surface from the floor perimeter. In this limit, the mean loss should depend on perimeter in a manner similar to the periodic loss.

Location	c_1	d_1	c_2	d_2
Medford, OR	0.978	-0.747	0.713	-0.999
Minneapolis, MN	0.997	-0.735	0.759	-0.999
Philadelphia, PA	1.007	-0.750	0.765	-0.995
Phoenix, AZ	1.041	-0.901	0.769	-0.997

Table III-5. Daily averaged heat loss model coefficients for climate variation tests. (Composite).

An indication of the magnitude of climatic variations in total heat loss from a typical floor is given by Table III-6, which compares the minimum, maximum, and average rates of heat loss over a year for an uninsulated 12 x 12 m floor in each of the four climates. The average annual heat loss varies by more than a factor of three from Phoenix to Minneapolis. With the exception of Phoenix, the floor experienced significant net heat loss to the ground throughout the entire year--losses approaching or exceeding a kilowatt on average and nearly two kilowatts maximum. Differences between maximum loss values (winter) were considerably larger

than those between minimum (summer) values. Here, again, is an instance of the difference between the summer and winter regimes. Above-ground climate dominates during the winter, causing large regional differences to appear. During the summer, the smaller floor/mean ground temperature difference determines the floor's heat loss and the distinction between climates is not so clearly defined. The difference between coastal and inland climates is evident in the extreme heat loss rates for Medford and Philadelphia. Although the Medford case has a larger mean loss by 40 W, Philadelphia has a larger maximum by more than 100 W and a smaller minimum by 80 W.

Location	Run ID	Q_{min} [W]	Q_{max} [W]	Q_{avg} [W]
Medford, OR	GR1A	388.8	1224.0	825.7
Minneapolis, MN	WMN1	403.2	1915.2	1088.9
Philadelphia, PA	WPH1	302.4	1339.2	784.3
Phoenix, AZ	WPX1	-14.4	734.4	336.3

Table III-6. Annual heat loss from an uninsulated 12 x 12 m slab in four climates.

III.B.3. EFFECT OF POTENTIAL EVAPOTRANSPIRATION BOUNDARY CONDITION

The set of runs identified as series "E" in Appendix D provided data to demonstrate the effect of suppressed latent loss at the ground surface. The series comprised four runs with different A/P values in Minneapolis weather and one run each for Medford, Philadelphia, and Phoenix--all with evapotranspiration turned off.

The Minneapolis results were used to compute a daily flux model (Eqn. III-9) for comparison with the corresponding series W model.

Table III-7 summarizes ground surface temperature statistics for the zero evapotranspiration cases. Mean temperatures are higher than average air temperature by 1 to 4 C and surface temperature amplitude exceeds air temperature amplitude. In contrast, the corresponding potential evapotranspiration cases summarized in Table III-3 yielded mean ground temperatures several degrees lower than air temperature and ground temperature amplitudes that were generally smaller than those of air. The difference in mean ground temperature due to inclusion or neglect of latent loss at the ground surface varied from a minimum value of 3.5 C for Minneapolis, to a maximum of 10 C for Phoenix. The respective differences in magnitude of surface temperature amplitude for these two cases were 2.8 C and 4.5 C.

	$I_{air,\ mean}$	ΔI_{air}	ζ_{air}	$I_{g,\ mean}$	ΔI_g	ζ_g
Medford, OR	11.4 C	-9.7 C	69.2 days	13.2 C	-13.8 C	74.6 days
Minneapolis, MN	7.2	-17.0	72.3	8.3	-19.1	74.6
Philadelphia, PA	12.4	-12.6	68.9	13.4	-14.1	71.1
Phoenix, AZ	21.9	-11.7	72.2	25.9	-12.8	75.2

Table III-7. Mean, amplitude, and phase shift for sinusoidal least squares models of daily averaged air and ground surface temperatures without evapotranspiration.

Figure III-15 compares potential evapotranspiration and zero evapotranspiration ground surface temperatures for Minneapolis and Phoenix to the coincident outdoor dry bulb in those locations. Differences between air and ground temperature are smallest during the winter and largest during the summer because of seasonal variation in both evapotranspiration and solar radiation. The high potential latent loss created by the warm, dry climate of Phoenix causes the evapotranspiration curve to fall considerably below those for air temperature and no evapotranspiration. In Minneapolis, the difference between the three is much smaller throughout the year and virtually vanishes during the winter.

Comparative heat loss data for 12 x 12 m uninsulated slabs under zero evapotranspiration conditions are given in Table III-8. Due to upward shifted ground temperature means, the average loss in each case is considerably lower than in the analogous potential evapotranspiration case (Table III-6). Phoenix, which showed a small net heat loss with evapotranspiration, now experiences a net gain of the same magnitude. The respective absolute and percentage changes in mean heat loss for Minneapolis, Medford, Philadelphia, and Phoenix were -203.9 W/-18.7%, -267.1 W/-32.4%, -227.8 W/-28.4%, and -573.1W/-170.4%. Two of the other cases which previously had net loss minima now have days of net heat gain. The seasonal differences in heat loss between potential and zero evapotranspiration cases are analogous to the variations in surface temperatures considered above. Maximum heat loss values, which occur during the winter, differ by less than minimum values, which occur during the summer. Consequently, the impact of the surface

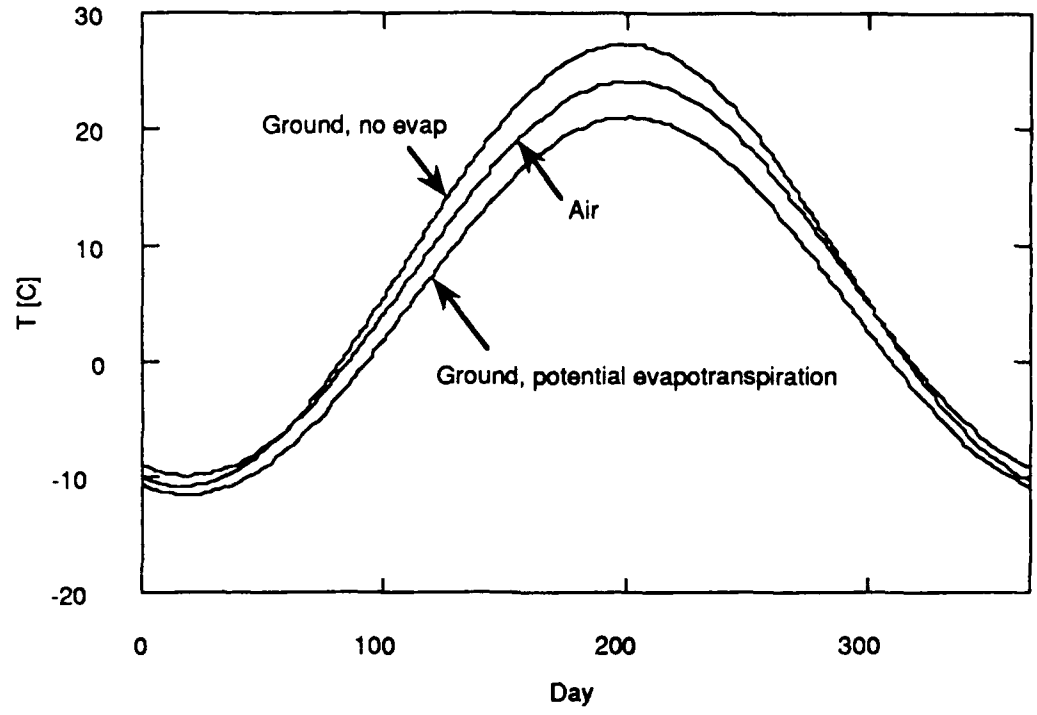

a) Minneapolis, MN

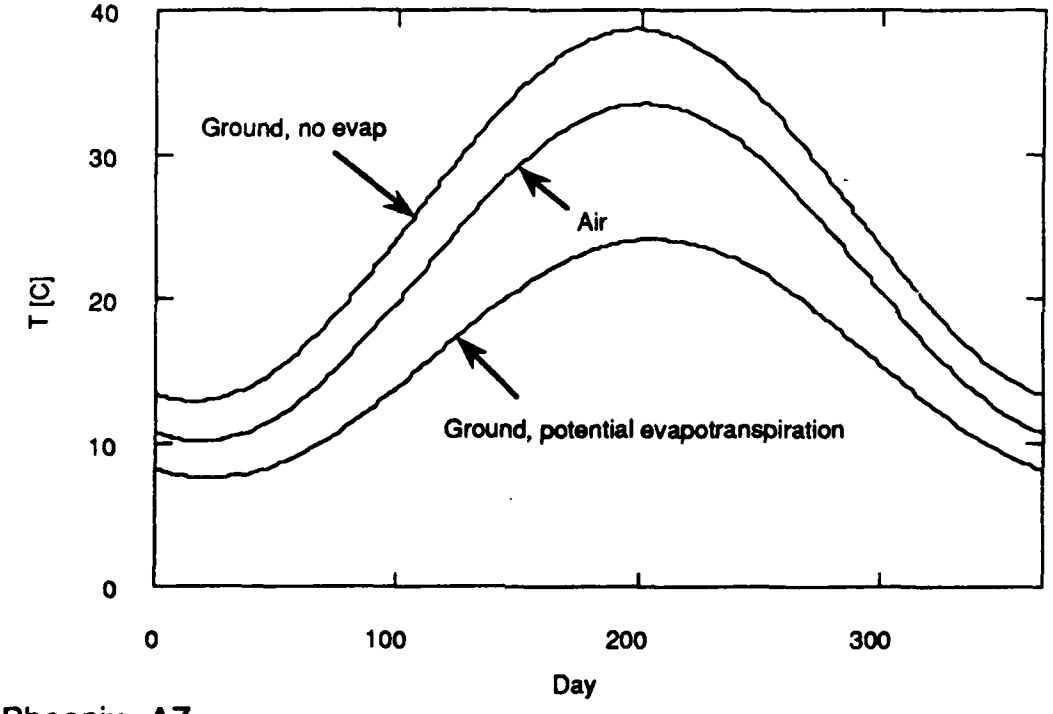

b) Phoenix, AZ

Figure III-15. Effect of boundary latent heat transfer on daily-averaged ground surface temperature.

latent loss is a greater source of potential error during the cooling season. The differences in Q_{max} between the potential evapotranspiration and no evapotranspiration cases are -81 W/ -4.2%, -129.6 W/-10.6%, -144.0 W/-10.8%, and -345.6 W/-47.1%, respectively for Minneapolis, Medford, Philadelphia, and Phoenix. Because evapotranspiration potential increases with air temperature, changes in both mean and extreme heat loss increased with site mean air temperature.

Location	Run ID	Q_{min} [W]	Q_{max} [W]	Q_{avg} [W]
Medford, OR	EMD1	-57.6	1094.4	558.6
Minneapolis, MN	EMN1	86.4	1843.2	885.0
Philadelphia, PA	EPH1	-14.4	1195.2	561.5
Phoenix, AZ	EPX1	-806.4	388.8	-236.8

Table III-8. Annual heat loss from an uninsulated 12 x 12 m slab in four different climates. No evapotranspiration.

The influence of evapotranspiration on the area dependence of floor heat loss was investigated by comparing least squares models based on the four Minneapolis cases of series W and E (respectively, potential and zero evapotranspiration). Coefficients c_1, d_1, c_2, and d_2 had values of 0.980, -0.700, 0.756, and -0.992, respectively in the no evapotranspiration case. The corresponding potential evapotranspiration values (Table III-5) were 0.997, -0.735, 0.759, and -0.992. The primary difference was a small (perhaps insignificant) increase in area dependence of the steady state flux in the zero evapotranspiration case. There is no clear-cut explanation for this behavior. A possible cause is the effect of a fixed lower

boundary temperature when it differs from the average surface temperature. In the potential evapotranspiration case, the mean ground surface temperature for Minneapolis was 4.8 C while the deep ground temperature was maintained at 7.2 C. When evapotranspiration is turned off, the average surface temperature increased to 8.3 C, a higher value than the deep ground temperature. The existence of a greater mean temperature difference between the floor and deep ground than between the floor and ground surface could, perhaps, cause the heavier weighting of area in the no evapotranspiration case.

III.B.4. EFFECT OF GROUND SHADOW FROM BUILDING

The influence on floor heat loss of the building shadow cast on the ground is a question which, perhaps justly, has received no attention in the literature heretofore. Intuitively, one would imagine that this is a negligible effect. In order to decide the issue "once and for all," however, a series of runs was performed to assess the magnitude of its contribution. Because full three-dimensional computations with a refined surface grid are quite time consuming, only a 144 m^2 plan area was considered. The height of this residential sized building was four meters in all cases. Three uninsulated rectangular cases were simulated, all with Medford weather and potential evapotranspiration: square, 6 x 24 m long north-south, and 6 x 24 m long east-west. Two additional 12 x 12 m square runs, one with no evapotranspiration and one with Phoenix

weather and potential evapotranspiration were performed to obtain information about surface boundary and climate effects.

Figure III-16 shows daily averaged heat loss values for the 12 x 12 m Medford case with evapotranspiration. Heat loss from the simulation with shading is greater than that from the no shade case throughout the year, but more so during the summer. This pattern is more apparent in the comparison of monthly averaged heat loss rate results, Figure III-17. Averaged over the entire year, heat loss from the shaded slab is 6.5% greater than from the unshaded slab (a difference of 53 W). The greatest monthly average difference, 17.2%

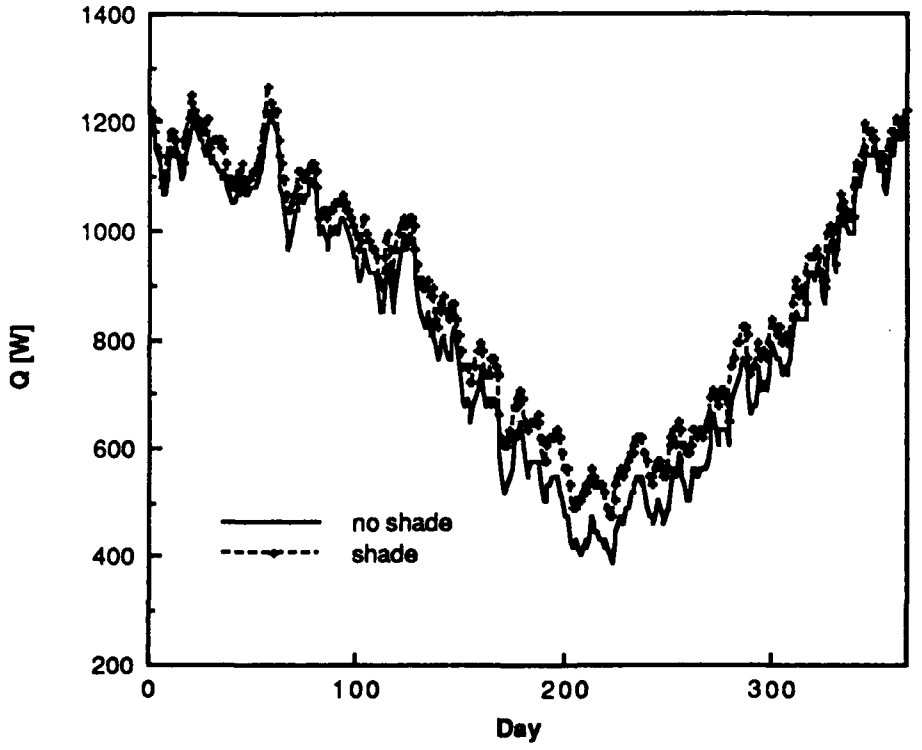

Figure III-16. Effect of building shadow on daily-averaged heat loss from a 12 x 12 m uninsulated slab in Medford, OR.

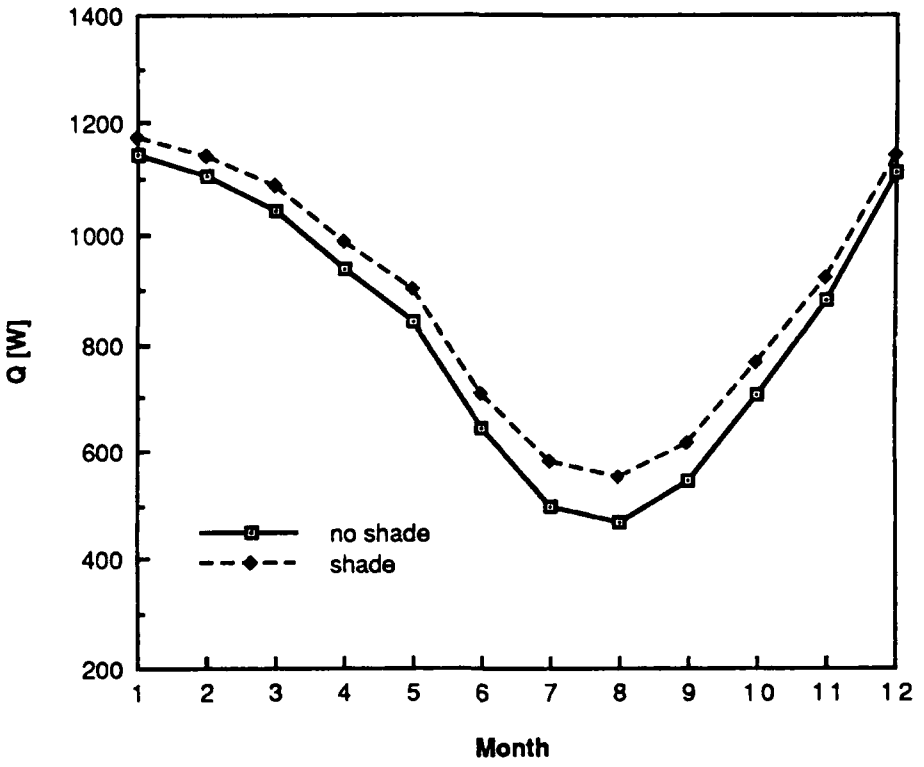

Figure III-17. Effect of building shadow on monthly-averaged heat loss from a 12 x 12 m uninsulated slab in Medford, OR.

(84 W) occurs during July. Differences between shade and no shade heat loss for the two 6 x 24 m runs were only slightly larger than those for the square case (7.3% annually and 19.6% maximum.) Somewhat surprisingly, orientation did not have a significant effect on heat loss. Values for north-south and east-west major axis orientations were virtually identical. In the absence of evapotranspiration, the effect of shade was more pronounced. Annual average heat loss increased by 14% (78 W) for the 12 x 12 m slab in Medford while the maximum difference on a monthly average basis climbed to 127 W. The impact of shade may have been less with evapotranspiration included because the latent loss provided a

mechanism for removing solar energy without raising ground temperature. Without evapotranspiration, shade prevents energy from reaching the ground that otherwise would have contributed directly to a rise in surface temperature.

The effect of shade in the warmer, sunnier Phoenix climate is qualitatively and quantitatively different from that in more northern Medford. The mean difference in heat loss resulting from shade is larger: 92 W / 27.4% greater than the no shade case. As Figure III-18 shows, seasonal differences between shade and no shade cases

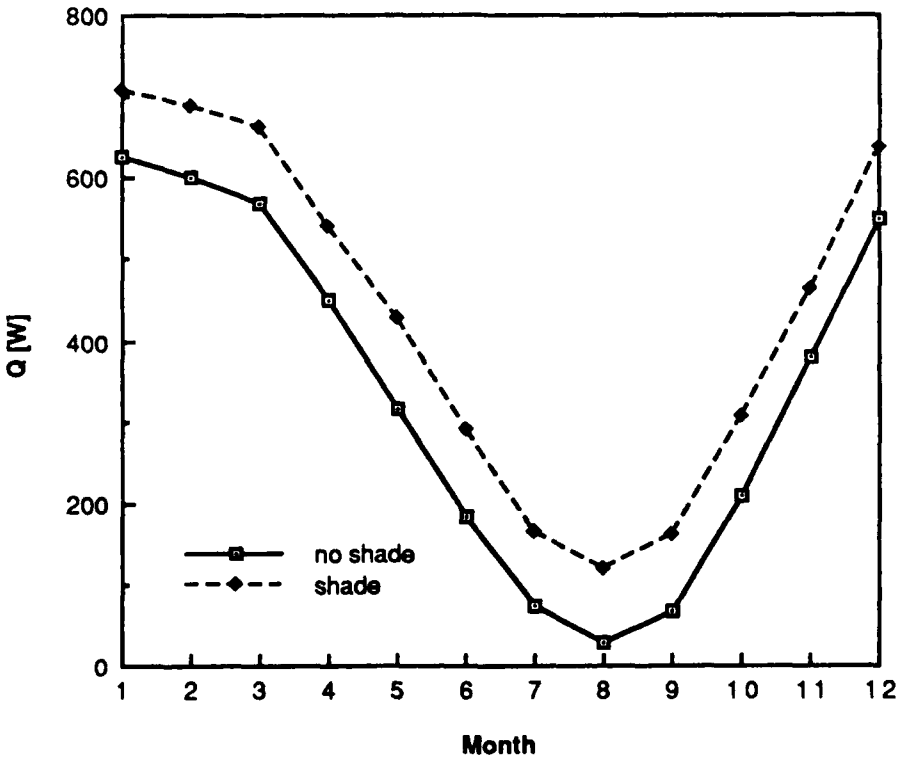

Figure III-18. Effect of building shadow on monthly-averaged heat loss from a 12 x 12 m uninsulated slab in Phoenix, AZ.

are much smaller than in Medford. To some extent, this difference is the result of sky conditions. The Medford TMY weather file used in this study contains a long period of time during the winter months when beam solar radiation is quite small due to overcast skies. Phoenix, on the other hand, has generally clear skies all year.

In the northern hemisphere, shadows fall predominantly on the north side of objects, leading humans to glaze south facades heavily and causing moss to grow on the north sides of trees. This asymmetry of the shadow pattern causes the ground on the north side of a building to be somewhat cooler than that on the south side. This localized cooling effect causes the increases in floor heat loss noted above. Figure III-19 indicates the extent of asymmetry in the

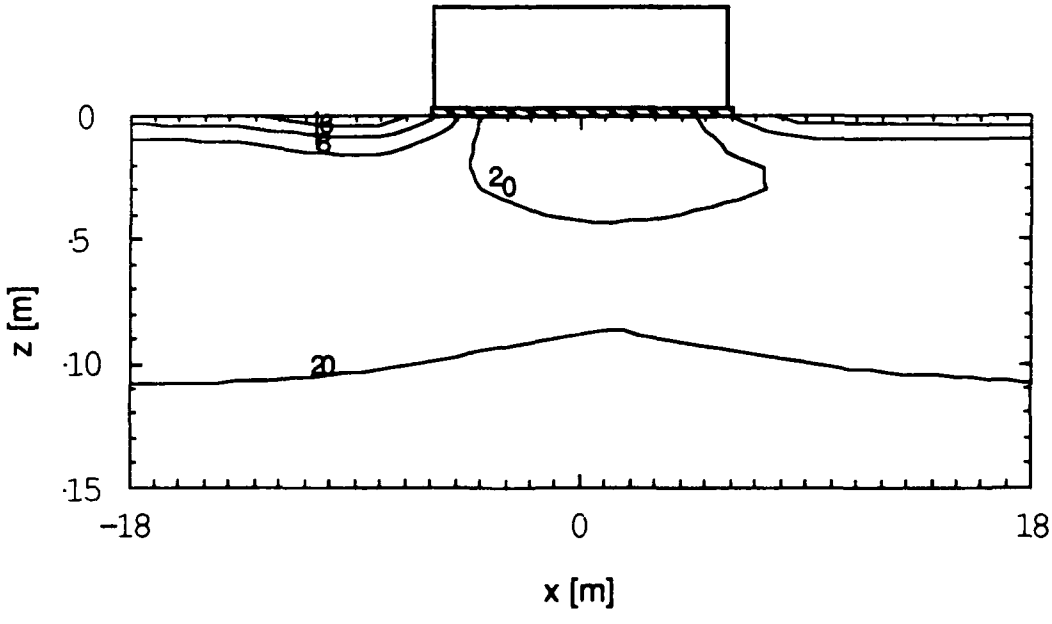

Figure III-19. Daily-averaged October 21 soil isotherms beneath a 12 x 12 m uninsulated slab in Phoenix with ground shadowing .

temperature distribution on the vertical section along the north-south axis of a 12 x 12 m slab in Phoenix. The north edge of the slab (x = -6 m) is roughly two degrees cooler than the south edge. The effect of the surface condition penetrates deeply enough to influence the size of the warm core beneath the floor to a depth of at least five meters. On the north side of the building, the disturbance to surface temperature caused by shade is concentrated in a zone extending roughly five meters horizontally outward from its edge.

III.B.5. EFFECTS OF SOIL THERMAL PROPERTY VARIATION

In series K, four different combinations of soil k and α were applied to uninsulated floors with four values of A/P in Philadelphia weather. The standard boundary conditions applied in other series also applied to this group, namely, potential evapotranspiration at the ground surface and fixed temperature in the deep ground. The series W Philadelphia runs, which had "base case" properties, provided a fifth set of results. The five property groups are listed in Table II-2. Property sets were chosen in such a way as to permit isolation of thermal conductivity and thermal diffusivity effects. Two pairs (base case/B and A/D) have like conductivity but different diffusivity values, and two (base case/A and B/C) have like diffusivity but different conductivity values. In total, three values each of diffusivity and conductivity were considered. Conductivity varied by a factor of two in both directions from the base value.

Diffusivity varied from a factor of two smaller to a factor of 1.3 larger than the base value.

Although soil property variations produced large changes in floor heat loss, undisturbed ground surface temperatures were little affected by either conductivity or diffusivity. The many competing surface flux components apparently adjusted to soil property variations in such a way that soil temperature was effectively unchanged. Across the five property sets, mean ground temperature varied from a low of 9.33 C to a high of 10.01 C, a range of only 0.68 C. Extreme surface temperature values varied somewhat more, but no more than 2.5 C. The only noticeable effect on the soil temperature profile was an increase in penetration depth with increasing thermal diffusivity, a behavior predicted by the semi-infinite medium solution.

The total, daily averaged heat loss results for varied property runs summarized in Table III-9 show that conductivity and diffusivity have much different impacts on heat loss. The most important effect of thermal conductivity is its role in determining the mean heat loss from a floor. For example, Q_{avg} for the 45 x 45 m floor varies from less than 2500 W to more than 7000 W over a thermal conductivity range from 0.5 W/m-K to 2.0 W/m-K. Thus, a four-fold increase in thermal conductivity produces a nearly three-fold increase in mean heat loss.

Diffusivity has a negligible effect on the mean value of heat loss because thermal mass is irrelevant to steady state heat transfer processes. (Thermal diffusivity vanishes from the heat conduction equation in the steady state case.) For example, consider

Dimensions (Area)	Properties	Q_{min}	Q_{max}	Q_{avg}
12 x 12 m (144 m^2)	Base	302.4 [W]	1339.2 [W]	784.3 [W]
"	A	547.2	1987.2	1226.6
"	B	345.6	1267.2	781.8
"	C	187.2	835.2	482.9
"	D	504.0	2030.4	1227.9
6 x 24 (144)	Base	331.2	1641.6	941.8
"	A	576.0	2419.2	1454.0
"	B	388.8	1555.2	937.2
"	C	201.6	1022.4	584.0
"	D	532.8	2476.8	1454.9
45 x 45 (2025)	Base	2227.5	6277.5	4152.6
"	A	4252.5	9922.5	7003.7
"	B	2632.5	6075.0	4207.6
"	C	1215.0	3847.5	2450.5
"	D	4252.5	10125.0	6997.6
18 x 112 (2016)	Base	2822.4	8467.2	5443.2
"	A	5241.6	13305.6	9018.9
"	B	3024.0	8064.0	5463.6
"	C	1612.8	5040.0	3232.2
"	D	5040.0	13507.2	9026.7

Table III-9. Heat loss data for varied thermal property cases. Philadelphia, PA weather and potential evapotranspiration.

the difference in mean heat loss between the base and set B property cases for an 18 x 112 m floor. The 20 W discrepancy is less than 0.5% of the mean, an insignificant difference for practical purposes. Diffusivity *does* influence the annual range of heat loss. For a given value of conductivity, larger ranges of heat loss correspond to larger diffusivity values. For instance, the difference between Q_{max} and Q_{min} for the property set B (k = 1 W/m-K, α = 3.5 x 10^{-7} m^2/s) 12 x 12 m floor is 921.6 W. The annual range with base case properties (same conductivity, but a larger diffusivity of 6.9 x 10^{-7} m^2/s) is 1036.8 W. An increase of approximately 100% in thermal diffusivity causes the annual range to widen by 115.2 W, an increase of only 12.5%.

Thermal conductivity, too, affects the amplitude of annual heat loss. Returning to the previous example, if the base case thermal diffusivity is fixed and conductivity is doubled (as in case A), the annual heat loss range increases to 1440.0 W, a change of 518.4 W, or 56.3%. The greater influence of conductivity shown by these examples indicates that heat loss on a daily averaged scale is quasi-steady with respect to the soil temperature distribution. Figure III-20 gives further evidence of the relative importance of conductivity and diffusivity on the daily scale. Fig. III-20a shows distance weighted least squares approximations to the daily averaged unit heat flux of the 12 x 12 m base and set B property groups. There is no significant change in mean heat loss and only a small change in amplitude. In Fig. III-20b, a large shift in mean heat loss is evident when conductivity changes by a factor of two with diffusivity held constant. The sizeable offset between the two

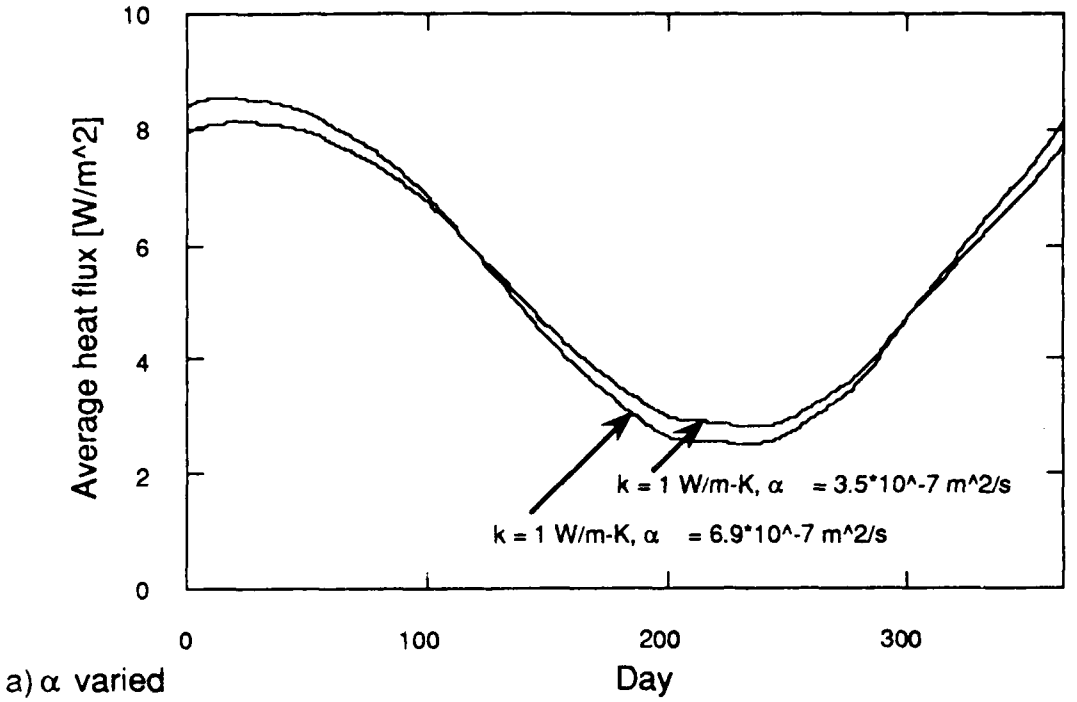

a) α varied

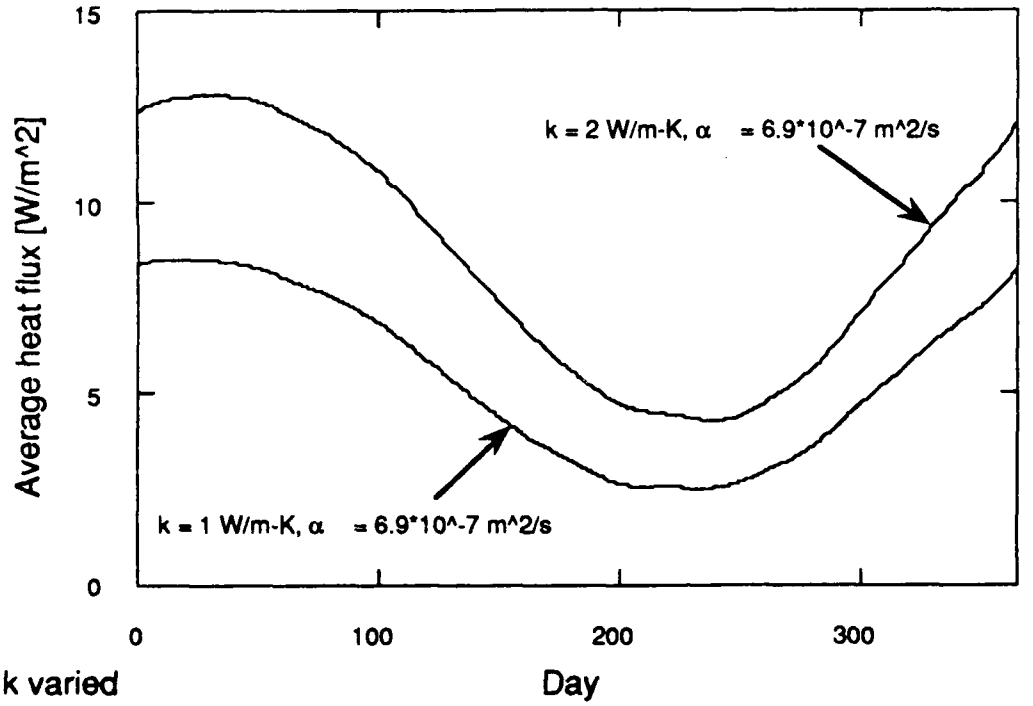

b) k varied

Figure III-20. Typical effects of k and α variation on smoothed, daily-averaged heat loss from a 12 x 12 m floor.

curves reduces the difference between the minimum values occurring during the summer and exaggerates the difference in winter maxima. The greatest difference approaches 5 W/m^2, considerably larger than the magnitude of the diffusivity effect in Fig. III-20a.

Thermal property values also influence the area dependence of floor heat loss. The nature of such effects can be shown through the use of the least squares model employed in previous sections. Figure III-21 shows K_1 and K_2 coefficients as a function of A/P for the cases summarized in Table III-9. Curves through the plotted values of K_1 and K_2 are instances of Eqns. III-8a and III-8b, respectively. Each curve is labelled to show its values of c_1 and d_1 or c_2 and d_2 as appropriate. The observations made above concerning conductivity and diffusivity dependence are readily apparent in these plots.

In Figure III-21a, K_1 values for cases with the same conductivity but different diffusivities essentially coincide, indicating the absence of a diffusivity effect on mean heat loss. Fractional changes in K_1 are comparable to, but smaller than, corresponding changes in k. The area effect of thermal conductivity on K_1 increases with increasing k. This is indicated by the decreasing magnitude of d_1 (the exponent of A/P) as k becomes larger. Area dependence increases because heat loss from the low gradient core region of the floor grows more rapidly than edge loss when k increases, thus weighting total area more heavily. The results presented in Table III-10 illustrate this phenomenon. For both 12 x 12 m and 45 x 45 m floors, the floor center heat loss

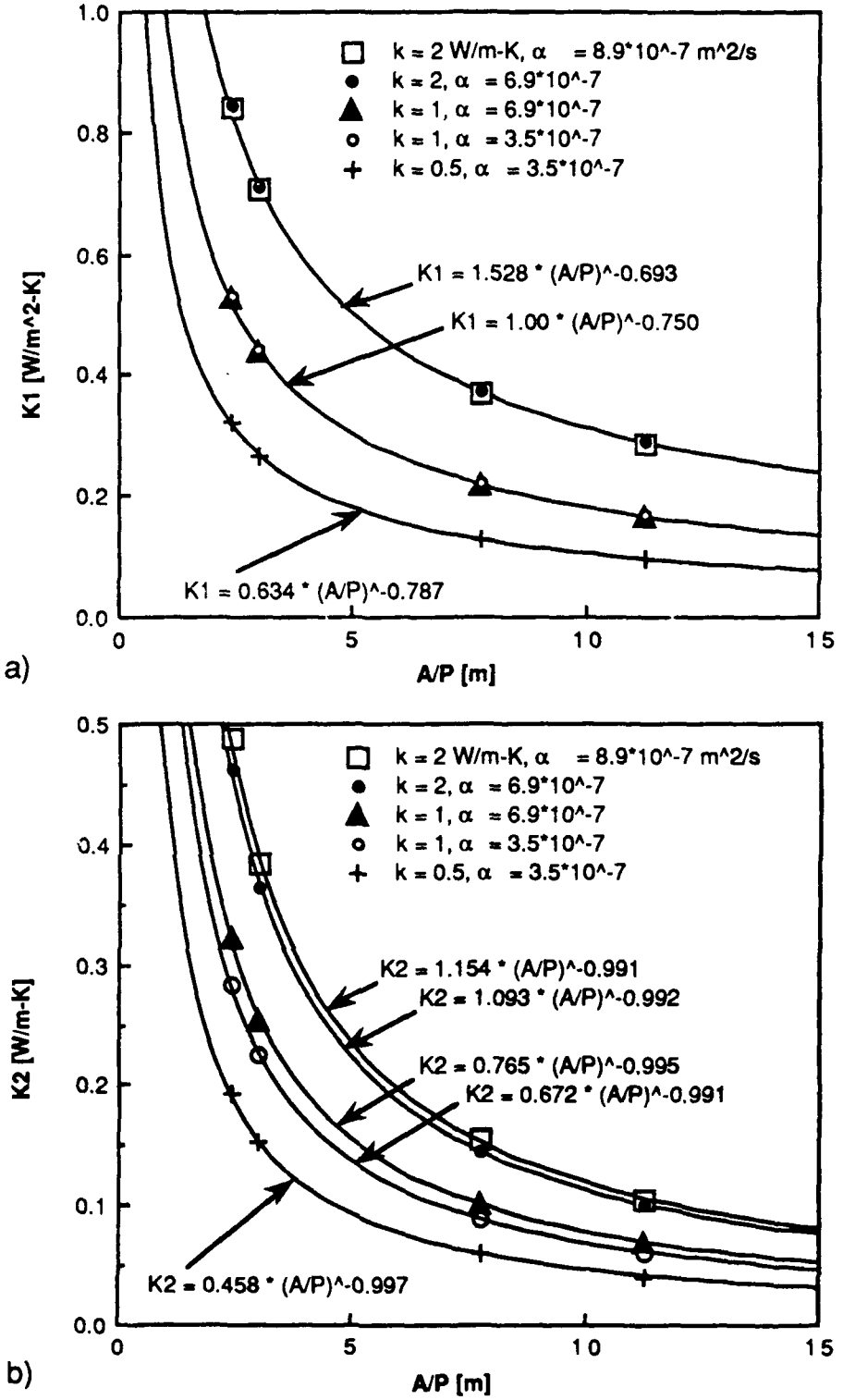

Figure III-21. Influence of soil properties on area dependence of floor heat loss. a) mean b) amplitude.

Property Set	k	q_{center}	Δq_{center}	$q_{edge,\ max}$	Δq_{edge}	q_{avg}	Δq_{avg}
Base	1 W/m-K	1.8 W/m^2	0%	69.0 W/m^2	0%	7.9 W/m^2	0%
A	2.0	3.5	94.4	78.9	14.4	12.2	54.4
C	0.5	0.9	-50.0	55.5	-19.6	4.7	-40.5

a) 12 x 12 m

Property Set	k	q_{center}	Δq_{center}	$q_{edge,\ max}$	Δq_{edge}	q_{avg}	Δq_{avg}
Base	1 W/m-K	0.7 W/m^2	0%	68.9 W/m^2	0%	2.7 W/m^2	0%
A	2.0	1.4	100.0	78.8	14.4	4.5	66.7
C	0.5	0.4	-42.9	55.5	-19.5	1.6	-40.7

b) 45 x 45 m

Table III-10. Thermal conductivity influence on floor center and edge heat loss values for two uninsulated slabs in Philadelphia, PA, January 21.

changes almost in direct proportion to the soil conductivity (i. e., if k is reduced by a factor of two, the center flux is halved.) Maximum edge flux values, however, change by 20% or less in response to two-fold increases and decreases in k. Thus, more of the difference in floor average heat loss results from changes in core loss.

The value of K_1 decreases more rapidly with increasing A/P for lower values of conductivity. Consequently, the fractional change in K_1 due to a given increase in conductivity grows with increasing A/P. The percentage change in mean heat loss resulting from an increase of k from 1 W/m-K to 2 W/m-K with α fixed at 6.9 x 10^{-7} (base case vs. set A properties), for a 6 x 24 m slab (A/P = 2.4 m) is 54.4%. When A/P increases to 3 m (12 x 12 m square), the fractional

change increases to 56.4%. Floors with A/P values of 7.75 m (18 x 112 m rectangle) and 11.25 m (45 x 45 m square) experience increases of 65.7% and 68.7%, respectively.

Figure III-21b, which shows K_2 as a function of A/P, confirms other observations made previously. This plot clearly indicates the subordinate role that thermal diffusivity plays to conductivity in the determination of K_2 and consequently, the periodic component of floor heat loss. Note that cases with like conductivity fall much closer together than those with like diffusivity but different conductivities. As in other cases examined above, K_2 for these varied property groups is essentially proportional to $(A/P)^{-1}$, indicating linear dependence on perimeter of the periodic component of total heat loss.

Floor heat loss phase lag results are summarized in Figure III-22. (Because of the convention for ϕ adopted in Eqn. III-7, a negative value of phase lag indicates floor heat flux *following* the ground temperature history.) For the cases considered, ϕ ranged from two to three weeks. Clearly, soil properties exercised a much stronger influence on phase lag than floor size. Although there is some pattern to the size dependence of these results, a clear relationship such as that deduced for K_1 and K_2 is not apparent. For a given set of properties, ϕ varied by two days or less. Lower values of soil conductivity corresponded to less phase lag, and for a given conductivity, an increase in thermal diffusivity of the soil caused ϕ to decrease. Phase lag, like the conductances K_1 and K_2, was more responsive to changes in conductivity than to changes in diffusivity. While the magnitudes of ϕ observed in this study were not

particularly large, two to three week lags are significant because they support an argument against models based on instantaneous indoor outdoor temperature differences. The floor heat loss on a particular day results from weather events over a prior period of several weeks.

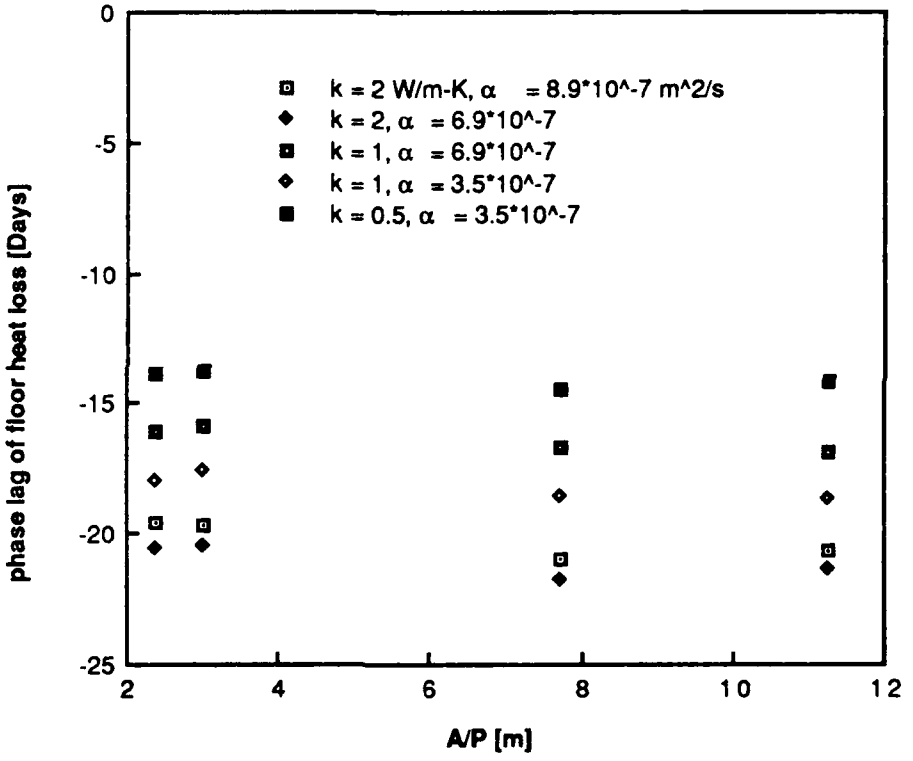

Figure III-22. Effects of thermal conductivity and thermal diffusivity on phase lag of floor heat loss.

The results of this series of tests clearly show that soil thermal conductivity must be a parameter in any simplified model of

slab-on-grade heat loss that purports to be both general and accurate. If k is incorrectly specified, heat loss rates could easily err by a factor of 2. The effect of conductivity on both "c" coefficients of Eqn. III-9 is quite strong. Conductivity also exercises some influence over the exponent d_1, and consequently, on the area dependence of the steady state heat loss component. Variation in thermal diffusivity, however, does not seem to have much effect on heat loss and probably does not need to be included as an explicit model parameter.

Building parameters such as details of foundation configuration, material properties, insulation, and floor covering all have the potential to change the overall conductance of a floor. The effects of these parameters are confounded with the effect of soil properties in the coefficients of Eqns. III-5 and 9 and can be separated only by the comparison of parametric sets of simulations. Therefore, if one were to construct a manual method based on Eqn. III-9, it would be necessary to select a variety of foundation designs and to perform sets of runs with several (perhaps two or three) soil conductivity values for each foundation type in order to produce a "general" model. If, as this study suggests, only four cases of A/P are sufficient to produce a model for one building type and set of environmental conditions, then twelve runs per foundation type would be needed. The conductivity dependence of c_1, c_2, and d_1 could be incorporated by fitting these results to simple interpolating functions, or by creating sets of parametric curves for graphical determination of these coefficients. The utility of constructing such a method would depend to a great extent on the importance of

foundation losses in the intended application and the expense incurred to acquire and validate the necessary base of numerical results.

III.B.6 EFFECT OF ZERO-FLUX LOWER BOUNDARY CONDITION

It was noted previously that the lower soil boundary condition exercises only a small influence on ground surface temperature (see Figure III-3 and associated discussion). Because conditions in the soil near the ground surface are relatively insensitive to deep ground conditions, slab on grade heat loss is unlikely to show strong dependence on deep ground conditions unless one or more special conditions exist. These might include a high water table (one which lies above the annual penetration depth of the ground temperature cycle), a sharp change in soil properties, or conditions which maintain a large mean temperature difference between the ground surface and the deep ground (such as frequent watering in an arid climate). In any of these cases, the ground temperature distribution could lose its close resemblance to the semi-infinite medium solution.

The quantitative difference between heat loss with fixed temperature and zero flux conditions was investigated by comparing the series W Minneapolis runs with the runs of series Z. Series Z was identical to Minneapolis series W except for the substitution of a zero flux lower boundary condition. In the fixed temperature series, deep ground temperature was set equal to the mean air temperature, 7.2 C. With potential evapotranspiration, the mean

ground surface temperature was 4.8 C, creating a mean temperature difference of 2.4 C between the upper and lower boundaries. As predicted by linear, constant property theory, the zero flux lower boundary in series Z runs assumed a temperature equal to the annual average surface temperature--also 4.8 C. Consequently, the lower boundary temperature was lower in series Z and the temperature difference between the ground surface and lower boundary was zero.

The lower deep ground temperature of the zero flux cases presented a stronger heat sink to the underside of the floor. Consequently, one would expect to find greater heat loss in the zero flux case than in the fixed temperature case. As the summary contained in Table III-11 shows, this was the result. Table III-12 compares the results from Table III-11 in terms of both the absolute heat loss rate difference in watts and the percentage difference with respect to the fixed lower boundary case. Absolute differences in mean heat loss are larger than differences in extreme values. It has been shown that the fluctuating component of heat transfer is driven by the surface conditions acting on the perimeter of a floor while the mean component is determined by global influences. It is not surprising, then, that a change in deep ground conditions is reflected more strongly in the mean than in extreme values. Percentage differences in mean heat loss are larger for larger floors. This is consistent with the prior observation that a floor disturbs the ground temperature over distances comparable to its characteristic length. In this regard, note that the percentage change in mean heat loss for the cases shown in Table III-12 increases monotonically with A/P.

	Fixed Lower Boundary Temperature			Zero Flux Lower Boundary		
Dimensions [m]	Q_{min} [W]	Q_{max} [W]	Q_{avg} [W]	Q_{min} [W]	Q_{max} [W]	Q_{avg} [W]
12 x 12	403.2	1915.2	1088.9	417.6	1929.6	1107.3
6 x 24	432.0	2347.2	1303.3	460.8	2361.6	1320.5
45 x 45	3240.0	9112.5	5895.8	3442.5	9315.0	6162.7
18 x 112	3830.4	12297.6	7653.6	4032.0	12499.2	7923.2

Note: Lower boundary temperature in fixed T case is equal to mean dry bulb, 7.2 C. Mean ground surface temperature is 4.8 C in both cases (potential evapotranspiration boundary).

Table III-11. Heat loss data for floors in Minneapolis with fixed temperature and zero flux deep ground boundary conditions.

		ΔQ_{min}		ΔQ_{max}		ΔQ_{avg}	
Dimensions [m]	A/P [m]	[W]	%	[W]	%	[W]	%
12 x 12	3	14.4	3.6	14.4	0.75	18.4	1.8
6 x 24	2.4	28.8	6.7	14.4	0.61	17.2	1.3
45 x 45	11.25	202.5	6.3	202.5	2.2	266.9	4.5
18 x 112	7.75	201.6	5.3	201.6	1.6	269.6	3.5

Table III-12. Change in floor heat loss due to substitution of zero flux lower boundary for fixed temperature lower boundary (data from Table III-11).

Figure III-23 shows distance weighted least squares approximations to the daily averaged heat loss from the two 45 x 45 m cases. The primary effect of the change in lower boundary conditions for a given floor is a shift in its mean heat loss. No change in the amplitude of the daily averaged heat loss curve is apparent. In the case of general A/P, the change in boundary

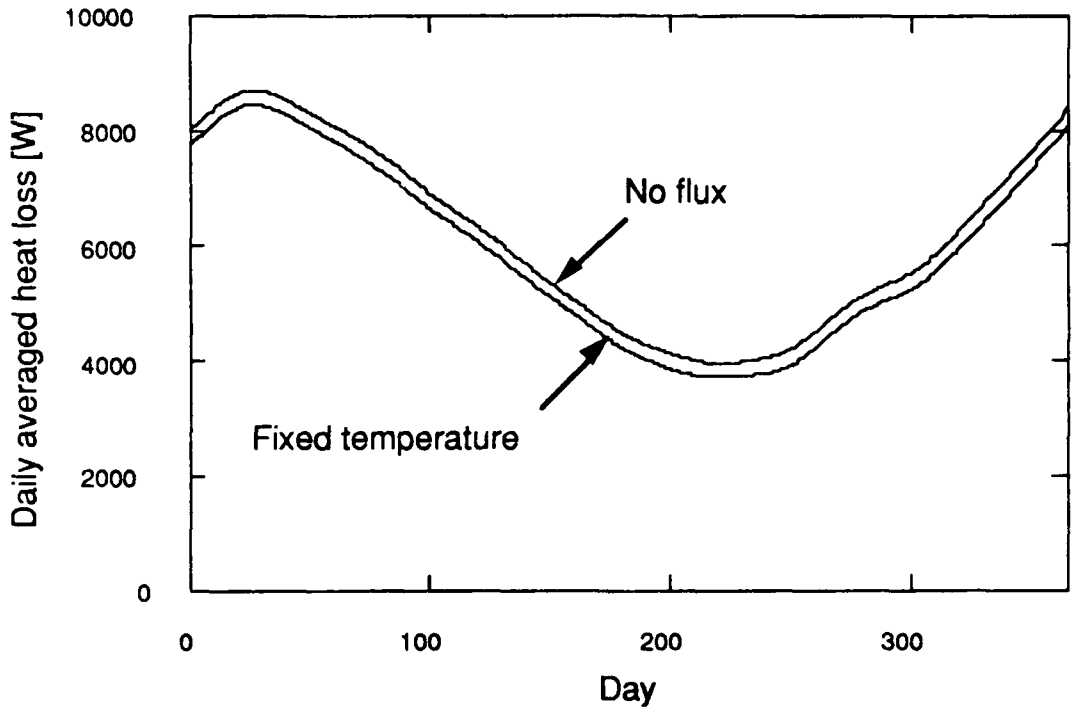

Figure III-23. Smoothed, daily-averaged heat loss from a 45 x 45 m slab floor in Minneapolis, MN with zero flux and fixed temperature deep ground boundary conditions.

condition type has a modest effect on coefficient d_1 and no perceptible effect on values of c_1, c_2, and d_2 (which were 0.994, 0.759, and -0.999 respectively, in both cases). The zero flux series displayed an increased dependence on area as indicated by the change in d_1 from -0.735 in the fixed temperature case to -0.717 for the zero flux set. As suggested previously, this may be a result of the increased core heat loss caused by a decrease in deep ground temperature.

The conclusion suggested by this limited investigation of lower boundary condition type effects is that they are probably not significant when the domain is deep and the specified lower boundary temperature is close to the mean surface temperature. If

the lower boundary temperature exceeds mean surface temperature, the substitution of a zero flux condition will lead to greater heat loss and area dependence. If the opposite is true, decreased heat loss and area dependence would result. Such effects could be exaggerated or suppressed as a result of other influences, for example, by soil property values.

III.B.7. EFFECTS OF INSULATION

A recent U. S. Department of Energy report [2] documents the large potential for energy savings through the insulation of building foundations. Many prior studies have dealt with the design and optimization of insulation systems [7, 24, 52, 53]. A similarly detailed consideration of insulation effects is beyond the scope of the present study. However, a limited examination of insulation effects was included to determine how well a simplified model like Eqn. III-9 could accommodate insulated slab floors. Limitations on the range of parameters considered in the series I insulation runs included:

- Minneapolis weather only
- Insulation limited to 1" or 2" thicknesses of expanded extruded polystyrene board (k=0.029 W/m-K)
- Two configurations: edge + 1 m under slab perimeter and edge + entire external surface of slab

As noted in Ch. II, the effect of insulation was represented by added surface resistance in the effective thermal conductivity formulation (Eqn. II-23) rather than by additional finite difference cells.

Figure III-24 shows typical summer and winter isotherms beneath a floor with perimeter insulation. Isotherms for the same floor without insulation appear in Fig. III-5. Comparison of these two figures reveals some of the interesting qualitative effects of insulation. First, the extent of the region warmed by the insulated floor is smaller than that affected by the uninsulated floor. Because heat loss is reduced by the edge insulation, the ground near the building becomes colder. Another result of the perimeter insulation is the creation of a larger region of high horizontal temperature gradient beneath the slab, as indicated by the more closely bunched and nearly vertical isotherms under the outer two meters of floor in Figure III-24a.

Figure III-25, which shows January 21 average centerline profiles for the outer three meters of floors treated with varying amounts of one inch insulation, illustrates the effect of insulation on floor surface temperature. The addition of a one meter wide strip causes the floor edge temperature to rise by approximately 5 C, but the temperature profile for this case converges rapidly with the uninsulated profile as distance from the edge increases. A probable cause for this behavior is that the width of the perimeter insulation band was not sufficiently large to prevent substantial losses around the inner edge of the insulation. Note, too, that in the case of the fully insulated floor, temperature near the slab edge is several degrees higher than with perimeter insulation. This gives further

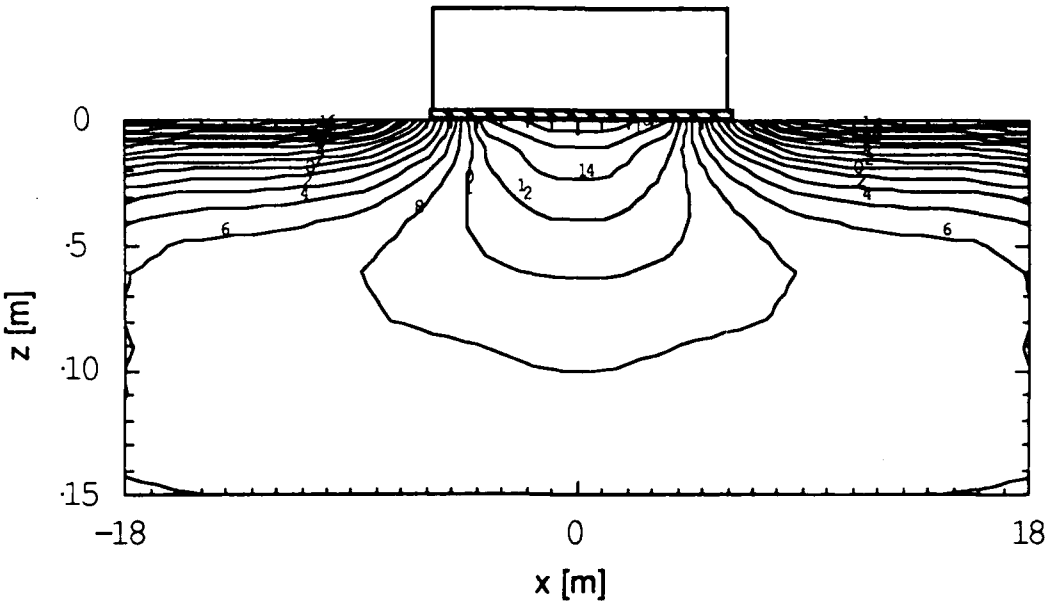

a) January 21

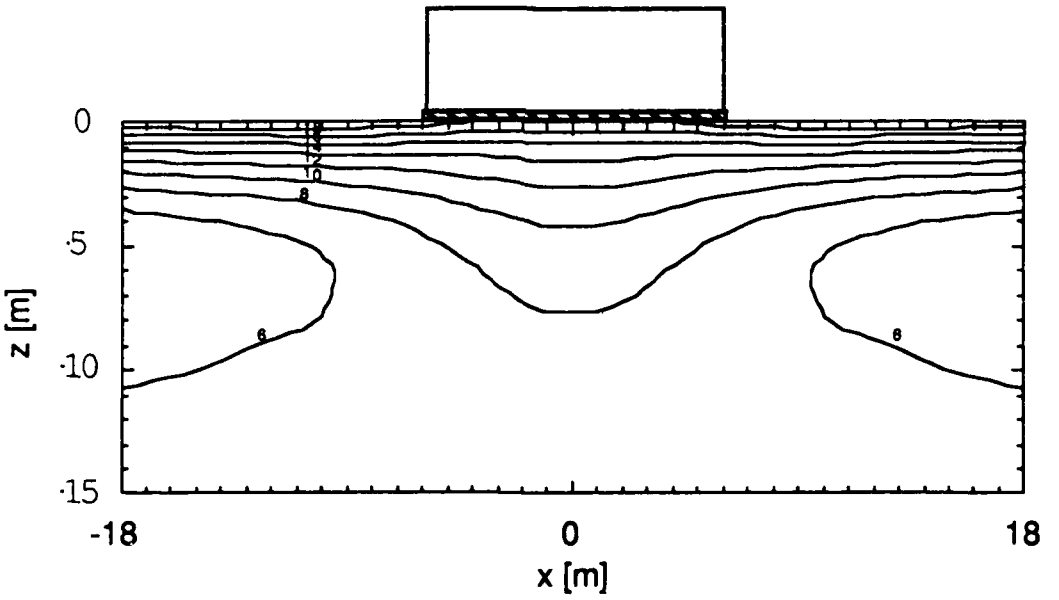

b) July 21

Figure III-24. Daily averaged isotherms beneath a 12 x 12 m concrete slab in Minneapolis with 2" of exterior polystyrene perimeter insulation (edge and one meter under slab).

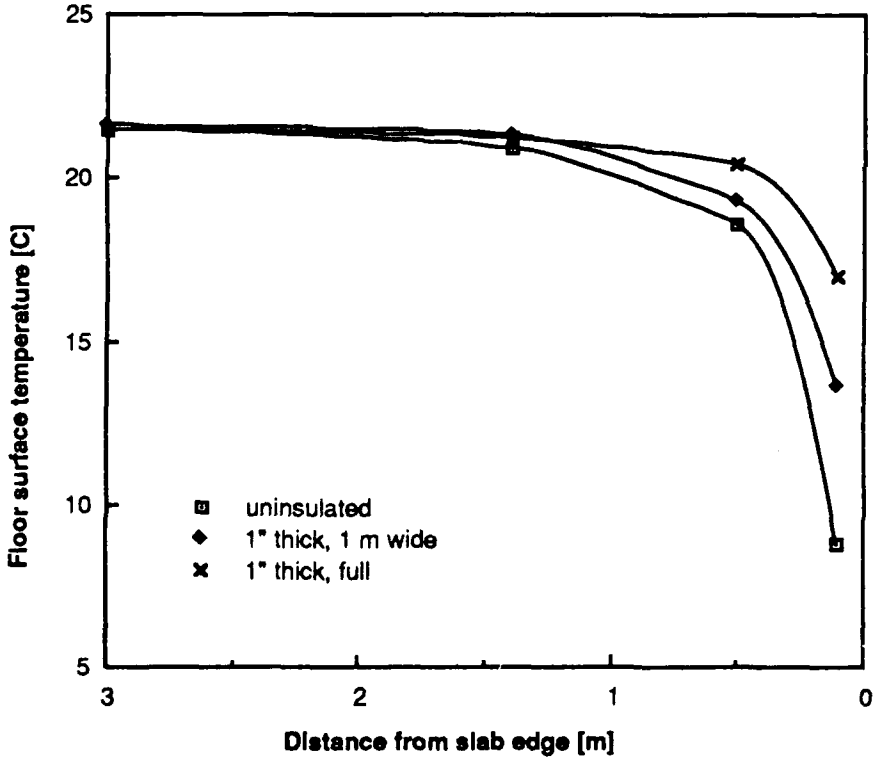

Figure III-25. Centerline floor surface temperature profiles near the edge of 12 x 12 m slabs with various insulation treatments for January 21 in Minneapolis, MN.

evidence of significant secondary heat flow in the perimeter insulated case. Figure III-26 shows heat flux distributions corresponding to the temperature profiles of Fig. III-25. Both insulation treatments result in large perimeter heat loss reductions relative to the uninsulated case.

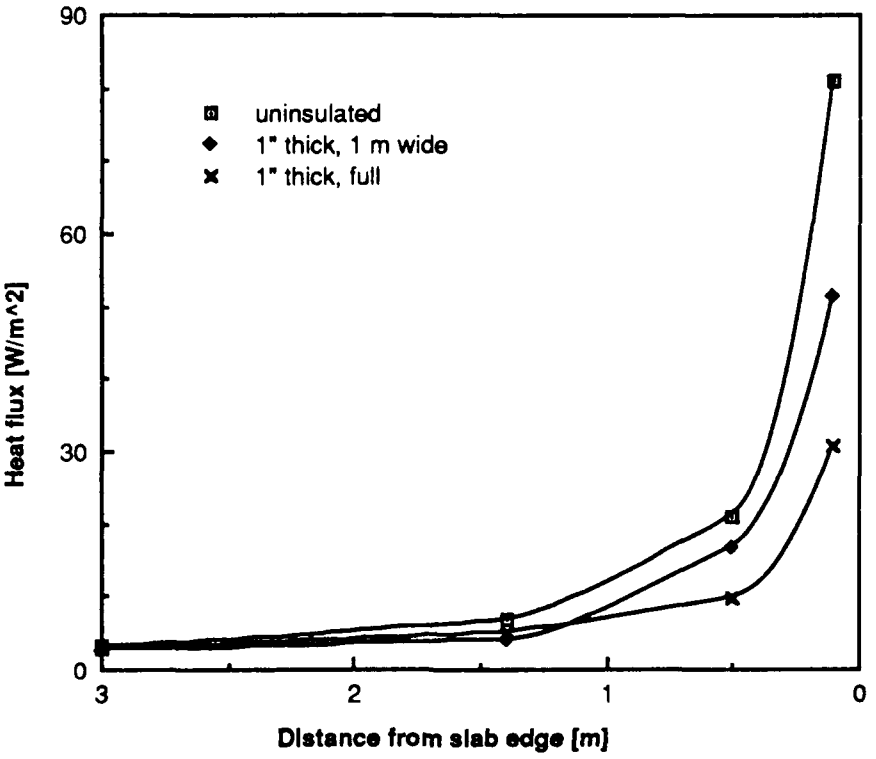

Figure III-26. Average centerline heat flux distributions for three 12 x 12 m floors with various insulation treatments on January 21 in Minneapolis, MN.

Figures III-27 and 28 show the effect of insulation on daily low floor temperature during January. In Fig. III-27, the uninsulated case, daily low temperature is over 10 C below the daily average and approaches freezing on several days. The variation in low temperature is approximately 8 C during this period. When two

inches of perimeter insulation are added to this floor, the difference between the daily average and low temperatures is reduced by more than half and variation in the daily low is also much smaller. This illustrates two important subsidiary benefits of foundation insulation. First, higher floor temperature levels in the winter are more conducive to thermal comfort. Secondly, the smaller variation of temperature with time contributes to levelling of demands on equipment.

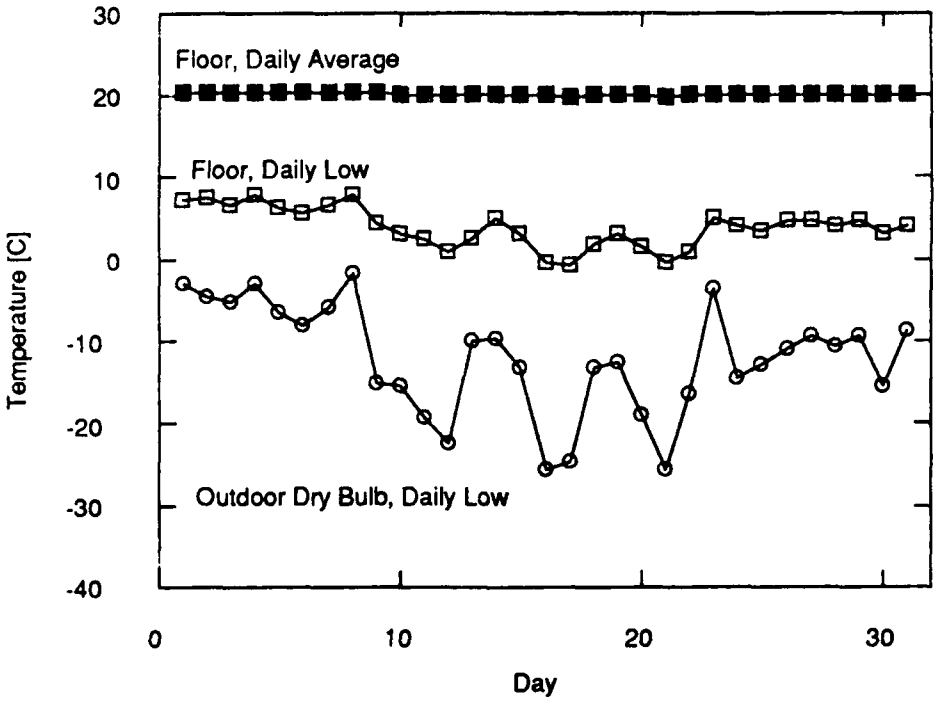

Figure III-27. January daily low and average floor surface temperatures for a 12 x 12 m uninsulated floor in Minneapolis, MN.

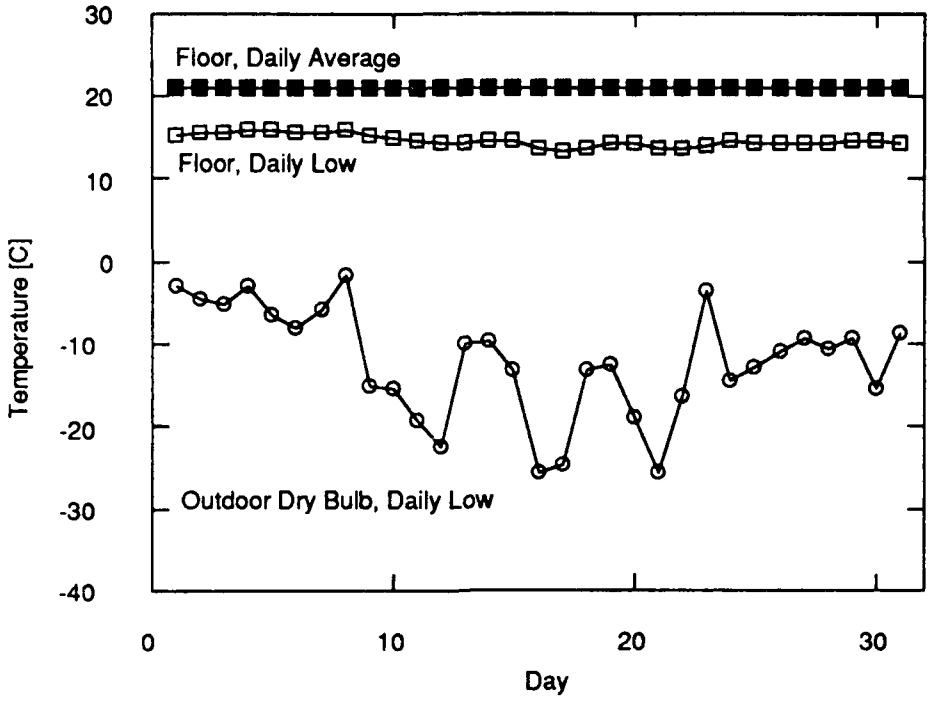

Figure III-28. January daily low and average floor surface temperatures for a 12 x 12 m floor with 1 m of 2 inch thick perimeter insulation in Minneapolis, MN.

Figure III-29 shows daily averaged heat loss from a 12 x 12 m floor for three different insulation treatments. The raw results have been smoothed to facilitate comparison. As insulation is added to the bare slab, both the mean and amplitude of the daily heat loss decrease. Consequently, the maximum heat loss is reduced by a much greater amount than the minimum. The resulting benefit in winter heating load avoided is much greater than the penalty paid in cooling lost during the summer. The result for full one inch thick insulation, which is not shown, would lie almost directly on top of the curve for the two inch thick, one meter wide configuration. The nearly identical performance of these two much different

treatments illustrates the importance of effective insulation placement. The full, one inch thick treatment requires 64% more material to achieve the same performance as the heavy perimeter insulation configuration.

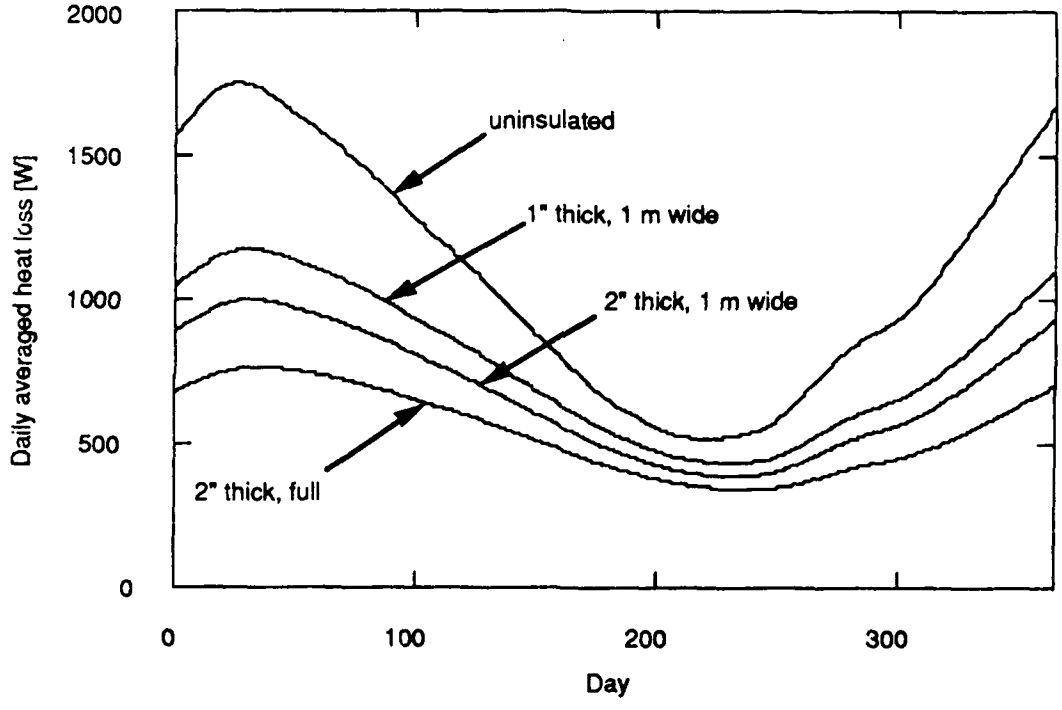

Figure III-29. Smoothed, daily-averaged heat loss from a 12 x 12 m Minneapolis slab floor with various insulation treatments.

The preceding discussion focused on the academic issue of how insulation alters the character of heat transfer from a slab floor. A more practical issue from the perspective of the building owner/operator is the bottom line of net energy savings due to the foundation insulation. Table III-13 compares heating, cooling, and

net energy consumption as well as peak heating load for two floor sizes (12 x 12 m and 45 x 45 m) and all five insulation configurations considered in this study. Heating and cooling loads were defined to be energy exchanges occurring when the outdoor dry bulb was, respectively, below and above the indoor temperature of 22 C. No dead band was assumed. For the 1979 Minneapolis TMY file used in these runs, there were 314 days of heating and 51 days of cooling. This created a considerable bias in favor of the use of insulation to reduce heating energy consumption. Another factor that enhances the desirability of insulation to mitigate heating load is the previously noted effect of simultaneous decrease in the mean and amplitude of floor heat loss when insulation is added. Peak heating load is reduced by a much larger amount than the peak cooling contribution is decreased. For both floor sizes, the first increment of insulation produces the greatest benefit. The addition of more material consistently leads to increased energy savings, but the marginal gains become increasingly smaller. This fact coupled with the linear cost of materials is the crucial trade-off in the insulation optimization problem.

The reduction in contribution to peak heating load is even greater than the reduction in heating energy. Although the fractional contribution of the floor to heating load at design conditions would probably be at its smallest, insulation could be a factor in reducing equipment size for small, well built structures such as super-insulated homes. Energy savings and load reductions are smaller in the 45 x 45 m case than in the 12 x 12 m case by 7-10%. Because of its larger associated core soil mass, the 45 x 45 m slab is less

	Insulation Thickness and Configuration				
	None	1"/1m	1"/full	2"/1m	2"/full
Heating Energy [GJ]	31.9	22.5	19.9	19.4	15.5
Savings [GJ]	0	9.5	12.0	12.5	16.5
Savings [%]	0	29.6	37.6	39.2	51.6
Heating Q_{max} [W]	1915.2	1238.4	1080.0	1051.2	806.4
Reduction [W]	0	676.8	835.2	864.0	1108.8
Reduction [%]	0	35.4	43.6	45.1	57.9
Cooling Energy [GJ]	-2.4	-2.1	-1.9	-1.8	-1.6
Savings [GJ]	0	-0.3	-0.5	-0.5	-0.7
Savings [%]	0	-13.7	-18.8	-22.4	-31.3
Net Savings [GJ]	0	9.1	11.6	12.0	15.8
Net Savings [% of net load]	0	30.9	39.1	40.6	53.1

a) 12 x 12 m

	Insulation Thickness and Configuration				
	None	1"/1m	1"/full	2"/1m	2"/full
Heating Energy [GJ]	169.1	132.2	122.6	119.2	104.5
Savings [GJ]	0	36.9	46.5	49.9	64.6
Savings [%]	0	21.8	27.5	29.5	38.2
Heating Q_{max} [W]	9112.5	6480.0	5872.5	5670.0	4657.5
Reduction [W]	0	2632.5	3240.0	3442.5	4455.0
Reduction [%]	0	28.9	35.6	37.8	48.9
Cooling Energy [GJ]	-16.8	-15.3	-14.9	-14.2	-13.7
Savings [GJ]	0	-1.5	-1.9	-2.6	-3.2
Savings [%]	0	-8.9	-11.5	-15.7	-18.8
Net Savings [GJ]	0	35.4	44.6	47.3	61.4
Net Savings [% of net load]	0	23.3	29.3	31.0	40.3

b) 45 x 45 m

Table III-13. Influence of insulation treatment on heating and cooling energy requirements for two slab floors in Minneapolis, MN.

affected than the smaller floor by changes at the slab perimeter. This difference in fractional savings might make it economically feasible to insulate the smaller structure more heavily than the larger.

Another way of assessing the importance of insulation is through the concept of an annual energy budget. The net annual energy consumption per unit area of the uninsulated cases in Table III-13 is 204.9 $MJ/m^2/yr$ (18.03 $KBTU/ft^2/yr$) for the 12 x 12 m floor and 75.2 $MJ/m^2/yr$ (6.62 $KBTU/ft^2/yr$) for the 45 x 45 m floor. Whole building energy targets such as those used in military construction range from 40-60 $KBTU/ft^2/yr$ for housing and from 35-45 $KBTU/ft^2/yr$ for office space over 8000 ft^2 (743.2 m^2) depending on the climate region in which a building resides [54]. Clearly, the contributions of the uninsulated floors toward the building energy budget are substantial. Particularly in the 12 x 12 m residential sized case, an energy target might prove difficult to meet if the floor is not insulated. For a designer working with such criteria, floor insulation relaxes constraints on the design of the above ground envelope and mechanical systems of the building.

A final matter of interest concerning insulation is its effect on the coefficients of Eqn. III-9. The simplified model seems quite capable of handling insulated floors. Insulation, however, has a significant effect on the model coefficients. Coefficient values for the uninsulated slab and the two perimeter insulated cases appear in Table III-14. As insulation is added, the area dependence of both the steady and periodic components of heat loss increases. As in previous cases, the steady state component is more strongly

	c_1	d_1	c_2	d_2
Uninsulated	0.997	-0.735	0.759	-0.999
1" Thick, 1 m wide	0.603	-0.623	0.408	-0.953
2" Thick, 1 m wide	0.475	-0.570	0.308	-0.921

Table III-14. Comparison of daily averaged heat loss model coefficients for three insulation treatments in Minneapolis, MN.

affected. The maximum fractional change in d_1 is over three times greater than the corresponding change in d_2. With two inches of insulation on the perimeter, d_2 still deviates from -1 by only 7.8%, thus the strict perimeter dependence of the periodic heat loss component is not seriously violated. An interesting and superficially contradictory effect of insulation demonstrated by these results is that a more uniform floor temperature distribution enhances the shape dependence of heat loss. By decreasing heat loss at the floor perimeter, insulation raises the contribution of interior area to total heat loss. Thus, while the floor temperature distribution is "less three dimensional", heat transfer is *more* three dimensional. In light of this fact, the predictions of perimeter heat loss factor methods may be especially misleading for well insulated floors.

IV. CONCLUSIONS AND RECOMMENDATIONS

This study has examined the effects of a variety of modelling assumptions, environmental conditions, and design features on the heat loss predictions of a highly detailed three-dimensional, hourly slab-on-grade model. Because this model incorporated far fewer *a priori* simplifying assumptions than most prior numerical models, the results obtained from it provide a firm basis for describing the essential characteristics of a design model for earth-coupled building heat transfer. Few factors influencing the soil temperature distribution were neglected without concrete evidence of their insignificance. Various parametric studies were discussed in detail in the preceding chapter. A simple model of slab-on-grade heat loss based on appropriate reference temperature differences proved a valuable aid in the analysis of these results and may be suitable for further development as a manual design technique This chapter presents the global conclusions of this investigation with respect to the nature of slab-on-grade heat loss and reasonable approaches to its modelling.

IV.A. CONCLUSIONS

IV.A.1. TEMPORAL AND SPATIAL TEMPERATURE AND HEAT LOSS VARIATION

This study generally supports previous qualitative findings concerning the soil temperature distribution near a slab-on-grade

and the floor heat transfer regime:

- During the heating season, heat loss is predominantly from the floor perimeter. A zone of one to two meters in width is strongly affected by above ground conditions while the remainder of the floor surface constitutes a core zone that is under the influence of mean conditions.
- The temperature and heat flux distributions in the perimeter zone are essentially independent of floor size for a given foundation design.
- Core conditions depend on the size and shape of a building. Floor center heat flux may vary by a factor of two or three from a small building to a large one.
- Variations in floor total heat loss on a time scale shorter than twenty-four hours appear to be insignificant for general purpose calculations. More localized hourly effects on perimeter zones, however, may be of consequence in passive building design.
- Seasonal variations in the soil temperature regime cause heat loss to be more uniform over the surface of a floor in the summer than during the winter. This fact makes perimeter loss coefficient methods unacceptable for purposes other than heating load calculations. They are not suitable for annual energy consumption estimates.

IV.A.2. DEPENDENCE OF HEAT LOSS ON FLOOR SHAPE AND SIZE

Prior investigations of three-dimensional floor heat loss [27, 29] demonstrated substantial differences between two- and three-

dimensional predictions but did not offer models to explain these discrepancies. The results of the present study indicate that influences of shape and size on floor heat loss in three dimensions can be related to the effect of the characteristic length A/P on heat loss per unit area for rectangular and L-shaped floor plans. Given the nature of this relationship, there is every reason to expect that it extends to more arbitrarily defined shapes, as well.

Analysis using a simple daily averaged heat loss model (Eqns. III-4 to III-9) showed that floor area strongly influences the mean component of heat loss but has little impact on the periodic component. Consequently, mean heat loss from floors with large A/P may exceed predictions based on small floor results by as much as a factor of two.

Phase lag of floor heat transfer with respect to ground surface temperature varied between two and three weeks over a large range of sizes and soil properties. Property values had more influence on phase lag than geometric factors.

IV.A.3 DEEP GROUND BOUNDARY CONDITION EFFECTS

Floor heat loss was relatively insensitive to changes in deep ground conditions in the cases considered. Two types of effect were investigated: the difference between zero flux and fixed temperature boundary types, and the difference between fixed temperature conditions specified at depths of 10 m and 15 m. In fixed lower boundary temperature runs, the lower boundary temperature was equal to the annual average air temperature and the

surface boundary condition included potential evapotranspiration, so mean surface temperature was lower than deep ground temperature.

In both boundary depth and boundary condition type comparisons, differences in heat loss increased as A/P became larger. The position of the lower boundary caused greater changes in heat loss than the change of boundary condition type. The range of differences in mean heat loss due to 50% reduction of the lower boundary depth varied from 0.33 to 12.6%. Differences in mean heat loss resulting from change of boundary condition type were in the range 1.3 to 3.5%. In view of the magnifying effect of lower boundary proximity, it seems inappropriate to conclude that boundary condition type is less important than boundary location. A change of boundary condition type on a plane ten meters below the surface would probably have caused greater differences in floor heat loss than the same change at a depth of fifteen meters. A more defensible conclusion, therefore, is that the nearer the lower boundary lies to the ground surface, the more significant is the effect of a given change in conditions.

IV.A.4 CLIMATE EFFECTS

This study considered the effects of four different climates on the performance of uninsulated slab-on-grade floors. For three climates with cold winters: Medford, OR; Minneapolis, MN; and Philadelphia, PA; the differences in heat loss related directly to differences in the statistical properties of the annual temperature distribution, i.e., to variation in the mean and amplitude of ground

surface temperature. For example, the ratio of mean fluxes for 12 x 12 m slabs in Medford and Minneapolis was 0.758 (825.7 W/1088.9 W) while the ratio of mean temperature differences for these two sites was 0.779. The steady state and periodic conductances for the three locations agreed well, with all showing comparable degrees of area dependence.

Results for Phoenix, AZ showed weaker dependence on area of the steady state heat loss. Both the mean and periodic total heat losses were nearly proportional to floor perimeter. The anomalous behavior of the Phoenix cases lacks a full explanation, however, it seems possible that the small difference between the indoor and deep ground temperatures (0.1 C) was an important factor. Since the lower boundary in these cases presented a very weak heat sink to the floor, most of the mean component of heat loss was to the ground surface, maintained at a lower temperature by evapotranspiration. Under these conditions, mean heat flow paths would resemble transient winter paths and heat loss should depend more strongly on perimeter.

IV.A.5. GROUND SURFACE BOUNDARY CONDITION EFFECTS

The effect of change from a potential evapotranspiration condition to one of zero latent loss was investigated. Potential evapotranspiration caused mean ground temperature to fall several degrees below mean air temperature and also decreased the amplitude of the annual cycle. The effect was most pronounced during the summer when evapotranspiration potential is highest.

Without a latent loss component at the ground surface, the mean and amplitude of surface temperature increased substantially and ground temperature exceeded air temperature through most of the year. The difference between air and surface temperature in the no evapotranspiration case also was greatest during the summer because of the effect of greater solar gain.

The effect of evapotranspiration was much stronger in the warm, dry climate of Phoenix than in any of the other locations considered. Evapotranspiration increased maximum floor heat loss by 4 to 11% relative to the zero latent loss case for a representative group of runs from Philadelphia, Medford, and Minneapolis while the corresponding Phoenix simulation showed a change of nearly 50%. Mean values were affected to an even greater extent. For Philadelphia, Medford, and Minneapolis, mean heat loss decreased by 18 to 32% when evapotranspiration was suppressed. Phoenix mean heat loss, however, changed by 170%, turning a net loss into a net gain.

On the basis of this study, one must conclude that the possible effects of latent heat loss on soil temperature are substantial. A boundary condition that includes radiation but neglects evaporation will predict ground surface temperatures that are generally elevated above air temperature during the day, sometimes by 10 C or more. Conversely, a boundary condition that includes potential evapotranspiration will predict lower daytime ground temperatures and a lower mean.

IV.A.6. GROUND SHADOWING BY A BUILDING

The effect of a building's shadow on ground temperature was measurable, but generally minor. Climate played a role in determining both the magnitude and seasonal variation of this effect. The increase in mean heat loss from a 12 x 12 m house as a result of shadowing was 6.5% in Medford with potential evapotranspiration, 14% in Medford with no evapotranspiration, and 27.4% in Phoenix with evapotranspiration. Although the effect of the building shadow is probably not worth including in most numerical models, the ability of localized shading to cause modest changes in foundation heat loss demonstrated in this study provides added incentive to use seasonal detached shading (e. g., deciduous trees) for cooling load mitigation. Furthermore, as the Phoenix results demonstrated, there can be considerable variation in the importance of this effect with climate.

IV.A.7. SOIL PROPERTY EFFECTS

Soil thermal conductivity has a profound effect on both the mean and transient components of heat loss. With the exception of foundation design, it is clearly the most crucial parameter affecting heat loss. It is entirely correct to say that reliable estimates of slab-on-grade heat loss without consideration of soil conductivity are impossible. This is unfortunate, since soil thermal properties are among the least certain parameters in a typical foundation heat loss analysis. In this study, variation of soil conductivity produced

greater change in heat loss than did variation in climate. Factor of two changes in conductivity, which may occur in the field, produced comparable changes in heat loss. Thermal diffusivity of the soil, however, did not exert much influence on floor heat loss over the range of values considered. As should be the case, thermal diffusivity had no effect on mean loss. The amplitude of the periodic loss changed by approximately 12% when diffusivity changed by a factor of two, a small change relative to the thermal conductivity effect.

IV.A.8. EFFECT OF INSULATION

The study of insulation effects confirmed the importance of insulating slab floors to reduce winter losses and the economic superiority of perimeter insulation to full slab insulation. For the case of Minneapolis weather, the benefit of insulation to reduce heating load far outweighed the penalty paid in lost cooling potential. The area dependence of the heat loss from an insulated floor was greater than that of the same floor without insulation because insulation made floor temperature and heat loss more uniform. This finding casts suspicion on the validity of F_2 method heat loss predictions for highly insulated floors. It is encouraging, however, that the performance of an insulated floor can be described by Eqn. III-9 without any substantive modifications. The coefficients for an insulated slab may be obtained in precisely the same way as those for an uninsulated slab. A comparison of observed heat loss values with U. S. Army design energy targets for

residential and office space types showed that the annual energy consumption of an uninsulated floor may be as much as 30 to 50% of the energy budget for new construction. The floor load contributed a larger fraction of the building target in the case of a residential sized structure. It also was shown that perimeter insulation can reduce this contribution by as much as 50%, and perhaps more.

IV.B. RECOMMENDATIONS

IV.B.1 GUIDELINES FOR MODELLING

On the basis of the results reviewed above, one may conclude that an accurate model of slab on grade heat loss should, at a minimum, account explicitly for the following:

- soil thermal conductivity
- surface boundary effects on soil temperature
- foundation design and insulation treatment
- area effects (A/P dependence of q)

Neglect or improper specification of any of these items could cause model predictions to err by 50% or more. The omission of lower boundary conditions from this list is only marginally justified and would restrict the applicability of a model. Shadow effects are, at the present level of refinement of the modelling art, not worth considering. Likewise, thermal diffusivity effects on slab heat loss are small enough that they could be omitted from a design oriented model. (For foundations extending substantial distances into the ground, however, the phase lag and penetration depth of surface

effects are more important and diffusivity most probably could not be neglected.)

Whenever possible, manual methods should employ soil temperature rather than air temperature as an environmental reference. In a northern, heating-dominated climate, it may be acceptable to use outdoor dry bulb, or a smoothed approximation of it, as a reference ambient condition rather than the actual ground surface temperature determined by a detailed surface energy balance such as Eqn. II-16. However, this practice could be the source of considerable error and some effort should be made to determine and account for air/ground temperature differences. It is essential that the coefficients of manual methods be based on a soil temperature reference for reasons explained in Ch. III. Manual methods must also separate the mean and periodic components of heat loss in order to have year-round validity. The F_2 method, which does not distinguish between mean and periodic heat loss, is applicable (and then, to a limited extent) only during the heating season.

A model such as Eqn. III-9 could be the basis of a manual design method with year-round validity. In order to generate such a model, however, it would be necessary to compute a large number of cases corresponding to various combinations of foundation design, soil properties, and boundary conditions. Also, the question of how to incorporate the combined effects of soil properties and foundation type into the mean and periodic conductances K_1 and K_2 needs to be addressed. It would be most practical in such a model to adopt conventions for specifying parameters which have relatively

little effect on heat loss, such as the depth of the lower boundary and the lower boundary condition type. For example, it might be advisable to eliminate the effect of the lower boundary by applying a zero flux condition at a large depth in all cases. This would greatly reduce both the number of runs required to generate model coefficients and the number of coefficient sets generated.

With the A/P scaling relationship observed in this study, it is possible to obtain results valid in three dimensions directly from two-dimensional models. Since two-dimensional heat transfer from a slab corresponds to the three-dimensional, infinite aspect ratio case (for which A/P = L/2), there is an equivalent two-dimensional case for any three-dimensional floor. This mapping procedure is potentially of great significance, since it would permit the heat loss from any number of arbitrarily shaped floors to be obtained from the heat loss of a single two-dimensional case with the same value of A/P. For example, a 20 x 20 m three-dimensional square (A/P = L/4 = 5 m) should have heat loss per unit area that is the same as that of a 10 m wide two-dimensional slab. Likewise, a square floor of side 6, a circle of radius 3, an L-shaped floor filling three quadrants of a square with a side of 8, a 4 x 12 rectangle, and an infinite strip of width 3 all have the same value of A/P (namely, 1.5) and so, should have the same heat loss per unit area under equivalent environmental conditions.

Because of the complexity of earth coupled heat loss, simulation rather than the use of correlated results is preferable whenever possible. In order to facilitate the widespread use of simulation, a number of simplifications may be made to reduce

hardware requirements and execution time. The findings of this study indicate that a clear, accurate picture of daily averaged heat loss may be obtained from models based on a simple sinusoidal approximation to ground temperature. The use of such models can save a great deal of computational effort if a one dimensional model of the soil temperature distribution is used to generate the raw ground temperature data on which they are based. While a shorter time step may be needed to obtain accurate estimates of convection and evapotranspiration in a detailed model of soil temperature, daily time steps appear to be adequate for the actual building simulation. Reasonable approximations in model formulation combined with the rapidly increasing capability of affordable workstations should make multi-dimensional simulation of building foundations for design purposes practical in the foreseeable future.

IV.B.2. GENERAL RECOMMENDATIONS

The commonly used design techniques for slab on grade heat loss, such as the F_2 method, are seriously limited in applicability and represent an obsolete view of earth-coupled heat loss. Because of the increased importance of building/ground thermal interactions in contemporary construction, it is imperative that the methods for earth-coupled heat transfer analysis be upgraded to reflect the current state of knowledge. This objective could be accomplished both through the development of better manual methods and through computer aided design tools.

Heat loss predictions and model coefficients reported in this study should be used only in a comparative manner and not taken as absolute. The results of this study would require experimental validation before being acceptable as design data. It would be appropriate and worthwhile for the conclusions of this study to be evaluated by application to data from real buildings.

Because a variety of model parameters were considered in this study, the coverage of individual parameters was not as deep as it might have been. Soil property and surface boundary condition effects, in particular, offer many opportunities for additional study. Examination of such issues as moisture movement, phase change, spatially and temporally variable soil conductivity, and the effects of non-uniform surface cover (for example, a combination of grass and asphalt covered surfaces) would provide very useful additions to existing knowledge.

Finally, the critical role of soil thermal conductivity demonstrated in this and previous studies underscores the need for an improved, expanded base of soil thermal property data for energy calculations. Until better methods of calculation are coupled with adequate knowledge of soil properties, the accurate estimation of earth-coupled heat loss for real buildings will remain a nearly impossible task.

APPENDIX A. COMPUTATION OF ZENITH AND SOLAR AZIMUTH ANGLES

This appendix summarizes the calculations required to obtain the zenith and solar azimuth angles from fundamental quantities during shading calculations performed by the three-dimensional model. These angles were introduced in section II.B.3 and are shown in Fig. II-6. For a detailed discussion of solar geometry and derivations of the relationships used in these calculations, the reader should consult one of the standard texts on solar engineering, for example, [48].

Zenith Angle

The zenith angle (θ_Z) depends on latitude (ϕ), hour angle (ω), and declination (δ), according to the following formula:

$$\Theta_z = \cos^{-1} \cdot [\cos\delta \cdot \cos\phi \cdot \cos\omega + \sin\delta \cdot \sin\phi] \qquad (A\text{-}1)$$

Angles in Eqn. A-1 and elsewhere in this appendix are expressed in radians, with the exception of longitude and latitude, which are given in their customary units of degrees.

The declination is the angle of the noonday sun above or below the equator and is positive north. Declination varies between ±0.409 radians (i.e., between ± 23.45°) and is approximated by

$$\delta = \frac{23.45\pi}{180} \cdot \sin\left(2\pi \cdot \frac{284+n}{365}\right) \qquad \text{(A-2)}$$

where n is the day of the year ($1 \leq n \leq 365$).

The hour angle indicates deviation from local solar noon. It varies between $-\pi$ and π with negative values occurring in the AM. Clearly, ω increases by $\pi/12$ radians per hour, therefore,

$$\omega = \frac{\pi}{12} \cdot (t_{solar} - 12) \qquad \text{(A-3)}$$

where t_{solar} is measured in decimal hours.

Solar time may be determined, given knowledge of standard time (t_{std}), longitude (Long), standard time meridian ($Long_{std}$), and the so-called "equation of time" (E):

$$t_{solar} = t_{std} + \left[\frac{4\,(Long_{std} - Long) + E}{60}\right] \qquad \text{(A-4)}$$

The equation of time is a seasonally varying correction (in minutes) to the solar time and is approximated by

$$E = 9.87\sin 2B - 7.53\cos B - 1.5\sin B \qquad \text{(A-5)}$$

where

$$B = \left[2\pi \cdot \frac{n-81}{364}\right] \qquad \text{(A-6)}$$

Solar Azimuth

The solar azimuth angle is a function of declination, zenith angle, and hour angle, all of which are defined above:

$$\gamma_s = \sin^{-1}\left[\frac{\cos\delta \cdot \sin\omega}{\sin\theta_z}\right] \qquad \text{(A-7)}$$

Procedure

The calculations leading to the zenith and solar azimuth angles for each hour occur in the following sequence:

i. equation of time
ii. solar time
iii. declination
iv. zenith angle
v. solar azimuth

It may be necessary to transpose the solar azimuth early and late in the day during portions of the winter because of the possibility that γ_S may fall outside the range $-\pi/2$ to $\pi/2$ returned by the Fortran inverse sine function.

APPENDIX B. SOURCE LISTINGS

This appendix contains listings of the routines comprising the three-dimensional slab-on-grade model:

- SLAB3D, the main program which reads input and data files, performs the explicit solution of the difference model, and creates output
- TEARTH, a subroutine which compiles an hourly file of ground temperatures from a one-dimensional model
- AIRPROPS, a subroutine which calculates air properties from weather data
- CHMTC, a subroutine called by TEARTH to compute heat and mass transfer coefficients at the ground surface
- TRIDI, a tridiagonal matrix reduction subroutine used to solve the implicit one-dimensional model of soil temperature in TEARTH
- SHADE, a subroutine which performs ground shading calculations and writes a file of hourly shade switches for outside surface cells
- COEFFS, a subroutine which precalculates and saves certain coefficients used repeatedly in the three-dimensional model

Major symbols are given in variable dictionaries near the beginning of each routine. Comments intended to clarify structure are distributed throughout the source.

B.1. MAIN PROGRAM SLAB3D

```
      PROGRAM SLAB3D
C
C*** THIS PROGRAM CALCULATES THE HOURLY, THREE-DIMENSIONAL TEMPERATURE
C*** DISTRIBUTION BENEATH A SLAB ON GRADE BUILDING BY THE EXPLICIT
C*** METHOD.
C
C*** VERSION 1.0, 5 AUGUST 1988
C
C*** WM. BAHNFLETH
C
C*** DECLARATIONS:
C
      REAL ELEV,RHO(4),C(4),TCON(4),RINS,DINS,ALBEDO(2),EPSLW(2),
     +     Z0(2),XFACE(-20:20),YFACE(-20:20),ZFACE(0:20),HBLDG,
     +     TIN,HIN(2),TDB(24),TWB(24),PBAR(24),HRAT(24),WND(24),
     +     RBEAM(24),RDIF(24),TG(0:20),T(-20:19,-20:19,0:19),
     +     TOLD(-20:19,-20:19,0:19),TCVG(-20:19,-20:19,0:19),
     +     XC(-20:19),YC(-20:19),ZC(0:19),DX(-20:19),
     +     DY(-20:19),DZ(0:19),DXP(-20:19),DYP(-20:19),
     +     DZP(0:19),
     +     SHADOW(-20:19,-20:19,2),GOFT(-20:19,-20:19,2),
     +     CXM(-20:19,-20:19,0:19),CYM(-20:19,-20:19,0:19),
     +     CZM(-20:19,-20:19,0:19),CXP(-20:19,-20:19,0:19),
     +     CYP(-20:19,-20:19,0:19),CZP(-20:19,-20:19,0:19),
     +     TS(-20:19,-20:19),QS(-20:19,-20:19),TV(-20:19,0:19),
     +     DA(-20:19,-20:19),LONG,LAT,MSTD
C
      INTEGER NMAT,NX,NY,NZ,IBOX,JBOX,SHAPE,IYRS,
     +        ISNW(24),NDIM(12),NFDM(12), MTYPE(-20:19,-20:19,0:19),
     +        MSURF(-20:19,-20:19),INS(-20:19,-20:19)
C
      LOGICAL OLDTG,OLDSHD,EVTR,FIXBC,CVG,CVG1D,QUIT,SYM
C
      CHARACTER*4 RUNID
      CHARACTER*6 WEATHER
      CHARACTER*7 FILNA,FILNB,FILNC,FILND,FILNE,TGNAM,SHDNAM
C
      DATA NDIM/31,28,31,30,31,30,31,31,30,31,30,31/,
     +     NFDM/1,32,60,91,121,152,182,213,244,274,305,335/
C
C*** INITIALIZE SWITCHES TO (RESPECTIVELY) PRODUCE OUTPUT AND
C*** TERMINATE EXECUTION AFTER CONVERGENCE
C
      CVG=.FALSE.
      QUIT=.FALSE.
C
C*** LOGICAL UNIT ASSIGNMENTS:
C
C***   UNIT 10    INPUT
C***   UNIT 11    B.C.S (GROUND TEMPERATURE, TRANSFER COEFFICIENTS)
C***   UNIT 12    SHADOWING FILE
C***   UNIT 13    WEATHER FILE
C***   UNIT 14    INPUT ECHO
C***   UNIT 15    OUTPUT: DAILY OUTPUT
```

```
C***   UNIT 16    OUTPUT: HOURLY SURFACE TEMPS, 21 JAN.
C***   UNIT 17    OUTPUT: DAILY AVG. SURFACE Q & T, 21ST OF MONTH
C***   UNIT 18    OUTPUT: DAILY AVG. X-Z PLANE TEMPS, 21ST OF MONTH
C
C*** VARIABLE DEFINITIONS
C
C*** INPUT FILE CONTENTS:
C
C*** RUNID         IDENTIFIER FOR RUN, OUTPUT FILE PREFIX
C*** WEATHER       NAME OF ASCII WEATHER FILE
C*** LONG          SITE LONGITUDE [DEGREES]
C*** LAT           SITE LATITUDE
C*** MSTD          LOCAL STANDARD TIME MERIDIAN
C*** ELEV          SITE ELEVATION [M]
C*** OLDTG         TRUE MEANS THERE IS AN EXISTING BC FILE
C*** TGNAM         NAME OF BC FILE
C*** OLDSHD        TRUE MEANS THERE IS AN OLD SHADE FILE
C*** SHDNAM        NAME OF SHADE FILE (NOSHADE MEANS SHADOWING OFF)
C*** NMAT          NUMBER OF MATERIAL TYPES
C*** RHO           DENSITY OF SOLID, [KG/M**3]
C*** C             SPECIFIC HEAT OF SOLID, [J/KG/K]
C*** TCON          THERMAL CONDUCTIVITY OF SOLID, [W/M/K]
C*** RINS          RESISTANCE OF FOUNDATION INSULATION [K/(W/M**2)]
C*** DINS          WIDTH OF INSULATION ON FOUNDATION [M]
C*** INS           INTEGER SWITCH: '1' IF CELL BOTTOM IS INSULATED,
C                 '0' IF NOT INSULATED
C*** ALBEDO        SURFACE SOLAR ALBEDO ARRAY
C*** EPSLW         SURFACE INFRARED EMISSIVITY ARRAY
C*** Z0            SURFACE ROUGHNESS HEIGHT ARRAY [CM]
C*** EVTR          TRUE MEANS POTENTIAL EVAPORATION ON
C*** FIXBC         TRUE MEANS FIXED TEMP. LOWER BC
C*** NX, NY        # CELL FACES ON EACH SIDE OF AXES.  (E.G., X RUNS
C***               -NX TO NX).  X IS POSITIVE SOUTH, Y IS POSITIVE WEST
C*** NZ            # CELLS FACES IN Z DIRECTION (K RUNS FROM 0 TO NZ)
C*** XFACE         ARRAYS OF CELL FACE COORDINATES [M]
C*** YFACE
C*** ZFACE
C*** IBOX, JBOX    INDICES THAT DESCRIBE BOX IN WHICH FLOOR OF BUILDING
C***               LIES (E.G., XFACE(IBOX) AND XFACE(-IBOX) BOUND X)
C*** SHAPE         0 FOR RECTANGULAR FLOOR PLAN
C***               1 FOR L-SHAPE WITH 1ST QUAD EMPTY
C***               2  "     "      "  2ND  "     "
C***               3  "     "      "  3RD  "     "
C***               4  "     "      "  4TH  "     "
C*** HBLDG         HEIGHT OF BUILDING FOR SHADOWING CALCULATION [M]
C*** TIN           INSIDE DRY BULB TEMPERATURE [C]
C*** HIN           INSIDE OVERALL HEAT TRANSFER COEFFICIENT [W/M**2/K]
C***               HIN(1): VALUE FOR Q DOWN, HIN(2): VALUE FOR Q UP
C*** IYRS          MAX # OF YEARS TO LOOP IN 3-D SOL'N.
C
C*** WEATHER DATA FILE:
C
C*** ISNW          1/0 FOR SNOW/NO SNOW ON GROUND
C*** TDB           AMBIENT DRY BULB [C]
C*** TWB           AMBIENT WET BULB
C*** PBAR          BAROMETRIC PRESSURE [N/M**2]
C*** HRAT          HUMIDITY RATIO
C*** WND           WIND SPEED [M/S]
```

```
C*** RBEAM          BEAM SOLAR RADIATION [W/M**2]
C*** RDIF           DIFFUSE SOLAR RADIATION
C
C*** DATA:
C
C*** NDIM           NUMBER OF DAYS IN MONTH
C*** NFDM           NUMBER OF THE FIRST DAY OF THE MONTH
C
C*** PHYSICAL VARIABLES:
C
C*** TG             CURRENT GROUND TEMPERATURE [C]
C*** T              TEMPERATURE, 3-D DOMAIN
C*** TOLD           LAST HOUR'S TEMPERATURES
C*** TCVG           3-D TEMPERATURE FIELD SAVED FOR CONVERGENCE TEST
C*** GOFT           SURFACE HEAT FLUXES FOR EXTERIOR CELLS
C***                GOFT(I,J,1)=CURRENT HOUR VALUE
C***                GOFT(I,J,2)=PREVIOUS HOUR VALUE
C*** RTOT           NET RADIANT FLUX TO THE GROUND
C
C*** MISCELLANEOUS VARIABLES
C
C*** NDIM           # DAYS IN EACH MONTH
C*** NFDM           # NUMBER OF THE FIRST DAY OF EACH MONTH
C*** XC, YC, ZC     ARRAYS OF CELL CENTER  COORDINATES
C*** DX, DY, DZ     ARRAYS OF CELL DIMENSIONS
C*** DXP,DYP,DZP    ARRAYS OF DISTANCES BETWEEN CENTERS (I) & (I+1)
C*** MTYPE          ARRAY OF MATERIAL PROPERTY INDICES THAT DEFINE BLDG
C***                (AT PRESENT, 1 FOR BUILDING, 2 FOR GROUND)
C*** MSURF          ARRAY OF SURFACE MATERIAL TYPES FOR USE IN SHADE CALC
C*** CXM,CYM,CZM    INTERFACE COEFFICIENTS USED IN FINITE DIFFERENCE
C***                EQNS:  CX(I,J,K)=KEFF(I-1/I)/DX(I)/DXP(I-1), ETC.
C*** CXP,CYP,CZP    INTERFACE COEFFICIENTS USED IN FINITE DIFFERENCE
C***                EQNS:  CX(I,J,K)=KEFF(I+1/I)/DX(I)/DXP(I), ETC.
C*** DA             AREA OF EACH SURFACE CELL [M^2]
C*** AFLOR          TOTAL SURFACE AREA OF FLOOR
C*** ATOT           TOTAL SURFACE AREA OF DOMAIN
C*** PERIM          PERIMETER OF SLAB [M]
C*** SYM            LOGICAL VARIABLE SET 'TRUE' IF SYMMETRY CAN BE USED
C***                TO REDUCE CALCULATION EFFORT
C*** SMULT          MULTIPLIER: '1' IF NO SYMMETRY, '4' IF SYMMETRY
C
C*** VARIABLES FOR OUTPUT STATISTICS
C
C*** TMNA, TMXA     MIN. AND MAX. SPACE-AVERAGED FLOOR TEMPS. FOR A DAY
C*** TBAR           TIME- AND SPACE-AVERAGED TEMPERATURE FOR A DAY
C*** TMN, TMX       MIN. AND MAX. FLOOR TEMPERATURES FOR A DAY
C*** QMNA, QMXA     DAILY MIN. AND MAX. SPACE-AVERAGED FLOOR HEAT FLUXES
C*** QBAR           TIME- AND SPACE-AVERAGED DAILY HEAT FLUX
C*** TS, QS         DAILY TIME-AVERAGED TEMPERATURE AND HEAT FLUX
C*** TV             DAILY TIME-AVERAGED TEMPERATURES IN N/S PLANE Y=0.
C*** TDBA           DAILY AVERAGED OUTDOOR DRY-BULB TEMPERATURE
C*** TDMN           DAILY MINIMUM OF HOURLY OUTDOOR DRY-BULB TEMPERATURE
C*** TDMX           DAILY MAXIMUM OF HOURLY OUTDOOR DRY-BULB TEMPERATURE
C
C*** FILE FOR DEBUG OUTPUT
C
      OPEN(UNIT=20,FILE='DBOUT',STATUS='NEW')
C
```

```
C*** READ NAME OF INPUT FILE
C
      OPEN(UNIT=10,FILE='RUNNAM',STATUS='OLD')
      READ(10,*) RUNID
      CLOSE(10)
C
C*** READ INPUT FILE
C
      OPEN(UNIT=10,FILE=RUNID,STATUS='OLD')
      READ(10,*) WEATHER,LONG,LAT,MSTD,ELEV,OLDTG,TGNAM,OLDSHD,SHDNAM,
     +           NMAT
C
      DO 100 I=1,NMAT
      READ(10,*) RHO(I), C(I), TCON(I)
  100 CONTINUE
C
      READ(10,*) RINS, DINS, ALBEDO,EPSLW,Z0,EVTR,FIXBC,NX,NY,NZ
      READ(10,*) (XFACE(I),I=-NX,NX)
      READ(10,*) (YFACE(I),I=-NY,NY)
      READ(10,*) (ZFACE(I),I=0,NZ)
      READ(10,*) IBOX,JBOX,SHAPE,HBLDG,TIN,HIN,IYRS
C
C*** COMPUTE SOME CELL GEOMETRY FACTORS
C
      NXM1=NX-1
      NYM1=NY-1
      NZM1=NZ-1
C
      DO 150 I=-NX,NXM1
      XC(I)=(XFACE(I)+XFACE(I+1))/2.
      DX(I)=XFACE(I+1)-XFACE(I)
  150 CONTINUE
C
      DO 151 I=-NX,NX-2
      DXP(I)=XC(I+1)-XC(I)
  151 CONTINUE
C
      DO 152 I=-NY,NYM1
      YC(I)=(YFACE(I)+YFACE(I+1))/2.
      DY(I)=YFACE(I+1)-YFACE(I)
  152 CONTINUE
C
      DO 153 I=-NY,NY-2
      DYP(I)=YC(I+1)-YC(I)
  153 CONTINUE
C
      DO 154 I=0,NZM1
      ZC(I)=(ZFACE(I)+ZFACE(I+1))/2.
      DZ(I)=ZFACE(I+1)-ZFACE(I)
  154 CONTINUE
      ZC(0)=0.
C
      DO 155 I=0,NZ-2
      DZP(I)=ZC(I+1)-ZC(I)
  155 CONTINUE
C
C*** ASSIGN MATERIAL PROPERTIES (I.E., DEFINE BUILDING LOCATION)
C*** THE SLAB IS, BY DEFINITION, ONE CELL THICK.
```

```
c*** MTYPE=1 FOR BLDG., MTYPE=2 FOR SOIL
C
      AFLOR=0.
      ATOT=(XFACE(NX)-XFACE(-NX))*(YFACE(NY)-YFACE(-NY))
C
      DO 200 I=-NX,NXM1
      DO 190 J=-NY,NYM1
      DO 180 K=0,NZM1
C
      IF(K.GE.1) THEN
        MTYPE(I,J,K)=2
      ELSE
        IF(XC(I).LT.XFACE(-IBOX).OR.XC(I).GT.XFACE(IBOX).OR.
     +     YC(J).LT.YFACE(-JBOX).OR.YC(J).GT.YFACE(JBOX)) THEN
          MTYPE(I,J,0)=2
        ELSE
          MTYPE(I,J,0)=1
          IF(SHAPE.EQ.1) THEN
            IF(XC(I).GT.0..AND.YC(J).GT.0.) THEN
              MTYPE(I,J,0)=2
            END IF
          ELSE IF(SHAPE.EQ.2) THEN
            IF(XC(I).LT.0..AND.YC(J).GT.0.) THEN
              MTYPE(I,J,0)=2
            END IF
          ELSE IF(SHAPE.EQ.3) THEN
            IF(XC(I).LT.0..AND.YC(J).LT.0.) THEN
              MTYPE(I,J,0)=2
            END IF
          ELSE IF(SHAPE.EQ.4) THEN
            IF(XC(I).GT.0..AND.YC(J).LT.0.) THEN
              MTYPE(I,J,0)=2
            END IF
          END IF
        END IF
      END IF
C
      IF(K.EQ.0) MSURF(I,J)=MTYPE(I,J,0)
C
  180 CONTINUE
C
C*** (CALCULATE FLOOR AREA OF BUILDING)
C
      DA(I,J)=DX(I)*DY(J)
      IF(MSURF(I,J).EQ.1) AFLOR=AFLOR+DA(I,J)
C
  190 CONTINUE
  200 CONTINUE
C
C*** CALCULATE PERIMETER OF BUILDING
C
      PERIM=2.*(XFACE(IBOX)-XFACE(-IBOX)+YFACE(JBOX)-YFACE(-JBOX))
C
C*** DETERMINE WHICH CELLS ARE INSULATED (IF ANY)
C
      DO 210 I=-NX,NXM1
      DO 209 J=-NY,NYM1
        IF(MSURF(I,J).EQ.1) THEN
```

```
            IF(XC(I).LT.(XFACE(-IBOX)+DINS).OR.
     +         XC(I).GT.(XFACE(IBOX)-DINS).OR.
     +         YC(J).LT.(YFACE(-JBOX)+DINS).OR.
     +         YC(J).LT.(YFACE(JBOX)-DINS)) THEN
              INS(I,J)=1
            ELSE IF(SHAPE.EQ.1) THEN
              IF(XC(I).GT.-DINS.OR.YC(J).GT.-DINS) INS(I,J)=1
            ELSE IF(SHAPE.EQ.2) THEN
              IF(XC(I).LT.DINS.OR.YC(J).GT.-DINS) INS(I,J)=1
            ELSE IF(SHAPE.EQ.3) THEN
              IF(XC(I).LT.DINS.OR.YC(J).LT.DINS) INS(I,J)=1
            ELSE IF(SHAPE.EQ.4) THEN
              IF(XC(I).GT.-DINS.OR.YC(J).LT.DINS) INS(I,J)=1
            END IF
          ELSE
            INS(I,J)=0
          END IF
  209   CONTINUE
  210   CONTINUE
C
C*** PRE-CALCULATE SOME FINITE-DIFFERENCE CONSTANTS
C
        CALL COEFFS(NXM1,NYM1,NZM1,DX,DY,DZ,DXP,DYP,DZP,MTYPE,
     +              TCON,RINS,INS,CXM,CYM,CZM,CXP,CYP,CZP)
C
C*** CONNECT WEATHER FILE
C
        OPEN(UNIT=13,FILE=WEATHER,STATUS='OLD')
C
C*** IF THERE IS AN OLD BOUNDARY CONDITION FILE FOR THIS PROBLEM,
C*** CONNECT IT AND CLOSE THE INPUT FILE. OTHERWISE, READ INITIAL
C*** CONDITION AND CREATE A NEW FILE WITH 1-D MODEL
C
        IF(OLDTG) THEN
          CLOSE(10)
          OPEN(UNIT=11,FILE=TGNAM,STATUS='OLD')
        ELSE
          READ(10,*) (TG(I),I=0,NZ)
          CLOSE(10)
          OPEN(UNIT=11,FILE=TGNAM,STATUS='NEW')
          CALL TEARTH(WEATHER,ELEV,TCON(2),RHO(2),C(2),ALBEDO,EPSLW,Z0,
     +                EVTR,FIXBC,NZ,ZC,DZ,DZP,TG,CVG1D)
C
        IF(.NOT.CVG1D) THEN
          STOP
        END IF
C
        END IF
C
C*** IF SHADE IS TURNED OFF IN THIS RUN, CONTINUE.
C*** IF THERE IS AN OLD SHADE FILE FOR THIS BUILDING, CONNECT IT
C*** AND CONTINUE.  OTHERWISE, CREATE A NEW FILE
C
        IF(SHDNAM.NE.'NOSHADE') THEN
          IF(OLDSHD) THEN
            OPEN(UNIT=12,FILE=SHDNAM,STATUS='OLD')
          ELSE
            OPEN(UNIT=12,FILE=SHDNAM,STATUS='NEW')
```

```
          CALL SHADE(LONG,LAT,MSTD,NX,NY,XC,YC,XFACE(IBOX),
     +     XFACE(-IBOX),YFACE(JBOX),YFACE(-JBOX),SHAPE,HBLDG,MSURF)
        END IF
      END IF
C
C*** ECHO INPUT DATA TO LFN 14
C
      FILNA=RUNID//'INP'
      OPEN(UNIT=14,FILE=FILNA,STATUS='NEW')
C
      WRITE(14,1100) RUNID,WEATHER,LONG,LAT,MSTD,ELEV
 1100 FORMAT( ' 3-D SLAB MODEL INPUT SUMMARY',//,
     + ' RUN IDENTIFIER: ',A,/,' WEATHER FILE ID: ',A6,/,
     + ' LONGITUDE (DEG): ',F5.1,'  LATITUDE (DEG): ',F5.1,/,
     + ' STANDARD TIME MERIDIAN (DEG): ',F5.1,/,
     + ' ELEVATION (M): ',F6.1)
C
      WRITE(14,1101) ALBEDO(1),ALBEDO(2),EPSLW(1),EPSLW(2),Z0(1),Z0(2),
     + RHO(2),C(2),TCON(2)
 1101 FORMAT(/,' SOIL AND SURFACE PROPERTIES:',//,
     + ' ALBEDO:',/,'    NO SNOW: ',F5.3,'  SNOW: ',F5.3,/,
     + ' LONG-WAVE EMISSIVITY:',/,'    NO SNOW: ',F5.3,
     + '  SNOW: ',F5.3,/,' ROUGHNESS LENGTH (CM):',/,
     + '    NO SNOW: ',F7.4,'  SNOW: ',F7.4,/,
     + ' DENSITY (KG/M**3): ',F6.1,/,
     + ' SPECIFIC HEAT (J/KG/K): ',F6.1,/,
     + ' THERMAL CONDUCTIVITY (W/M/K): ',F5.2)
C
      WRITE(14,1102) RHO(1),C(1),TCON(1),RINS,DINS,SHAPE,AFLOR,PERIM,
     +     XFACE(-IBOX),XFACE(IBOX),YFACE(-JBOX),YFACE(JBOX),
     +     ZFACE(1),HBLDG
 1102 FORMAT(/,' FLOOR MATERIAL PROPERTIES AND DIMENSIONS:',//,
     + ' DENSITY: ',F6.1,/,' SPECIFIC HEAT: ',F6.1,/,
     + ' THERMAL CONDUCTIVITY: ',F5.2,/,' UNDER-SLAB INSULATION:',
     + '    RESISTANCE (M**2 K/W): ',F5.1,'  WIDTH (M): ',F5.1,/,
     + ' FLOOR SHAPE: ',I1,/,' FLOOR AREA (M**2): ',F7.1,/,
     + ' PERIMETER (M): ',F6.1,/,
     + ' MIN X (M): ',F6.1,'  MAX X: ',F6.1,
     + /,' MIN Y (M): ',F6.1,'  MAX Y: ',F6.1,/,
     + ' FLOOR THICKNESS (M): ',F4.1,/,' BUILDING HEIGHT (M): ',
     + F4.1)
C
      WRITE(14,1103) TIN,HIN(1),HIN(2)
 1103 FORMAT(/,' BOUNDARY CONDITIONS:',//,' INSIDE AIR TEMP. (C): ',
     + F4.1,/,' FLOOR-AIR HEAT TRANSFER COEFF. (W/M**2/K): ',/,
     + '   Q INTO FLOOR: ',F4.2,'  Q OUT OF FLOOR: ',F4.2)
C
      IF(EVTR) THEN
        WRITE(14,1104)
 1104   FORMAT( ' POTENTIAL EVAPOTRANSPIRATION SURFACE BOUNDARY')
      ELSE
        WRITE(14,1105)
 1105   FORMAT( ' ZERO EVAPORATION SURFACE BOUNDARY')
      END IF
C
      IF(SHDNAM.EQ.'NOSHADE') THEN
        WRITE(14,1106)
 1106   FORMAT( ' NO SHADING OF GROUND BY BUILDING')
```

```
      ELSE
        WRITE(14,1107)
 1107   FORMAT( ' SHADING BY BUILDING INCLUDED')
      END IF
C
      IF(FIXBC) THEN
        WRITE(14,1108)
 1108   FORMAT( ' FIXED TEMPERATURE LOWER BOUNDARY')
      ELSE
        WRITE(14,1109)
 1109   FORMAT( ' ZERO FLUX LOWER BOUNDARY')
      END IF
C
      WRITE(14,1110) (XFACE(I),I=-NX,NX)
 1110 FORMAT( ' CELL X-COORDINATES (M):',/,4(10F7.2,/))
      WRITE(14,1111) (YFACE(J),J=-NY,NY)
 1111 FORMAT( ' CELL Y-COORDINATES (M):',/,4(10F7.2,/))
      WRITE(14,1112) (ZFACE(K),K=0,NZ)
 1112 FORMAT( ' CELL Z-COORDINATES (M):',/,3(10F7.2,/))
C
      CLOSE(14)
C
C*** CONNECT OUTPUT FILES
C
      FILNB=RUNID//'DLY'
      FILNC=RUNID//'HST'
      FILND=RUNID//'MTQ'
      FILNE=RUNID//'MTV'
C
      OPEN(UNIT=15,FILE=FILNB,STATUS='NEW')
      OPEN(UNIT=16,FILE=FILNC,STATUS='NEW')
      OPEN(UNIT=17,FILE=FILND,STATUS='NEW')
      OPEN(UNIT=18,FILE=FILNE,STATUS='NEW')
C
C*** INITIALIZE TEMPERATURES IN 3-D DOMAIN:
C***   T(X,Y,X)=TG(Z) (I.E., EQUAL TO B.C.)
C
      READ(11,*) RSKY,HHEAT,HMASS,(TG(I),I=0,NZM1)
      DO 220 I=-NX,NXM1
      DO 219 J=-NY,NYM1
      DO 218 K=0,NZM1
        T(I,J,K)=TG(K)
        TCVG(I,J,K)=TG(K)
  218 CONTINUE
  219 CONTINUE
  220 CONTINUE
C
C*** INITIALIZE SURFACE HEAT FLUX VALUES
C
      GINIT=TCON(2)*(TG(0)-TG(1))/DZP(0)
      DO 222 I=-NX,NXM1
      DO 221 J=-NY,NYM1
      GOFT(I,J,2)=GINIT
  221 CONTINUE
  222 CONTINUE
C
C*** DETERMINE WHETHER SYMMETRY CAN BE USED TO REDUCE DOMAIN SIZE
C*** FLOOR MUST BE RECTANGULAR AND SHADE MUST BE TURNED OFF
```

```
C
      IF(SHAPE.EQ.0.AND.SHDNAM.EQ.'NOSHADE') THEN
        NXMIN=0
        NYMIN=0
        SYM=.TRUE.
        SMULT=4.
      ELSE
        NXMIN=-NX
        NYMIN=-NY
        SYM=.FALSE.
        SMULT=1.
      END IF
C
C*** TIME LOOP FOR 3-D CALCULATION
C
      DO 800 IYR=1,IYRS
C
C*** IF SOLUTION HAS CONVERGED, SET SWITCH TO TERMINATE EXECUTION
C*** AFTER THIS YEAR
C
      IF(CVG) QUIT=.TRUE.
C
C*** POSITION WEATHER FILE AT BEGINNING OF YEAR (REWIND, SKIP HEADER)
C
      REWIND(13)
      READ (13,2000)
 2000 FORMAT(/)
C
C*** REWIND BOUNDARY CONDITION AND SHADE FILES
C
      REWIND(11)
      IF(SHDNAM.NE.'NOSHADE') THEN
        REWIND(12)
      END IF
C
      IMON=1
      DO 600 IDAY=1,365
      IF(IDAY.EQ.NFDM(IMON)+NDIM(IMON)) IMON=IMON+1
C
C*** IF THIS IS FINAL YEAR, INITIALIZE VARIABLES FOR OUTPUT STATISTICS
C
      IF(CVG.OR.IYR.EQ.IYRS) THEN
        TMNA=999.
        TMXA=-999.
        TBAR=0.
        TMN=999.
        TMX=-999.
        QMNA=999999.
        QMXA=-999999.
        QBAR=0.
        QMN=999999.
        QMX=-999999.
        TDBA=0.
        TDMN=999.
        TDMX=-999.
C
        DO 230 I=-NX,NXM1
        DO 228 J=-NY,NYM1
```

```
          TS(I,J)=0.
          QS(I,J)=0.
  228   CONTINUE
        DO 229 K=0,NZM1
          TV(I,K)=0.
  229   CONTINUE
  230   CONTINUE
C
      END IF
C
C*** READ ONE DAY OF WEATHER DATA
C
      READ(13,2010) ISNW,TDB,TWB,PBAR,HRAT,WND,RBEAM,RDIF
C
 2010 FORMAT( 33X,24I1,/,
     +       6(8F10.6,/),
     +       4(6F12.5,/),
     +       2(12F6.4,/),
     +       3(8F10.5,/),
     +       //,
     +       5(8F10.6,/),
     +       8F10.6)
C
C*** IF SHADING IS INCLUDED, CHECK FIRST LINE OF FILE
C*** FOR TODAY'S SUNRISE AND SUNSET HOURS
C
      IF(SHDNAM.NE.'NOSHADE') THEN
        READ(12,*) IJUNK,ISR,ISS,IJUNK
      END IF
C
      DO 400 IHR=1,24
C
C*** READ ONE HOUR OF GROUND TEMPERATURES, ETC.
C
      READ(11,*) RSKY,HHEAT,HMASS,DODPG,(TG(I),I=0,NZ)
C
C*** SET SHADE SWITCHES IF CALCULATION INCLUDES SHADE AND THE
C*** SUN IS UP
C
      IF(SHDNAM.NE.'NOSHADE') THEN
        IF(IHR.GE.ISR) THEN
          IF(IHR.LE.ISS+1) THEN
            DO 240 I=-NX,NXM1
            DO 239 J=-NY,NYM1
              IF(IHR.EQ.ISR) THEN
                SHADOW(I,J,2)=1.
              ELSE
                SHADOW(I,J,2)=SHADOW(I,J,1)
              END IF
  239       CONTINUE
  240       CONTINUE
          END IF
          IF(IHR.LE.ISS) THEN
            READ(12,*) ((SHADOW(I,J,1),J=-NY,NYM1),I=-NX,NXM1)
          END IF
          IF(IHR.LT.ISS) THEN
            READ(12,*)
          END IF
```

```
        END IF
      END IF
C
C*** FOR EXTERIOR SURFACE CELLS, COMPUTE SURFACE
C*** BOUNDARY CONDITION G(T) FOR THIS HOUR
C
C*** SET OLD VALUES OF BEAM AND DIFFUSE SOLAR RADIATION
C
      IF(IHR.GT.1) THEN
        RBO=RBEAM(IHR-1)
        RDO=RDIF(IHR-1)
      ELSE
        RBO=RBEAM(1)
        RDO=RDIF(1)
      END IF
C
C*** SET SURFACE PROPERTIES FOR THIS HOUR
C
      ISP=1+ISNW(IHR)
      EPS=EPSLW(ISP)
      ALB=ALBEDO(ISP)
C
C*** LOOP THROUGH EXTERIOR SURFACE CELLS
C
      DO 250 I=NXMIN,NXM1
      DO 249 J=NYMIN,NYM1
      IF(MSURF(I,J).EQ.2) THEN
C
C*** DETERMINE RADIATIVE FLUX TO CELL SURFACE
C
      RGRND=5.670E-08*(T(I,J,0)+273.15)**4
        IF(SHDNAM.EQ.'NOSHADE') THEN
          RTOT=(1.-ALB)*(RBEAM(IHR)+RBO+RDIF(IHR)+RDO)/2.+
     +          EPS*(RSKY-RGRND)
        ELSE IF(IHR.LT.ISR.OR.IHR.GT.ISS+1)THEN
          RTOT=(1.-ALB)*(RDIF(IHR)+RDO)/2.+EPS*(RSKY-RGRND)
        ELSE IF(IHR.EQ.ISS+1) THEN
          RTOT=(1.-ALB)*(SHADOW(I,J,2)*RBO+RDIF(IHR)+RDO)/2.+
     +          EPS*(RSKY-RGRND)
        ELSE
          RTOT=(1.-ALB)*(SHADOW(I,J,1)*RBEAM(IHR)+SHADOW(I,J,2)*RBO+
     +           RDIF(IHR)+RDO)/2.+EPS*(RSKY-RGRND)
        END IF
C
C*** CALCULATE G(T) FOR EVAPORATION OFF/ON CASES
C
        GOFT(I,J,1)=RTOT-HHEAT*(T(I,J,0)-TDB(IHR))
        IF(EVTR) THEN
          GOFT(I,J,1)=GOFT(I,J,1)-DODPG*(RTOT-GOFT(I,J,2))
     +                -HMASS*(TDB(IHR)-TWB(IHR))
        END IF
      END IF
C
C*** IF DOMAIN IS SYMMETRIC, ASSIGN VALUES BY REFLECTION
C
      IF(SYM) THEN
        GOFT(I,-J-1,1)=GOFT(I,J,1)
        GOFT(-I-1,J,1)=GOFT(I,J,1)
```

```
        GOFT(-I-1,-J-1,1)=GOFT(I,J,1)
      END IF
  249 CONTINUE
  250 CONTINUE
C
C*** SOLUTION BY THE EXPLICIT METHOD:
C
      DO 300 I=NXMIN,NXM1
      DO 299 J=NYMIN,NYM1
      DO 298 K=0,NZM1
C
C*** X-DIFFUSION TERM
C
      IF(I.EQ.-NX) THEN
        XDIF=TCON(MTYPE(-NX,J,K))*(TG(K)-TOLD(-NX,J,K))/DX(-NX)/DX(-NX)
     +       +CXP(-NX,J,K)*(TOLD(-NX+1,J,K)-TOLD(-NX,J,K))
      ELSE IF(I.EQ.NXM1) THEN
        XDIF=CXM(NXM1,J,K)*(TOLD(NX-2,J,K)-TOLD(NXM1,J,K))
     +       +TCON(MTYPE(NXM1,J,K))*(TG(K)-TOLD(NXM1,J,K))/
     +        DX(NXM1)/DX(NXM1)
      ELSE
        XDIF=CXM(I,J,K)*TOLD(I-1,J,K)
     +       -(CXM(I,J,K)+CXP(I,J,K))*TOLD(I,J,K)
     +       +CXP(I,J,K)*TOLD(I+1,J,K)
      END IF
C
C*** Y-DIFFUSION TERM
C
      IF(J.EQ.-NY) THEN
        YDIF=TCON(MTYPE(I,-NY,K))*(TG(K)-TOLD(I,-NY,K))/DY(-NY)/DY(-NY)
     +       +CYP(I,-NY,K)*(TOLD(I,-NY+1,K)-TOLD(I,-NY,K))
      ELSE IF(J.EQ.NYM1) THEN
        YDIF=CYM(I,NYM1,K)*(TOLD(I,NY-2,K)-TOLD(I,NYM1,K))
     +       +TCON(MTYPE(I,NYM1,K))*(TG(K)-TOLD(I,NYM1,K))/
     +        DY(NYM1)/DY(NYM1)
      ELSE
        YDIF=CYM(I,J,K)*TOLD(I,J-1,K)
     +       -(CYM(I,J,K)+CYP(I,J,K))*TOLD(I,J,K)
     +       +CYP(I,J,K)*TOLD(I,J+1,K)
      END IF
C
C*** Z-DIFFUSION TERM
C
      IF(K.EQ.0) THEN
        IF(MTYPE(I,J,0).EQ.2) THEN
          ZDIF=GOFT(I,J,1)/DZ(0)+CZP(I,J,0)*(TOLD(I,J,1)-TOLD(I,J,0))
        ELSE IF(MTYPE(I,J,0).EQ.1) THEN
          IF(TIN.GT.T(I,J,0)) THEN
            HROOM=HIN(1)
          ELSE
            HROOM=HIN(2)
          END IF
          ZDIF=HROOM*(TIN-TOLD(I,J,0))/DZ(0)
     +         +CZP(I,J,0)*(TOLD(I,J,1)-TOLD(I,J,0))
        END IF
      ELSE IF(K.EQ.NZM1) THEN
        ZDIF=CZM(I,J,NZM1)*(TOLD(I,J,NZ-2)-TOLD(I,J,NZM1))
     +       +TCON(MTYPE(I,J,NZM1))*2.*(TG(NZ)-TOLD(I,J,NZM1))
```

```
     +        /DZ(NZM1)/DZ(NZM1)
      ELSE
        ZDIF=CZM(I,J,K)*TOLD(I,J,K-1)
     +       -(CZM(I,J,K)+CZP(I,J,K))*TOLD(I,J,K)
     +       +CZP(I,J,K)*TOLD(I,J,K+1)
      END IF
C
C*** UPDATE TEMPERATURE AT THIS NODE
C
      T(I,J,K)=TOLD(I,J,K)
     +         +(XDIF+YDIF+ZDIF)*3600./RHO(MTYPE(I,J,K))/C(MTYPE(I,J,K))
C
C*** IF DOMAIN IS SYMMETRIC, ASSIGN VALUES BY REFLECTION
C
      IF(SYM) THEN
        T(I,-J-1,K)=T(I,J,K)
        T(-I-1,J,K)=T(I,J,K)
        T(-I-1,-J-1,K)=T(I,J,K)
      END IF
C
  298 CONTINUE
  299 CONTINUE
  300 CONTINUE
C
C*** RESET TOLD AND GOFT(I,J,2)
C
      DO 303 I=-NX,NXM1
      DO 302 J=-NY,NYM1
        GOFT(I,J,2)=GOFT(I,J,1)
      DO 301 K=0,NZM1
        TOLD(I,J,K)=T(I,J,K)
  301 CONTINUE
  302 CONTINUE
  303 CONTINUE
C
C*** COMPUTE SPATIAL AVERAGES (WEIGHTED BY AREA) AND CHECK FOR
C*** NEW LOCAL MIN/MAX OF FLOOR TEMP. AND HEAT FLUX, MAKE OUTPUT
C
      IF(CVG.OR.IYR.EQ.IYRS) THEN
        TSUM=0.
        QSUM=0.
        DO 310 I=NXMIN,NXM1
        DO 309 J=NYMIN,NYM1
          IF(MSURF(I,J).EQ.1) THEN
            TSUM=TSUM+T(I,J,0)*SMULT*DA(I,J)
            TMN=MIN(TMN,T(I,J,0))
            TMX=MAX(TMX,T(I,J,0))
              IF(TIN.GT.T(I,J,0)) THEN
                HROOM=HIN(1)
              ELSE
                HROOM=HIN(2)
              END IF
            QQ=HROOM*(TIN-T(I,J,0))
            QSUM=QSUM+QQ*SMULT*DA(I,J)
            QMN=MIN(QMN,QQ)
            QMX=MAX(QMX,QQ)
          END IF
  309   CONTINUE
```

```
  310   CONTINUE
C
C*** CHECK FOR MAX/MIN HOURLY SPATIAL AVERAGE VALUES
C
        TMNA=MIN(TMNA,TSUM/AFLOR)
        TMXA=MAX(TMXA,TSUM/AFLOR)
        QMNA=MIN(QMNA,QSUM/AFLOR)
        QMXA=MAX(QMXA,QSUM/AFLOR)
C
C*** CHECK FOR HOURLY MIN/MAX OUTDOOR DRY-BULB
C
      TDMN=MIN(TDMN,TDB(IHR))
      TDMX=MAX(TDMX,TDB(IHR))
C
C*** CALCULATE DAILY, SPATIALLY AVERAGED FLOOR TEMP AND HEAT FLUX
C
        TBAR=TBAR+TSUM/AFLOR/24.
        QBAR=QBAR+QSUM/AFLOR/24.
        TDBA=TDBA+TDB(IHR)/24.
C
C*** CALCULATE TIME-AVERAGED SURFACE AND X-Z PLANE INFORMATION ON 21ST
C*** OF EACH MONTH
C
        IF(IDAY.EQ.NFDM(IMON)+20) THEN
          DO 320 I=-NX,NXM1
C
C*** SURFACE
C
          DO 318 J=-NY,NYM1
            TS(I,J)=TS(I,J)+T(I,J,0)/24.
            IF(MSURF(I,J).EQ.1) THEN
              IF(TIN.GT.T(I,J,0)) THEN
                HROOM=HIN(1)
              ELSE
                HROOM=HIN(2)
              END IF
              QS(I,J)=QS(I,J)+HROOM*(TIN-T(I,J,0))/24.
            ELSE IF(MSURF(I,J).EQ.2) THEN
              QS(I,J)=QS(I,J)+GOFT(I,J,1)/24.
            END IF
  318     CONTINUE
C
C*** VERTICAL PLANE
C
          DO 319 K=0,NZM1
            TV(I,K)=TV(I,K)+T(I,0,K)/24.
  319     CONTINUE
  320     CONTINUE
C
        END IF
C
C*** MAKE HOURLY SURFACE TEMPERATURE DISTRIBUTION OUTPUT ON JAN 21
C
      IF(IDAY.EQ.21) THEN
        DO 330 I=-NX-1,NX
          IF(I.EQ.-NX-1) THEN
            XH=XC(-NX)-DX(-NX)
          ELSE IF(I.EQ.NX) THEN
```

```
            XH=XC(NXM1)+DX(NXM1)
          ELSE
            XH=XC(I)
          END IF
        DO 329 J=-NY-1,NY
          IF(J.EQ.-NY-1) THEN
            YH=YC(-NY)-DY(-NY)
          ELSE IF(J.EQ.NY) THEN
            YH=YC(NYM1)+DY(NYM1)
          ELSE
            YH=YC(J)
          END IF
          IF(I.EQ.-NX-1.OR.I.EQ.NX.OR.J.EQ.-NY-1.OR.J.EQ.NY) THEN
            TH=TG(0)
          ELSE
            TH=T(I,J,0)
          END IF
          WRITE(16,1300) IHR,XH,YH,TH
 1300     FORMAT( I3,2(2X,F7.2),2X,F5.1)
  329   CONTINUE
  330   CONTINUE
      END IF
C
      END IF
C
  400 CONTINUE
C
C*** MAKE DAILY AVERAGE SURFACE AND X-Z PLANE TEMPERATURE OUTPUT
C*** ONCE EACH MONTH
C
      IF(CVG.OR.IYR.EQ.IYRS) THEN
        WRITE(15,1200) IDAY,TMN,TMX,TMNA,TMXA,TBAR,TIN,TDMN,
     +                 TDMX,TDBA,QMN,QMX,QMNA,QMXA,QBAR
 1200   FORMAT( I4,14(2X,F5.1))
        IF(IDAY.EQ.NFDM(IMON)+20) THEN
          DO 450 I=-NX,NXM1
          DO 448 J=-NY,NYM1
            WRITE(17,1400) IMON,XC(I),YC(J),TS(I,J),QS(I,J)
 1400       FORMAT( I2,2(2X,F7.2),F5.1,F6.1)
  448     CONTINUE
          DO 449 K=0,NZM1
            WRITE(18,1500) IMON,XC(I),ZC(K),TV(I,K)
 1500       FORMAT( I2,2X,F7.2,2X,F6.2,F5.1)
  449     CONTINUE
  450     CONTINUE
        END IF
      END IF
C
  600 CONTINUE
C
C*** TEST FOR CONVERGENCE AT END OF YEAR
C
      CVG=.TRUE.
C
      DO 650 K=0,NZM1
      DO 649 I=-NX,NXM1
      DO 648 J=-NY,NYM1
        IF(ABS(T(I,J,K)-TCVG(I,J,K)).GE.0.1) CVG=.FALSE.
```

```
        TCVG(I,J,K)=T(I,J,K)
  648 CONTINUE
  649 CONTINUE
  650 CONTINUE
C
      WRITE(20,*) ' YEAR = ', IYR
C
C*** DETERMINE WHETHER EXECUTION SHOULD CONTINUE.  IF NOT,
C*** CLOSE ALL OPEN FILES AND STOP
C
      IF(QUIT.OR.IYR.EQ.IYRS) THEN
C
C*** DATA FILES
C
        CLOSE(11)
        CLOSE(12)
        CLOSE(13)
C
C*** OUTPUT FILES
C
        CLOSE(15)
        CLOSE(16)
        CLOSE(17)
        CLOSE(18)
C
C*** DEBUG FILE
C
        WRITE(20,*) 'CVG = ',CVG
C
        CLOSE(20)
C
        STOP
      END IF
  800 CONTINUE
      STOP
      END
```

B.2. SUBROUTINE TEARTH

```
      SUBROUTINE TEARTH(WEATHER,ELEV,TCON,RHO,CG,ALBEDO,EPSLW,Z0,EVTR,
     +                  FIXBC,NZ,ZC,DZ,DZP,TG,CVG)
C
C*** THIS SUBROUTINE CALCULATES THE 1-D, HOURLY TEMPERATURE
C*** DISTRIBUTION IN THE GROUND.  IT WRITES ONE YEAR OF TEMPERATURES,
C*** SKY RADIATION, AND SURFACE CONVECTION COEFFICIENTS TO LFN 8
C
C*** VERSION 1.0, 20 JULY, 1988
C
C*** WILLIAM BAHNFLETH
C
C*** DECLARATIONS:
C
      REAL ELEV,TCON,RHO,CG,ALBEDO(2),EPSLW(2),Z0(2),ZC(0:19),DZ(0:19),
     +   DZP(0:18),TG(0:19),TGCVG(0:19),CONST(0:19,2),
     +   TDB(24),TWB(24),PBAR(24),HRAT(24),WND(24),RBEAM(24),RDIF(24),
     +   A(21),B(21),C(21),X(21),R(21)
C
      INTEGER NZ,MAXYR,NDIM(12),NFDM(12),ISNW(24)
C
      LOGICAL EVTR,FIXBC,CVG
C
      DATA NDIM/31,28,31,30,31,30,31,31,30,31,30,31/,
     +     NFDM/1,32,60,91,121,152,182,213,244,274,305,335/,
     +     MAXYR/20/
C
      CVG=.FALSE.
C
C*** VARIABLE DEFINITIONS:  CONSULT LISTING OF SLAB3D
C
C*** NZ          THE NUMBER OF CELL FACES IN THE 3-D MODEL
C***             (THERE ARE NZ+1 TEMPS IN THE BC FILE)
C
C*** CALCULATE SOME CONSTANTS USED IN FINITE DIFFERENCE MATRIX
C
      DO 110 I=1,NZ-1
      CONST(I,1)=TCON*3600./RHO/CG/DZ(I)/DZP(I-1)
  110 CONTINUE
C
      DO 120 I=0,NZ-2
      CONST(I,2)=TCON*3600./RHO/CG/DZ(I)/DZP(I)
  120 CONTINUE
      CONST(NZ-1,2)=TCON*7200./RHO/CG/DZ(NZ-1)/DZ(NZ-1)
C
*** FOR FIXED TEMPERATURE LOWER B.C., SET BOUNDARY VALUE
C
      IF(FIXBC) TDEEP=TG(NZ)
C
C*** ESTIMATE CONDUCTION TO GROUND FOR FIRST STEP OF CALCULATION
C
      GOLD=TCON*(TG(0)-TG(1))/DZP(0)
C
C*** POSITION WEATHER FILE
C
```

```
      READ (13,1000)
 1000 FORMAT(/)
C
C*** TIME LOOP:
C
C*** YEARS:
C
      DO 800 IYR=1,MAXYR
C
C*** AT BEGINNING OF YEAR, UPDATE CONVERGENCE TEST TEMPERATURES
C
      DO 100 I=0,NZ
      TGCVG(I)=TG(I)
  100 CONTINUE
C
C
C*** MONTHS:
C
      DO 600 IMON=1,12
C
C*** DAYS:
C
      DO 400 IDAY=1,NDIM(IMON)
C
C*** READ ONE DAY OF WEATHER FROM FILE
C
      READ(13,1100) ISNW,TDB,TWB,PBAR,HRAT,WND,RBEAM,RDIF
C
 1100 FORMAT( 33X,24I1,/,
     +       6(8F10.6,/),
     +       4(6F12.5,/),
     +       2(12F6.4,/),
     +       3(8F10.5,/),
     +       //,
     +       5(8F10.6,/),
     +       8F10.6)
C
C*** CALCULATE AVERAGE WINDSPEED FOR DAY
C
      AVGWND=0.
      DO 150 I=1,24
        AVGWND=AVGWND+WND(I)/24.
  150 CONTINUE
C
C*** HOURS:
C
      DO 200 IHR=1,24
C
C*** SAVE OLD VALUES OF TDB AND R FOR LAGGED G(T) CALCULATION
C
      IF(IHR.EQ.1) THEN
        TDBO=TDB(IHR)
        RBMO=RBEAM(IHR)
        RDFO=RDIF(IHR)
      ELSE
        TDBO=TDB(IHR-1)
        RBMO=RBEAM(IHR-1)
        RDFO=RDIF(IHR-1)
```

```
      END IF
C
C*** SET SURFACE PROPERTIES FOR THIS HOUR
C
      ISP=1+ISNW(IHR)
C
      ALB=ALBEDO(ISP)
      EPS=EPSLW(ISP)
      ZZER=Z0(ISP)
C
C*** CALCULATE PROPERTIES OF AMBIENT AIR FOR THIS HOUR
C
      CALL AIRPROPS(HRAT(IHR),PBAR(IHR),TDB(IHR),ELEV,
     +              PVAP,RHOA,CPA,DODPG)
C
C*** CALCULATE CONVECTIVE HEAT & MASS TRANSFER COEFFICIENTS DH AND DW
C
      CALL CHMTC(ZZER,WND(IHR),AVGWND,TDB(IHR),TG(0),DH,DW)
C
C*** SET UP COEFFICIENT MATRIX
C
C*** INTERIOR CELLS
C
      DO 160 I=1,NZ-2
      II=I+1
      A(II)=-CONST(I,1)
      B(II)=1.+CONST(I,1)+CONST(I,2)
      C(II)=-CONST(I,2)
      R(II)=TG(I)
  160 CONTINUE
C
C*** LOWER BOUNDARY (2 CASES: FIXED TEMPERATURE (FIXBC=T) AND
C***                  ZERO HEAT FLUX (FIXBC=F))
C
      IF(FIXBC) THEN
        A(NZ)=-CONST(NZ-1,1)
        B(NZ)=1.+CONST(NZ-1,1)+CONST(NZ-1,2)
        R(NZ)=CONST(NZ-1,2)*TDEEP+TG(NZ-1)
      ELSE
        A(NZ)=-CONST(NZ-1,1)
        B(NZ)=1.+CONST(NZ-1,1)
        R(NZ)=TG(NZ-1)
      END IF
C
C*** UPPER BOUNDARY (GROUND SURFACE)
C
C*** CALCULATE G(T)
C
C*** INFRARED RADIATION:
C
C***   SKY RADIATION FROM ANGSTROM/GEIGER EQUATION
C
      RSKY=5.670E-08*((TDBO+273.15)**4)*
     +     (0.820-0.250*EXP(-0.002162*PVAP))
C
C***   NET INFRARED TO GROUND
C
      RLW=EPS*(RSKY-5.670E-08*(TG(0)+273.15)**4)
```

```
C
C*** NET SOLAR RADIATION
C
      RSW=(1.-ALB)*(RBMO+RDFO+RBEAM(IHR)+RDIF(IHR))/2.
C
C*** SENSIBLE CONVECTIVE LOSS
C
      QCS=RHOA CPA*DH*(TG(0)-TDBO)
C
C*** COMPUTE LATENT HEAT LOSSES IF EVTR=T
C
      IF(EVTR) THEN
        QEV=DODPG*(RLW+RSW-GOLD)
        QCL=RHOA*CPA*DW*(TDB(IHR)-TWB(IHR))
        ELSE
       QEV=0.
        QCL=0.
      END IF
C
C*** COMPUTE NET FLUX CONDUCTED INTO THE GROUND,G(T)
C
      GOFT=RSW+RLW-QCS-QEV-QCL
C
C*** RESET GOLD
C
      GOLD=GOFT
C
C*** COMPUTE COEFFICIENTS FOR SURFACE CELL
C
      B(1)=1.+CONST(0,2)
      C(1)=-CONST(0,2)
      R(1)=TG(0)+GOFT*3600./RHO/CG/DZ(0)
C
C*** SOLVE SYSTEM WITH TRIDIAGONAL MATRIX ALGORITHM
C
      CALL TRIDI(A,B,C,X,R,NZ)
C
      DO 165 I=0,NZ-1
      TG(I)=X(I+1)
  165 CONTINUE
      IF(.NOT.FIXBC) TG(NZ)=TG(NZ-1)
C
C*** IF TEMPERATURE FIELD HAS CONVERGED, RESULTS ARE WRITTEN TO
C*** LFN 8 (RSKY, CONVECTIVE HEAT AND MASS TRANSFER COEFFICIENTS
C*** (I.E., RHO*CPA*DH & RHO*CPA*DW), AND TG(I))
C
      IF(CVG) THEN
        WRITE(11,*) RSKY,RHOA*CPA*DH,RHOA*CPA*DW,DODPG
        WRITE(11,*) (TG(I),I=0,NZ)
      END IF
C
  200 CONTINUE
  400 CONTINUE
  600 CONTINUE
C
C*** TEST FOR CONVERGENCE AT 2400 HRS ON 31 DECEMBER
C
      IF(.NOT.CVG) THEN
```

```
C
        IF(IYR.EQ.MAXYR-1) THEN
          RETURN
        ELSE
          CVG=.TRUE.
          DO 650 I=0,NZ
          IF(ABS(TG(I)-TGCVG(I)).GT.0.05) CVG=.FALSE.
  650     CONTINUE
        END IF
C
      ELSE
      REWIND(11)
      RETURN
      END IF
C
C*** REWIND AND POSITION WEATHER FILE AT YEAR END
C
      REWIND(13)
      READ(13,1000)
C
  800 CONTINUE
C
      RETURN
      END
```

B.3. SUBROUTINE AIRPROPS

```
      SUBROUTINE AIRPROPS(HRAT,PBAR,TDB,ELEV,PVAP,RHOA,CPA,DODPG)
C
C*** THIS SUBROUTINE CALCULATES PROPERTIES OF AIR.
C*** VAPOR PRESSURE, DENSITY, AND CONSTANT PRESSURE SPECIFIC HEAT
C*** ARE COMPUTED WITH RELATIONS PUBLISHED IN THE ASHRAE HANDBOOK
C*** OF FUNDAMENTALS, 1985 SI VERSION.  THE EVAPORATION PARAMETER
C*** DELTA/(DELTA + GAMMA) IS COMPUTED BY A 2ND ORDER CURVE FIT TO
C*** DATA PUBLISHED IN "CONSUMPTIVE USE OF WATER," ASCE, 1973.
C
C*** VERSION 1.0, 21 JULY 1988
C
C*** WM. BAHNFLETH
C
C*** VARIABLES:
C
C***     HRAT: HUMIDITY RATIO, DIMENSIONLESS
C***     PBAR: BAROMETRIC PRESSURE [N/M**2]
C***     TDB: AMBIENT DRY BULB TEMPERATURE [C]
C***     ELEV: ELEVATION ABOVE SEA LEVEL [M]
C***     PVAP: VAPOR PRESSURE OF AMBIENT AIR [N/M**2]
C***     RHOA: AIR DENSITY [KG/M**3]
C***     CPA: CONSTANT PRESSURE SPECIFIC HEAT OF AIR [J/KG/K]
C***     DODPG: DELTA/(DELTA + GAMMA), DIMENSIONLESS
C
      PVAP=(HRAT/(HRAT+0.62198))*PBAR
      RHOA=(PBAR-0.3780*PVAP)/(287.055*(TDB+273.15))
      CPA=1007.+863*PVAP/PBAR
      DODPG=0.395643+
     1      0.170926E-01*TDB-0.140959E-03*TDB*TDB+
     2      0.309091E-04*ELEV+0.822511E-09*ELEV*ELEV-
     3      0.472208E-06*TDB*ELEV
C
      RETURN
      END
```

B.4. SUBROUTINE CHMTC

```
      SUBROUTINE CHMTC(Z0CM,WND,AVGWND,TDB,TG,DH,DW)
C
C*** THIS SUBROUTINE COMPUTES TURBULENT HEAT AND MASS TRANSFER
COEFFICIENTS
C*** FOR ONE HOUR USING THE CORELLATION OF SELLERS AND DRYDEN
C
C*** VERSION 1.0 21 JULY 1988
C
C*** WM. BAHNFLETH
C
C***    Z0CM: ROUGHNESS HEIGHT AS INPUT [CM]
C***    Z0: ROUGHNESS HEIGHT AS USED [M]
C***    WND: WIND SPEED [M/S]
C***    AVGWND: AVERAGE WIND SPEED FOR DAY [M/S]
C***    TDB: AMBIENT DRY BULB TEMPERATURE [C]
C***    TG: GROUND SURFACE TEMPERATURE [C]
C***    DM: NEUTRAL STABILITY COEFFICIENT [M/S]
C***    DTV2: STABILITY PARAMETER ANALOG. TO RICHARDSON NO. (RI)
C***    DH: STABILITY CORRECTED HEAT TRANSFER COEFFICIENT [M/S]
C***    DW:     "          "     MASS    "          "      [M/S]
C
      Z0=Z0CM/100.
      ALGZ0=ALOG(2./Z0)
C
C*** ESTIMATE 2M WIND SPEED FROM 10M SPEED BY LOG B.L. ASSUMPTION
C*** (IF 10M WINDSPEED IS ZERO, USE DAILY AVERAGE WIND)
C
      IF(WND.EQ.0.) THEN
      WND2=AVGWND*ALGZ0/ALOG(10./Z0)
      ELSE
      WND2=WND*ALGZ0/ALOG(10./Z0)
      END IF
C
      DM=0.164*WND2/ALGZ0/ALGZ0
      DTV2=(TG-TDB)/WND2/WND2
C
C*** SELECT APPROPRIATE FORM OF CORRECTION TERM (UNSTABLE/STABLE) AND
C*** COMPUTE COEFFICIENTS
C
      IF(DTV2.GE.0.) THEN
      DH=DM*(1.+14.*DTV2)**0.33333333
      DW=DM*(1.+10.5*DTV2)**0.33333333
      ELSE
      DH=DM*(1.-14.*DTV2)**(-0.33333333)
      DW=DM*(1.-10.5*DTV2)**(-0.33333333)
      END IF
C
      RETURN
      END
```

B.5. SUBROUTINE TRIDI

```
      SUBROUTINE TRIDI(A,B,C,X,R,N)
C
C*** THIS SUBROUTINE SOLVES A TRIDIAGONAL SYSTEM OF EQUATIONS
C*** BY THE THOMAS ALGORITHM.  THIS VERSION IS TAKEN FROM
C*** "NUMERICAL MARCHING TECHNIQUES FOR FLUID FLOWS WITH HEAT
C*** TRANSFER" BY ROBERT W. HORNBECK, NASA, 1973.
C
C*** A,B,AND C ARE, RESPECTIVELY, THE LOWER, MAJOR, AND UPPER
C*** DIAGONAL COEFFICIENT VALUES.  FOR A SYSTEM OF N EQUATIONS,
C*** INDICES OF A RUN FROM 2 TO N, INDICES OF B FROM 1 TO N, AND
C*** INDICES OF C FROM 1 TO N-1.  R IS THE RIGHT-HAND SIDE VECTOR
C*** OF THE SYSTEM.  THE UNKNOWN VECTOR IS RETURNED AS X.
C
      DIMENSION A(120),B(120),C(120),X(120),R(120)
C
      A(N)=A(N)/B(N)
      R(N)=R(N)/B(N)
C
      DO 1100 I=2,N
      II=-I+N+2
      BN=1./(B(II-1)-A(II)*C(II-1))
      A(II-1)=A(II-1)*BN
      R(II-1)=(R(II-1)-C(II-1)*R(II))*BN
 1100 CONTINUE
C
      X(1)=R(1)
C
      DO 1101 I=2,N
      X(I)=R(I)-A(I)*X(I-1)
 1101 CONTINUE
C
      RETURN
      END
```

B.6. SUBROUTINE SHADE

```
      SUBROUTINE SHADE(LONG,LAT,MSTD,NX,NY,XC,YC,XMAX,XMIN,
     +                 YMAX,YMIN,SHAPE,HBLDG,MSURF)
C
C*** THIS SUBROUTINE CALCULATES THE SHADOW CAST ON THE GROUND
C*** BY A BUILDING.  THE LINE IN THE DIRECTION OF SOLAR BEAM
C*** RADIATION ORIGINATING AT THE CENTER OF EACH EXTERIOR
C*** SURFACE CELL IS TESTED TO DETERMINE WHETHER IT INTERSECTS
C*** THE BUILDING.  THE FRACTION OF EACH CELL IN SHADOW IS NOT
C*** COMPUTED.  IT IS ASSUMED THAT THE ENTIRE CELL IS SHADED
C*** IF ITS CENTER IS IN SHADOW AND THAT THE ENTIRE CELL IS
C*** UNSHADED IF ITS CENTER IS NOT IN SHADOW.  THE SUN IS
C*** ASSUMED TO BE "UP" IF BEAM RADIATION ON THE WEATHER TAPE
C*** IS NON-ZERO REGARDLESS OF WHETHER ZENITH ANGLE IS LESS
C*** THAN NINETY DEGREES.
C
C*** VERSION 1.0, 21 JULY 1988
C
C*** WM. BAHNFLETH
C
C*** DECLARATIONS:
C
      REAL MSTD,LONG,LAT,ENDS(6,2),VALUE(6),RBEAM(24),GAMMA(24),
     +     THETAZ(24),SHADOW(-20:19,-20:19),XC(-20:19),YC(-20:19)
C
      INTEGER SHAPE,MSURF(-20:19,-20:19),IDIR(6)
C
      DATA PI/3.14159/
C
C*** VARIABLE DEFINITIONS:
C
C***   LONG:        LONGITUDE [DEG]
C***   LAT:         LATITUDE [DEG]
C***   MSTD:        STANDARD TIME MERIDIAN [DEG]
C***   NX, NY:      CELL INDICES (E.G., -NX TO NX-1 IN THE X-DIR)
C***   XC, YC:      CELL CENTER COORDINATES [M]
C***   XMIN, XMAX: DEFINE X-LIMITS OF BOX AROUND BUILDING
C***   YMIN, YMAX: AS ABOVE FOR Y-DIRECTION
C***   SHAPE:       INDEX DEFINING BUILDING SHAPE.  0 FOR
C***                RECTANGLE, 1,2,3, OR 4 FOR L-SHAPE WITH
C***                THE INDICATED QUADRANT EMPTY.  QUADRANTS
C***                ARE COUNTER-CLOCKWISE IN THE X-Y PLANE
C***                WITH RESPECT TO A RIGHT-HANDED SYSTEM WITH
C***                Z INTO THE GROUND AND X FACING SOUTH.
C***   HBLDG:       HEIGHT OF THE BUILDING [M]
C***   MSURF:       2-D ARRAY OF SURFACE MATERIAL TYPE INDICES
C***   IDIR:        WALL DIRECTION ARRAY.  1 RUNS N/S, 2 RUNS E/W
C***   ENDS:        ARRAY OF WALL END POINT COORDINATES.
C***                FIRST VALUE IS MIN, SECOND IS MAX
C***   VALUE:       FOR E/W RUNNING WALL, THE X VALUE, FOR N/S WALL, Y
C***   NWALLS:      NUMBER OF WALLS:  4 FOR RECTANGLE, 6 FOR L-SHAPE
C***   RBEAM:       BEAM RADIATION READ FROM WEATHER TAPE
C***   B:           CONSTANT USED IN 'EQUATION OF TIME'
C***   ET:          SOLAR 'EQUATION OF TIME' [MIN]
C***   TCORR:       CORRECTION FROM LOCAL STANDARD TIME TO
```

```
C***                SOLAR TIME [HRS]
C***   TSOL:        SOLAR TIME [HRS]
C***   OMEGA:       HOUR ANGLE [RADIANS]
C***   THETAZ:      ZENITH ANGLE [RADIANS]
C***   GAMMA:       SOLAR AZIMUTH ANGLE [RADIANS]
C***   ISR:         HOUR OF SUNRISE (LOCAL STANDARD TIME,
C***                FIRST HOUR WITH BEAM RADIATION)
C***   ISS:         HOUR OF SUNSET (LOCAL STANDARD TIME,
C***                LAST HOUR WITH BEAM RADIATION)
C***   SHADOW:       ARRAY CONTAINING ONE HOUR OF SHADE SWITCHES
C***                SHADOW=0 FOR SHADE, 1 FOR NO SHADE, 2 FOR
C***                CELL INSIDE BUILDING
C***   XSMX:        X COMPONENT OF LONGEST SHADOW CAST BY BUILDING
C***   YSMX:        Y COMPONENT OF LONGEST SHADOW CAST BY BUILDING
C***   XW,YW:       INTERSECTION OF AZIMUTH THROUGH A CELL WITH THE
C***                PLANE OF A BUILDING WALL
C
C*** DESCRIBE BUILDING WALLS
C
      IDIR(1)=1
      ENDS(1,1)=XMIN
      ENDS(1,2)=XMAX
      VALUE(1)=YMAX
C
      IDIR(2)=2
      ENDS(2,1)=YMIN
      ENDS(2,2)=YMAX
      VALUE(2)=XMAX
C
      IDIR(3)=1
      ENDS(3,1)=XMIN
      ENDS(3,2)=XMAX
      VALUE(3)=YMIN
C
      IDIR(4)=2
      ENDS(4,1)=YMIN
      ENDS(4,2)=YMAX
      VALUE(4)=XMIN
C
      IF(SHAPE.EQ.0) THEN
        NWALLS=4
      ELSE
        IDIR(5)=1
        VALUE(5)=0.
        IDIR(6)=2
        VALUE(6)=0.
        NWALLS=6
C
        IF(SHAPE.EQ.1) THEN
          ENDS(1,2)=0.
          ENDS(2,2)=0.
          ENDS(5,1)=0.
          ENDS(5,2)=XMAX
          ENDS(6,1)=0.
          ENDS(6,2)=YMAX
        ELSE IF(SHAPE.EQ.2) THEN
          ENDS(4,2)=0.
          ENDS(1,1)=0.
```

```
            ENDS(5,1)=XMIN
            ENDS(5,2)=0.
            ENDS(6,1)=0.
            ENDS(6,2)=YMAX
          ELSE IF(SHAPE.EQ.3) THEN
            ENDS(3,1)=0.
            ENDS(4,1)=0.
            ENDS(5,1)=XMIN
            ENDS(5,2)=0.
            ENDS(6,1)=YMIN
            ENDS(6,2)=0.
          ELSE IF(SHAPE.EQ.4) THEN
            ENDS(2,1)=0.
            ENDS(3,2)=0.
            ENDS(5,1)=0.
            ENDS(5,2)=XMAX
            ENDS(6,1)=YMIN
            ENDS(6,2)=0.
          END IF
        END IF
C
C*** REWIND WEATHER FILE
C
        REWIND(13)
        READ(13,1000)
 1000 FORMAT(/)
C
C*** LOOP THROUGH ONE YEAR OF WEATHER
C
        DO 600 IDAY=1,365
C
C*** READ ONE DAY OF BEAM RADIATION VALUES FROM WEATHER FILE
C
        READ(13,1500) RBEAM
 1500 FORMAT( 18(/),3(8F10.6,/),//)
C
C*** CALCULATE CORRECTION FROM LOCAL STANDARD TIME TO
C*** SOLAR TIME (IN HOURS)
C
        B=2.*PI*(IDAY-81.)/364.
        ET=9.87*SIN(2.*B)-7.53*COS(B)-1.5*SIN(B)
        TCORR=(4.*(MSTD-LONG)+ET)/60.
C
C*** CALCULATE DECLINATION (IN RADIANS)
C
        DELTA=PI*(23.45*SIN(2.*PI*(284.+IDAY)/365.))/180.
C
C*** FIND LOCAL SUNRISE AND SUNSET HOURS
C
        ISR=24
        ISS=1
C
        DO 150, IHR=1,24
        IF(RBEAM(IHR).NE.0.) THEN
          IF(IHR.LT.ISR) THEN
            ISR=IHR
          ELSE IF(IHR.GT.ISS) THEN
            ISS=IHR
```

```
        END IF
      END IF
  150 CONTINUE
C
C*** COMPUTE RAW AZIMUTH VALUES
C
      DO 155 I=ISR,ISS
C
      TSOL=I+TCORR
      OMEGA=PI*(-1.+TSOL/12.)
      THETAZ(I)=ACOS(COS(DELTA)*COS(PI*LAT/180.)*COS(OMEGA)+
     +       SIN(DELTA)*SIN(PI*LAT/180.))
C
      IF(THETAZ(I).NE.0.) THEN
        GAMMA(I)=ASIN(COS(DELTA)*SIN(OMEGA)/SIN(THETAZ(I)))
      ELSE
        GAMMA(I)=GAMMA(I-1)
      END IF
C
  155 CONTINUE
C
C*** IF NECESSARY, CORRECT AZIMUTH VALUES
C
      DO 160 IHR=ISR,ISS-1
C
      IF(GAMMA(IHR+1).LT.GAMMA(IHR)) THEN
        IF(GAMMA(IHR).LT.0.) THEN
          GAMMA(IHR)=-PI-GAMMA(IHR)
        ELSE IF(GAMMA(IHR).GT.0.) THEN
          GAMMA(IHR+1)=PI-GAMMA(IHR+1)
        END IF
      END IF
C
  160 CONTINUE
C
C*** CHECK EXTERIOR CELLS FOR SHADE DURING SUNLIT HOURS
C
      DO 500 IHR=ISR,ISS
C
C*** CALCULATE MAXIMUM DISTANCE SHADOW CAN BE CAST IN X AND Y
C*** DIRECTIONS.  VALUE USED TO LIMIT SEARCH AREA FOR SHADOWS.
C
      XSMX=ABS(HBLDG*TAN(THETAZ(IHR))*COS(GAMMA(IHR)))
      YSMX=ABS(HBLDG*TAN(THETAZ(IHR))*SIN(GAMMA(IHR)))
C
      DO 400 I=-NX,NX-1
      DO 300 J=-NY,NY-1
C
C*** SELECT EXTERIOR CELLS (MATERIAL '2')

      IF(MSURF(I,J).EQ.2) THEN
C
C*** ELIMINATE AREAS OF THE DOMAIN THAT, A PRIORI, CANNOT BE SHADOWED.
C*** THESE ARE AREAS 'IN FRONT OF' THE BUILDING AND AREAS THAT ARE
C*** BEYOND THE FURTHEST SHADOW THAT CAN BE CAST AT A GIVEN HOUR.
C***
C
      SHADOW(I,J)=0.
```

```
C
        IF(GAMMA(IHR).GE.0.)THEN
          IF(YC(J).GT.YMAX.OR.YC(J).LT.YMIN-YSMX) SHADOW(I,J)=1.
        ELSE
          IF(YC(J).LT.YMIN.OR.YC(J).GT.YMAX+YSMX) SHADOW(I,J)=1.
        END IF
C
        IF(GAMMA(IHR).GE.-PI/2..AND.GAMMA(IHR).LE.PI/2.)THEN
          IF(XC(I).GT.XMAX.OR.XC(I).LT.XMIN-XSMX) SHADOW(I,J)=1.
        ELSE
          IF(XC(I).LT.XMIN.OR.XC(I).GT.XMAX+XSMX) SHADOW(I,J)=1.
        END IF
C
        IF(THETAZ(IHR).EQ.0.) SHADOW(I,J)=1.
C
C*** TEST REMAINING EXTERIOR CELLS FOR INTERSECTION OF BEAM LINES
C*** WITH BUILDING WALLS.  BECAUSE AREAS BEYOND THE FURTHEST SHADOW
C*** THAT CAN BE CAST HAVE BEEN ELIMINATED, IT IS ONLY NECESSARY TO
C*** SHOW THAT THE AZIMUTH LINE FROM ONE OF THE REMAINING CELLS
C*** INTERSECTS ONE OF THE WALLS OF THE BUILDING
C
      IF(SHADOW(I,J).EQ.0.)THEN
        SHADOW(I,J)=1.
        DO 310 IW=1,NWALLS
          IF(IDIR(IW).EQ.1.) THEN
            IF(ABS(GAMMA(IHR)).EQ.PI/2.) THEN
              XW=XC(I)
            ELSE
              XW=XC(I)+(VALUE(IW)-YC(J))/TAN(GAMMA(IHR))
            END IF
C
            IF(XW.GE.ENDS(IW,1).AND.XW.LE.ENDS(IW,2)) THEN
              SHADOW(I,J)=0.
            END IF
          ELSE IF(IDIR(IW).EQ.2. ..EN
            IF(GAMMA(IHR).EQ.0..OR.ABS(GAMMA(IHR)).EQ.PI) THEN
              YW=YC(J)
            ELSE
              YW=YC(J)+(VALUE(IW)-XC(I))*TAN(GAMMA(IHR))
            END IF
C
            IF(YW.GE.ENDS(IW,1).AND.YW.LE.ENDS(IW,2)) THEN
              SHADOW(I,J)=0.
            END IF
          END IF
  310   CONTINUE
      END IF
C
C*** POINTS INTERIOR TO THE BUILDING HAVE THEIR SHADE INDICES SET TO 2
C
      ELSE
        SHADOW(I,J)=2.
      END IF
C
  300 CONTINUE
  400 CONTINUE
```

```
C
C*** WRITE RESULTS FOR THIS HOUR TO THE SHADE FILE
C
      WRITE(12,*) IDAY,ISR,ISS,IHR
      WRITE(12,*) ((SHADOW(I,J),J=-NY,NY-1),I=-NX,NX-1)
C

  500 CONTINUE
  600 CONTINUE
C
      RETURN
      END
```

B.7. SUBROUTINE COEFFS

```
      SUBROUTINE COEFFS(NXM1,NYM1,NZM1,DX,DY,DZ,DXP,DYP,DZP,MTYPE,
     +                  TCON,RINS,INS,CXM,CYM,CZM,CXP,CYP,CZP)
C
C*** THIS SUBROUTINE COMPUTES CONSTANTS USED IN THE FINITE
C*** DIFFERENCE EQUATIONS SO THAT THEY DO NOT NEED TO BE REGENERATED
C*** AT EVERY TIME STEP.  THEY ARE FUNCTIONS OF CELL DIMENSIONS AND
C*** OF THERMAL CONDUCTIVITY.  THEY MUST BE RECOMPUTED EVERY TIME
C*** MATERIAL PROPERTIES ARE VARIED, BUT NEED BE CALCULATED ONLY
C*** ONCE IN A CONSTANT PROPERTY RUN.  SEE SLAB3D FOR MOST VARIABLE DEFS.
C
C*** 1 AUGUST 1988
C
C*** WM. BAHNFLETH
C
      REAL DX(-20:19),DY(-20:19),DZ(0:19),DXP(-20:19),DYP(-20:19),
     +     DZP(0:19),TCON(4),
     +     CXM(-20:19,-20:19,0:19),CYM(-20:19,-20:19,0:19),
     +     CZM(-20:19,-20:19,0:19),CXP(-20:19,-20:19,0:19),
     +     CYP(-20:19,-20:19,0:19),CZP(-20:19,-20:19,0:19)
C
      INTEGER INS(-20:19,-20:19),MTYPE(-20:19,-20:19,0:19)
C
C*** CXM, CYM, CZM ARE COEFFICIENTS REFERRING TO CELL FACES IN THE NEGATIVE
C***   COORDINATE DIRECTION INDICATED FROM THE CENTER CELL NODE
C*** CXP, CYP, AND CZP REFER TO FACES IN THE POSITIVE DIRECTION FROM THE
CENTER
C***   NODE
C
      NX=NXM1+1
      NY=NYM1+1
C
      DO 100 I=-NXM1,NXM1
      DO 90 J=-NY,NYM1
      DO 80 K=0,NZM1
C
C*** DETERMINE EFFECTIVE CONDUCTIVITY AT X INTERFACE (I-1/I).
C*** UNLESS NEIGHBOR CELLS ARE OF DIFFERENT MATERIALS OR THERE IS A
C*** SURFACE RESISTANCE, THE EFFECTIVE CONDUCTIVITY AT THE INTERFACE
C*** IS THE SAME AS THE ACTUAL CELL CONDUCTIVITY.
C
      IF(MTYPE(I,J,K).EQ.MTYPE(I-1,J,K)) THEN
        XK=TCON(MTYPE(I,J,K))
      ELSE IF(MTYPE(I,J,K).EQ.1.OR.MTYPE(I-1,J,K).EQ.1) THEN
        XK=DXP(I-1)/(DX(I-1)/TCON(MTYPE(I-1,J,K))/2.+
     +     DX(I)/TCON(MTYPE(I,J,K))/2.+RINS)
      ELSE
        XK=DXP(I-1)/(DX(I-1)/TCON(MTYPE(I-1,J,K))/2.+
     +     DX(I)/TCON(MTYPE(I,J,K))/2.)
      END IF
C
C*** CALCULATE COEFFICIENTS CXM, CXP
C
      CXM(I,J,K)=XK/DX(I)/DXP(I-1)
      CXP(I-1,J,K)=XK/DX(I-1)/DXP(I-1)
C
```

```
   80 CONTINUE
   90 CONTINUE
  100 CONTINUE
C
C*** REPEAT PREVIOUS STEPS AT Y INTERFACE (J-1/J)
C
      DO 200 I=-NX,NXM1
      DO 190 J=-NYM1,NYM1
      DO 180 K=0,NZM1
C
C*** EFFECTIVE CONDUCTIVITY
C
      IF(MTYPE(I,J,K).EQ.MTYPE(I,J-1,K)) THEN
        YK=TCON(MTYPE(I,J,K))
      ELSE IF(MTYPE(I,J,K).EQ.1.OR.MTYPE(I,J-1,K).EQ.1) THEN
        YK=DYP(J-1)/(DY(J-1)/TCON(MTYPE(I,J-1,K))/2.+
     +     DY(J)/TCON(MTYPE(I,J,K))/2.+RINS)
      ELSE
        YK=DYP(J-1)/(DY(J-1)/TCON(MTYPE(I,J-1,K))/2.+
     +     DY(J)/TCON(MTYPE(I,J,K))/2.)
      END IF
C
C*** CALCULATE COEFFICIENTS CYM, CYP
C
      CYM(I,J,K)=YK/DY(J)/DYP(J-1)
      CYP(I,J-1,K)=YK/DY(J-1)/DYP(J-1)
C
  180 CONTINUE
  190 CONTINUE
  200 CONTINUE
C
C*** ONE MORE TIME FOR THE Z INTERFACE (K-1/K)
C
      DO 300 I=-NX,NXM1
      DO 290 J=-NY,NYM1
      DO 280 K=1,NZM1
C
C*** DETERMINE INTERFACE CONDUCTIVITY
C
      IF(K.EQ.1) THEN
        IF(MTYPE(I,J,1).EQ.MTYPE(I,J,0)) THEN
          ZK=TCON(MTYPE(I,J,1))
        ELSE IF(MTYPE(I,J,0).EQ.1) THEN
          ZK=DZP(0)/(DZ(0)/TCON(1)+DZ(1)/TCON(MTYPE(I,J,1))/2.+
     +       RINS*INS(I,J))
        END IF
      ELSE
        IF(MTYPE(I,J,K).EQ.MTYPE(I,J,K-1)) THEN
          ZK=TCON(MTYPE(I,J,K))
        ELSE
          ZK=DZP(K-1)/(DZ(K-1)/TCON(MTYPE(I,J,K-1))/2.+
     +       DZ(K)/TCON(MTYPE(I,J,K))/2.)
        END IF
      END IF
C
C*** CALCULATE COEFFICIENTS CZM, CZP
C
      CZM(I,J,K)=ZK/DZ(K)/DZP(K-1)
```

```
      CZP(I,J,K-1)=ZK/DZ(K-1)/DZP(K-1)
C
  280 CONTINUE
  290 CONTINUE
  300 CONTINUE
C
      RETURN
      END
```

APPENDIX C. 3-D PROGRAM INPUT WORKSHEET

Item	Description	
RUNID	name of input file, 4 characters	_____
WEATHER	name of weather file, 6 characters	_____
LONG, LAT	longitude and latitude, [DEG]	_____ _____
MSTD	standard time meridian [DEG]	_____
ELEV	elevation [m]	_____
OLDTG	T/F: is there a ground temperature file for this run?	_____
TGNAM	7 char. name of ground temperature file (will be created if it doesn't exist)	_____
OLDSHD	T/F: is there a shade file for this run?	_____
SHDNAM	7 char. name of shade file ('NOSHADE' means shadowing is off)	_____
NMAT	number of material types (2)	_____
RHO/C/TCON	density [kg/m^3], specific heat [J/kg-K], thermal conductivity [W/m-K] for each material--1) floor, 2) soil	
	1) _____	_____ _____
	2) _____	_____ _____
RINS, DINS	thermal resistance [K/(W/m^2)] and width [m] of slab insulation	_____ _____

ALBEDO	solar albedo: no snow/snow	_____	_____
EPSLW	long-wave emissivity	_____	_____
Z0	roughness height [cm]	_____	_____
EVTR	T/F: is there evapotranspiration?		_____
FIXBC	T/F: is the deep ground condition fixed temp. or zero flux?		_____
NX, NY, NX	cell face indices (-NX to NX, -NY to NY, 0 to NZ)		
		_____ _____	_____

XFACE coordinates of cell x-faces [m]

_____ _____ _____ _____ _____ _____ _____ _____

_____ _____ _____ _____ _____ _____ _____ _____

_____ _____ _____ _____ _____ _____ _____ _____

_____ _____ _____ _____ _____ _____ _____ _____

_____ _____ _____ _____ _____ _____ _____ _____

YFACE coordinates of cell y-faces [m]

_____ _____ _____ _____ _____ _____ _____ _____

_____ _____ _____ _____ _____ _____ _____ _____

_____ _____ _____ _____ _____ _____ _____ _____

_____ _____ _____ _____ _____ _____ _____ _____

_____ _____ _____ _____ _____ _____ _____ _____

ZFACE coordinates of cell z-faces [m]

_____ _____ _____ _____ _____ _____ _____

_____ _____ _____ _____ _____ _____ _____

_____ _____ _____ _____ _____ _____ _____

IBOX, JBOX	face indices defining extent of slab: -IBOX to IBOX in x, -JBOX to JBOX in y	____ ____
SHAPE	index for shape: 0 for rectangle, 1, 2, 3, 4 for L-shaped (SHAPE is the number of the empty quadrant: SW, NW, NE, or SE)	_____
HBLDG	height of building [m] -- required, but only used when there is shadowing	_____
TIN	temperature above slab floor [C]	_____
HIN	indoor heat transfer coefficient [W/m^2-K] 1) Q to floor, 2) Q to room	____ ____
IYRS	limit on years to iterate	_____
TG	initial values for ground temperature [C]	____ ____

APPENDIX D. CATALOG OF RUNS

I. Series G

Rectangular and L-shaped plans. Evapotranspiration on, shadowing off. Medford, OR weather. Base case properties (k=1W/m-K, density=1200 Kg/m^3, specific heat=1200 J/m^3-K). Variable aspect ratio for areas of 144 m^2, 900 m^2, 2025 m^2, and 3600 m^2. All floors are 0.1m thick. Soil temperature is 11.7 C at a depth of 10 m or 15 m, as indicated. Side boundaries are approximately 12 m beyond the edge of the slab The objective of this series is to provide data for investigation of geometric influences on slab-on-grade heat loss. Ground temperature files generated in connection with this series of tests are TGMEDG1 (10 m deep domain) and TGMEDG2 (15 m deep domain).

ID	Plan Shape	Dimensions	Area	Comments
GR01	rectangle	12x12m	144 m^2	z_{max}=10 m
GR1A	rectangle	12x12m	144 m^2	z_{max}=15 m
GR02	rectangle	8.5x17m	144.5 m^2	z_{max}=10 m
GR03	rectangle	7x20.5m	143.5 m^2	z_{max}=10 m
GR04	rectangle	6x24m	144 m^2	z_{max}=10 m
GR05	rectangle	45x45m	2025 m^2	z_{max}=10 m
GR5A	rectangle	45x45m	2025 m^2	XMAX & YMAX > GR05
GR5B	rectangle	45x45m	2025 m^2	z_{max}=15 m
GR06	rectangle	32x63m	2016 m^2	z_{max}=10 m
GR6A	rectangle	32x63m	2016 m^2	z_{max}=15 m
GR07	rectangle	23x88m	2024 m^2	z_{max}=10 m
GR7A	rectangle	23x88m	2024 m^2	z_{max}=15 m
GR08	rectangle	18x112m	2016 m^2	z_{max}=10 m
GR8A	rectangle	18x112m	2016 m^2	z_{max}=15 m

GR09	rectangle	30x30m	900 m^2	z_{max}=10 m
GR9A	rectangle	30x30m	900 m^2	z_{max}=15 m
GR10	rectangle	20x45m	900 m^2	z_{max}=10 m
G10A	rectangle	20x45m	900 m^2	z_{max}=15 m
GR11	rectangle	17x53m	901 m^2	z_{max}=10 m
G11A	rectangle	17x53m	901 m^2	z_{max}=15 m
GR12	rectangle	15x60m	900 m^2	z_{max}=10 m
G12A	rectangle	15x60m	900 m^2	z_{max}=15 m
GR13	rectangle	60x60m	3600 m^2	z_{max}=10 m
G13A	rectangle	60x60m	3600 m^2	z_{max}=15 m
GR14	rectangle	30x120m	3600 m^2	z_{max}=10 m
G14A	rectangle	30x120m	3600 m^2	z_{max}=15 m
GR15	rectangle	20x180m	3600 m^2	z_{max}=10 m
G15A	rectangle	20x180m	3600 m^2	z_{max}=15 m
GR16	rectangle	20x20m	400 m^2	z_{max}=10 m
G16A	rectangle	20x20m	400 m^2	z_{max}=15 m
GR17	rectangle	10x40m	400 m^2	z_{max}=10 m
G17A	rectangle	10x40m	400 m^2	z_{max}=15 m
GL01	L-shaped	******	144.9 m^2	z_{max}=15 m
GL02	L-shaped	******	2028 m^2	z_{max}=10 m
GL2A	L-shaped	******	2028 m^2	z_{max}=15 m
GL03	L-shaped	******	897.9 m^2	z_{max}=10 m
GL3A	L-shaped	******	897.9 m^2	z_{max}=15 m

II. Series W

Rectangular plans. The basic decks are taken from the previous series. The only factor varied is the weather file. TMY files from Minneapolis MN, Phoenix AZ and Philadelphia PA. Ground temperature files generated for this series are TGMINW1, TGPHOW1, and TGPHIW1, all for a 15m deep domain.

ID	Plan Shape	Dimensions	Area	Location
WMN1	rectangle	12x12m	144 m^2	Minneapolis
WMN2	rectangle	45x45m	2025 m^2	Minneapolis
WMN3	rectangle	6x24m	144 m^2	Minneapolis
WMN4	rectangle	18x112m	2016 m^2	Minneapolis
WPX1	rectangle	12x12m	144 m^2	Phoenix
WPX2	rectangle	45X45m	2025 m^2	Phoenix
WPX3	rectangle	6x24m	144 m^2	Phoenix
WPX4	rectangle	18x112m	2016 m^2	Phoenix
WPH1	rectangle	12x12m	144 m^2	Philadelphia
WPH2	rectangle	45x45m	2025 m^2	Philadelphia
WPH3	rectangle	6x24m	144 m^2	Philadelphia
WPH4	rectangle	18x112m	2016m^2	Philadelphia

III. Series S

These runs show the effect of shade cast on the ground by a building. Sites are Medford and Phoenix. 15m deep domain. Evapotranspiration is included except as noted. Shade files are SHMEDSQ for square plan in Medford and Phoenix, SHMEDR1 and SHMEDR2 for E/W and N/S rectangular plans in Medford.

ID	Plan Shape	Dimensions	Area	Location
SMD1	rectangle	12x12m	144 m^2	Medford
SMD2	rectangle	6x24m	144 m^2	Medford, Long E/W
SMD3	rectangle	6x24m	144 m^2	Medford, Long N/S
SMD4	rectangle	12x12m	144 m^2	Medford, No evap.
SPX1	rectangle	12x12m	144 m^2	Phoenix

IV. Series K

These runs show the effect of thermal conductivity and thermal diffusivity. They are identical to the 'W' runs for Philadelphia except that the soil properties have been changed.

A. k=2 W/m-K, density=1700 kg/m^3,and specific heat=1700 J/m^3-K. (Ground temperature file TGPHW2)

ID	Plan Shape	Dimensions	Area	Location
KPH1	rectangle	12x12m	144 m^2	Philadelphia
KPH2	rectangle	45X45m	2025 m^2	Philadelphia
KPH3	rectangle	6x24m	144 m^2	Philadelphia
KPH4	rectangle	18x112m	2016 m^2	Philadelphia

B. k=1 W/m-K, density=1700 kg/m^3,and specific heat=1700 J/m^3-K. (Ground temperature file TGPHW3)

ID	Plan Shape	Dimensions	Area	Location
KPH5	rectangle	12x12m	144 m^2	Philadelphia
KPH6	rectangle	45X45m	2025 m^2	Philadelphia
KPH7	rectangle	6x24m	144 m^2	Philadelphia
KPH8	rectangle	18x112m	2016 m^2	Philadelphia

C. k=0.5 W/m-K, density=1200 kg/m^3,and specific heat=1200 J/m^3-K. (Ground temperature file TGPHW4)

ID	Plan Shape	Dimensions	Area	Location
KPH9	rectangle	12x12m	144 m^2	Philadelphia
KP10	rectangle	45X45m	2025 m^2	Philadelphia
KP11	rectangle	6x24m	144 m^2	Philadelphia
KP12	rectangle	18x112m	2016 m^2	Philadelphia

D. k=2 W/m-K, density=1500 kg/m^3,and specific heat=1500 J/m^3-K. (Ground temperature TGPHW5)

ID	Plan Shape	Dimensions	Area	Location
KP13	rectangle	12x12m	144 m^2	Philadelphia
KP14	rectangle	45X45m	2025 m^2	Philadelphia
KP15	rectangle	6x24m	144 m^2	Philadelphia
KP16	rectangle	18x112m	2016 m^2	Philadelphia

V. Series E

These runs are show the effect of turning off evaporation in the surface boundary condition. Otherwise, they are the same as the corresponding series G and W runs. New ground temperature files TGMINE1, TGMEDE1, TGPHIE1, and TGPHOE1 were generated.

ID	Plan Shape	Dimensions	Area	Location
EMN1	rectangle	12x12m	144 m^2	Minneapolis
EMN2	rectangle	6x24m	144 m^2	Minneapolis
EMN3	rectangle	45x45m	2025 m^2	Minneapolis
EMN4	rectangle	18x112m	2016 m^2	Minneapolis
EMD1	rectangle	12x12m	144 m^2	Medford
EPH1	rectangle	12x12m	144 m^2	Philadelphia
EPX1	rectangle	12x12m	144 m^2	Phoenix

VI. Series I

These runs indicate the effect of under-slab insulation. The insulating material is 2" extruded polystyrene board, k=0.029 W/m-K. The resistance of 1 and 2" layers are 0.8759 and 1.75 K/(W/m^2), respectively. Two treatments are considered: edge+1 m under slab, and edge+full under slab. Since insulation is applied primarily for the purpose of mitigating heating load, Minneapolis weather is used in these runs.

ID	Plan Shape	Dimensions	Area	Location
IMN1	rectangle	12x12m	144 m^2	2", 1 m strip

IMN2	rectangle	12x12m	144 m^2	2", full
IMN3	rectangle	45x45m	2025 m^2	2", 1m strip
IMN4	rectangle	45x45m	2025 m^2	2", full
IMN5	rectangle	6x24m	144 m^2	2", 1m strip
IMN6	rectangle	18x112m	2016 m^2	2", 1m strip
IMN7	rectangle	12x12m	144 m^2	1", 1 m strip
IMN8	rectangle	12x12m	144 m^2	1", full
IMN9	rectangle	45x45m	2025 m^2	1", 1m strip
IM10	rectangle	45x45m	2025 m^2	1", full
IM11	rectangle	6x24m	144 m^2	1", 1m strip
IM12	rectangle	18x112m	2016 m^2	1", full

VII. Series Z

Rectangular plans. The basic decks are the same as WMN1-4. The only factor varied is the deep ground boundary condition. Ground temperature file TGMINZ1 has a zero-flux condition at a depth of 15m. Evapotranspiration is on.

ID	Plan Shape	Dimensions	Area	Location
ZMN1	rectangle	12x12m	144 m^2	Minneapolis
ZMN2	rectangle	45x45m	2025 m^2	Minneapolis
ZMN3	rectangle	6x24m	144 m^2	Minneapolis
ZMN4	rectangle	18x112m	2016 m^2	Minneapolis

REFERENCES

1. Bareither, H.D., A.N. Fleming, and B.E. Alberty, TEMPERATURE AND HEAT LOSS CHARACTERISTICS OF CONCRETE FLOORS LAID ON THE GROUND, University of Illinois Small Homes Council Technical Report PB 93920, 1948.

2. Labs, K., J. Carmody, R. Sterling, L. Shen, Y. J. Huang, and D. Parker, BUILDING FOUNDATION DESIGN HANDBOOK, United States Department of Energy publication DE88-013350, May 1988.

3. Moreland, F., F. Higgs, and J. Shih, eds., EARTH COVERED BUILDINGS: TECHNICAL NOTES, US-DoE CONF-7806138-P1, 1979.

4. MacDonald, G.R., D.E. Claridge, and P.A. Oatman, "A Comparison of Seven Basement Heat Loss Calculation Methods Suitable for Variable-Base Degree-Day Calculations," ASHRAE Trans., v. 91, pt.1b, 1985.

5. Dill, R. S., W. C. Robinson, and H.D. Robinson, "Measurements of Heat Losses from Slab Floors," Building Materials and Structures Report BMS103, National Bureau of Standards, Washington D.C., 1943.

6. 1985 ASHRAE Fundamentals-SI Version, American Society of Heating, Refrigerating, and Air-Conditioning Engineers, Atlanta.

7. Wang, F.S., MATHEMATICAL MODELING AND COMPUTER SIMULATION OF INSULATION SYSTEMS IN BELOW GRADE APPLICATIONS, Proc. ASHRAE/DOE-ORNL Conf. Thermal Performance of the Exterior Envelopes of Buildings, Dec. 3-5, 1979.

8. Yard, D.C., M. Morton-Gibson, and J.W. Mitchell, "Simplified Dimensionless Relations for Heat Loss from Basements," ASHRAE Trans. v.90, pt.1b, 1984.

9. Kusuda, T., O. Piet, and J.W. Bean, "Annual Variation of Temperature Field and Heat Transfer under Heated Ground Surfaces: Slab-on-Grade Floor Heat Loss Calculations," Proc. ASHRAE/DOE Conf. Thermal Performance of the Exterior Envelopes of Buildings II, Dec. 6-9, 1982.

10. Lachenbruch, A. H., "Three-dimensional heat conduction in permafrost beneath heated buildings," U. S. Geological Survey Bulletin 1052-B, 1957.

11. Adamson, B., "Soil Temperature Under Houses Without Basements," Bygyforsknigen Handlinger, Nr 46 Transaction, 1964.

12. Delsante, A. E., A. N. Stokes, and P. J. Walsh, "Application of Fourier transforms to periodic heat flow into the ground under a building," International Journal of Heat and Mass Transfer, Dec. 1982.

13. Kusuda, T. and J.W. Bean, "Simplified Methods for Determining Seasonal Heat Loss from Uninsulated Slab-on Grade Floors," ASHRAE Trans., v. 90, pt. 1b, 1984.

14. Shen, L.S. and J.W. Ramsey, "A Simplified Thermal Analysis of Earth-Sheltered Buildings Using a Fourier-Series Boundary Method," ASHRAE Trans. 1983, pt. 1b.

15. Krarti, M., D. Claridge and J. Kreider, INTERZONE TEMPERATURE PROFILE ESTIMATION -SLAB-ON-GRADE HEAT TRANSFER RESULTS, in Heat Transfer in Buildings and Structures, ASME Heat Transfer Division HTD-Vol. 41, proceedings of a session held at the 23rd National Heat Transfer Conference, Aug. 4-7, 1985.

16. Mitalas, G.P., "Calculation of Basement Heat Loss," ASHRAE Trans. 1983, pt. 1b.

17. Kelvin, 1st Baron, "The Reduction of Observations of Underground Temperature," Transactions of the Royal Society of Edinburgh, vol. 22, 1861.

18. Lux, M.E., R.S. Dumont, J. Hayes, and A. Wilson, HOTCAN 3: HOUSING ENERGY PROGRAM, Proc. 9th National Passive Solar Conference, Columbus, OH, 23 Sep., 1984.

19. Yuill, G.K., and C.P. Wray, VERIFICATION OF A MICROCOMPUTER PROGRAM IMPLEMENTING THE MITALAS BELOW-GRADE HEAT LOSS MODEL, ASHRAE Trans., v. 93, pt. 1, 1987.

20. Shipp, P.H., THE THERMAL CHARACTERISTICS OF LARGE EARTH-SHELTERED STRUCTURES, Ph.D. thesis, Univ. of Minn., 1979.

21. Patankar, S.V., Numerical Heat Transfer and Fluid Flow, New York, Hemisphere 1980.

22. Kusuda, T., "The Effect of Ground Cover on Earth Temperature," in Alternatives in Energy Conservation: The Use of Earth Covered Buildings, NSF-RA-760006, 1975.

23. Meixel, G.D., "Computer Simulation of Heat Transfer from Earth Sheltered Structures: A Comparison of Varying Levels of Earth Sheltering in Five Different Climates," Proc. Third Miami International Conference on Alternative Energy Sources, Dec. 15-17, 1980.

24. Meixel, G.D., P.H. Shipp, and T.P. Bligh, THE IMPACT OF INSULATION PLACEMENT ON THE SEASONAL HEAT LOSS THROUGH BASEMENT AND EARTH-SHELTERED WALLS, Proc. ASHRAE/DOE-ORNL Conf. Thermal Performance of the Exterior Envelopes of Buildings, Dec. 3-5, 1979.

25. Szydlowski, R.F., and T.H. Kuehn, "Analysis of Transient Heat Loss in Earth-Sheltered Structures," Underground Space, v. 5, n. 4, 1981.

26. McBride, M. F., R. S. Blancett, C. F. Sepsy, and C.D. Jones, "Measurement of subgrade temperatures for prediction of heat loss in basements," ASHRAE Trans., 1985, pt. 1.

27. Speltz, J.J., A NUMERICAL SIMULATION OF TRANSIENT HEAT FLOW IN EARTH SHELTERED BUILDINGS FOR SEVEN SELECTED U.S. CITIES, MS thesis, Trinity University, 1980.

28. Speltz, J.J. and G.D. Meixel, A COMPUTER SIMULATION OF THE THERMAL PERFORMANCE OF EARTH COVERED ROOFS, Proc. Underground Space Conference and Exposition, Kansas City, MO, June 8-10, 1981.

29. Walton, G.N., ESTIMATING 3-D HEAT LOSS FROM RECTANGULAR BASEMENTS AND SLABS USING 2-D CALCULATIONS, ASHRAE Trans., v. 93, pt. 1., 1987.

30. Ceylan, H.T. and G.E. Meyers, "Long-Time Solutions to Heat-Conduction Transients with Time-Dependent Inputs," ASME J. Heat Transfer, v. 102, Feb. 1980.

31. Shen, L. S., J. Poliakova, and Y. J. Huang, CALCULATION OF BUILDING FOUNDATION HEAT LOSS USING SUPERPOSITION AND NUMERICAL SCALING, ASHRAE Trans., v. 94, pt. 2, 1988.

32. Huang, Y. J., L. S. Shen, J. C. Bull, and L. F. Goldberg, WHOLE-HOUSE SIMULATION OF FOUNDATION HEAT FLOWS USING THE DOE-2.1C PROGRAM, ASHRAE Trans., v. 94, pt. 2, 1988.

33. Kersten, M.S., THERMAL PROPERTIES OF SOILS, Univ. of Minnesota Institute of Technology Engineering Experiment Station Bulletin No. 28, v. LII, n. 21, June 1, 1949.

34. Eckert, E.R.G. and E. Pfender, "HEAT AND MASS TRANSFER IN POROUS MEDIA WITH PHASE CHANGE," Proc. 6th Int'l. Heat Transfer Conference, 1978.

35. Smith, W.O., THERMAL CONDUCTIVITIES IN MOIST SOILS, Proc., Soil Science Society of America, v.4, 1939.

36. Penner, E., "Thermal conductivity of frozen soils," Canadian J. of Earth Sciences, v. 7, 1970.

37. Gilpin, R.R. and B.K. Wong, ""Heat-Valve" Effects in the Ground Thermal Regime," ASME J. Heat Transfer, v. 98, 1976.

38. Philip, J.R., and D.A. deVries, "Moisture Movement in Porous Materials under Temperature Gradients," American Geophysical Union Trans., v. 38, no. 2, 1957.

39. Kusuda, T. and P.R. Achenbach, "Earth Temperature and Thermal Diffusivity at Selected Stations in the United States," ASHRAE Trans., v. 71, pt. 1, 1965.

40. Gilpin, R.R. and B.K. Wong, "The Ground Temperature Regime and its Relationship to Soil Properties and Ground Surface Cover," ASME paper 75-WA/HT-98, 1975.

41. Gold, L.W., "INFLUENCE OF SURFACE CONDITIONS ON GROUND TEMPERATURE," Canadian Journal of Earth Sciences, v. 4, 1967.

42. Sellers, W.D., PHYSICAL CLIMATOLOGY, Univ. of Chicago Press, Chicago, 1965.

43. Kreith, F. and W.D. Sellers, "General principles of natural evaporation," in Heat and Mass Transfer in the Biosphere, Part I: Transfer Processes in the Plant Environment, D.A. de Vries and N.H. Afgan, eds., Wiley, New York, 1975.

44. Geiger, R., The Climate Near the Ground, Harvard University Press, Cambridge, 1961.

45. Sellers, W.D. and P.S. Dryden, AN INVESTIGATION OF HEAT TRANSFER FROM BARE SOIL, Final Report, Grant No. DA-AMC-28-043-66-G27, Institute of Atmospheric Physics, Univ. of Arizona, Tucson, AZ, April 1967.

46. Jensen, M.E., ed., Consumptive Use of Water and Irrigation Water Requirements, ASCE, New York, 1973.

47. Thibault, J., "COMPARISON OF NINE THREE-DIMENSIONAL NUMERICAL METHODS FOR THE SOLUTION OF THE HEAT DIFFUSION EQUATION," Numerical Heat Transfer, v. 8, 1985.

48. Kreith, F. and J. F. Kreider, Principles of Solar Engineering, Hemisphere, Washington, D. C., 1978.

49. Labs, K., "Regional Analysis of Ground and Above-Ground Climate," Underground Space, v. 6, no. 6, and v. 7, no. 1, 1982.

50. Andersland, O.B. and D.M. Anderson, Geotechnical Engineering for Cold Regions, New York, McGraw-Hill, 1978.

51. Kung, E.C., R.A. Bryson, and D.H. Lenschow, "A STUDY OF CONTINENTAL SURFACE ALBEDO ON THE BASIS OF FLIGHT MEASUREMENTS AND STRUCTURE OF THE EARTH'S SURFACE COVER OVER NORTH AMERICA," Monthly Weather Review, v. 92, n. 12, 1964.

52. Christian, J.E. and W.R. Strzepek, "PROCEDURE FOR DETERMINING THE OPTIMUM FOUNDATION INSULATION LEVELS FOR NEW, LOW-RISE RESIDENTIAL BUIDINGS," ASHRAE Trans., v. 93, pt. 1, 1987.

53. Shipp, P.H. and T.B. Broderick, "Comparison of Annual Heating Loads for Various Basement Wall Insulation Strategies Using Transient and Steady-State Models," THERMAL INSULATION, MATERIALS, AND SYSTEMS FOR ENERGY CONSERVATION IN THE '80s, ASTM STP 789, F.A. Govan, D.M. Greason, and J.D. McAllister, eds., American Society for Testing and Materials, 1983.

54. Architectural and Engineering Instructions: Design Criteria. Office of the Chief of Engineers, Engineering Division, Washington, D.C., 13 March, 1987.

VITA

William P. Bahnfleth [redacted] After passing the greater part of his childhood in Downers Grove, Illinois, he moved with his parents and two brothers to Cincinnati, Ohio in the fall of 1972. In 1975, he graduated from Cincinnati Indian Hill High School where he achieved National Merit Scholar recognition, was a member of the track team, and captain of the cross-country team. During his high school years, he studied organ with W. Edwin Domb at the Cincinnati Conservatory of Music. He enrolled as an undergraduate James Scholar in mechanical engineering at the University of Illinois in the fall of 1975, and received the B.S. degree with University Honors in May, 1979. He was awarded Phi Kappa Phi and National Science Foundation fellowships in 1979. He continued his studies in mechanical engineering as a graduate student under the direction of Michael M. Chen, and received the M.S. in 1980. A paper based on his master thesis topic, "A MASS TRANSFER ANALOG FOR THE STUDY OF LOW PRANDTL NUMBER HEAT TRANSFER" (co-authored with Prof. Chen and Davood Moslemian) earned "best paper" recognition at the 1983 ASME-AIChE Heat Transfer Conference. He continued his athletic activities while a graduate student, serving as president of the Illinois Track Club and receiving three Avery Brundage scholarships. In 1984, he suspended his engineering studies to pursue a degree in organ performance at the University of Illinois. While thus occupied, he met his future bride, [redacted] a classmate in the organ studio of Jerald Hamilton. They

were married on December 28, 1985. He was a finalist in the 1987 Scarritt College undergraduate organ competion and received a B.Mus. degree with highest honors in May, 1988. Mr. Bahnfleth joined the staff of the US Army Construction Engineering Research Laboratory as a principal investigator in the Energy Systems Division in March, 1988, after three years of employment as a student contractor. He is a member of the Phi Eta Sigma, Pi Tau Sigma, Tau Beta Pi, Phi Kappa Phi, Sigma Xi, and Pi Kappa Lamba honorary societies. His professional affiliations include ASME, ASHRAE, and the American Guild of Organists. He remains active as a musician, occasionally appearing in recital with his wife.

USACERL DISTRIBUTION

Chief of Engineers
ATTN: CEEC-E

US Military Academy 10966
ATTN: Dept of Geography &
Computer Science

AMC - Dir., Inst., & Svcs.
Army Matls Tech Lab 02172
ATTN: DEH
Harry Diamond Laboratories 20783
ATTN: Library

Fort Belvoir, VA 22060
ATTN: Engr Studies Center
ATTN: Engr topographic Lab

CECRL, ATTN: Library 03755

CEWES, ATTN: Library 39180

Tyndall AFB, IL 32403
AFESC/Engineering & Serivce Lab

NCEL 93043
ATTN: Library (Code L08A)

Engineering Societies Library
New York, NY 10017

US Government Printing Office 22304
Receiving/Depository Section (2)

Nat'l Institute of Standards & Tech 20899

Defense Technical Info. Center 22314
ATTN: DDA (2)